Helsinki University of Technology Publications in Engineering Physics
Teknillisen korkeakoulun teknillisen fysiikan julkaisuja
Espoo 2004 TKK-F-A830

# SELF-ORGANIZED SUPRAMOLECULES OF π-CONJUGATED RODLIKE POLYMERS

Matti Knaapila

Dissertation for the degree of Doctor of Science in Technology to be presented with due permission of the Department of Engineering Physics and Mathematics of Helsinki University of Technology for public examination and debate in Auditorium E at the Main Building of Helsinki University of Technology (Espoo, Finland) on Friday, the 13 th August, 2004 at 12 o'clock noon.

Helsinki University of Technology
Department of Engineering Physics and Mathematics
Espoo, Finland

Teknillinen korkeakoulu
Teknillisen fysiikan ja matematiikan osasto
Espoo, Suomi

Distribution:
Matti Knaapila &
Helsinki University of Technology
P.O. Box 1000
FIN-02015 HUT
Tel. +358-9-4511
Fax. +358-9-456-077

E-mail: matti.knaapila@durham.ac.uk
http://www.helsinki.fi/people/matti.knaapila/
http://www.physics.helsinki.fi/~mknaapil/
http://www.dur.ac.uk/matti.knaapila/



ISBN 951-22-7147-8 (print)
ISBN 951-22-7148-6 (pdf)
ISSN 1456-3320 (print)
ISSN 1459-7268 (pdf)

Otamedia Oy
Espoo, June 8, 2004

# Preface

This thesis has been made in the Materials Physics Laboratory and in the Optics and Molecular Materials Laboratory, Department of Engineering Physics and Mathematics of Helsinki University of Technology in the course of February 2000-January 2001 and January 2001-October 2002, respectively. It has been conducted in the Division of X-Ray Physics at the Department of Physical Sciences of University of Helsinki during October 2002-October 2003. During October 2003-August 2004 it has been made in the Organic Electroactive Materials Research Group, Department of Physics of University of Durham, UK. The essence of the experimental results was done using synchrotron sources in the Durtch-Belgium Beamline of European Synchrotron Radiation Facility and W1.1 Beamline of Deutsches Electronen-Synchrotron in numerous instances during the period 1999-2003. The theory considerations were made in collaboration with the Polymer Physics Group of University of Groningen in 2003. The instructors were O. Ikkala of Helsinki University of Technology and A. Monkman of University of Durham.

# Acknowledgements

First of all, I thank Mika Torkkeli and Ritva Serimaa of University of Helsinki and Andrew Monkman of University of Durham. The best thanks belong to Mika Torkkeli for the excellent supervision and advice.


**Figure 1**. Matti Knaapila on the snow-covered road.

I acknowledge the Division of X-ray physics at the University of Helsinki and the Department of Physics at the University of Durham for the superb offices, superiour working conditions, and world-class opportunities, and my associates there for the great time and friendship. I highly appreciate Kaisa Kisko, Ulla Vainio, and Teemu Ikonen, and everyone at the Division of X-ray Physics. They really make the atmosphere. I express my best thanks to Lockhart Horsburgh of Avocado Research Chemicals and Benjamin Lyons, Lars-Olof Pålsson, Joel Foreman, and Naveed Zaidi of University of Durham. Moreover, I thank Roman Stepanyan of University of Twente very much for his extensive cooperation in theoretical discussions and experiment. Special thanks for excellent cooperation belong to Kaija Jokela of Instrumentarium Corporation and Gerrit ten Brinke of the Polymer Physics Group of University of Groningen. I thank Andrei Subbotin and Evgeny Polushkin of Groningen, as well. I acknowledge Wim Bras and Igor Dolbnya of the Durtch-Belgium Beamline of European Synchrotron Radiation Facility as well as Oliver Seeck and Milena Mihaylova of Institut für Festkörperforschung of Forschungszentrum Jülich and W1.1 Beamline of Deutsches Electronen-Synchrotron for very fluent cooperation and excellent opportunities. Working at these beamlines has always been a great pleasure. I thank Panu Hiekkataipale and Klas Lindfors of the Department of Engineering Physics and Mathematics of Helsinki University of Technology for important cooperation. I also thank Keijo Hämäläinen, Eero Rauhala, Seppo Manninen, Tiina Väänänen, and Mikko Hakala of the Department of Physical Sciences of University of Helsinki; Matti Kaivola of the Department of Engineering Physics and Mathematics, Kyösti Kontturi of the Department of Chemical Technology, and Panu Kuosmanen of the Innovation Centre of Helsinki University of Technology; László Almásy of Budapest Neutron Centre; and Thomas Hase of University of Durham for contribution which indirectly facilitated my work.

I thank Academy of Finland, National Technology Agency (Finland), Department of Physical Sciences of University of Helsinki, and University of Durham and One NorthEast (UK) for the primary financial support. I also thank Finnish Cultural Foundation; Foundation of Technology in Finland; Nordisk Forskerutdanningsacademi (NorFA) and University of Aarhus and Max-lab; Hungarian Academy of Sciences and Budapest Neutron Centre; The Netherlands Organization for Scientific Research (NWO); Spectra Isotope Group and the Collaborative Computational Project for Fibre Diffraction and Non-crystalline Diffraction in UK; as well as French HERCULES organization for excellent opportunities and support. I think highly of the world-leading research training in the use of synchrotron and neutron facilities.

Finally, I thank heart and soul my parents, my sister, and my brother, and all the friends of mine, for unforgettable support.

# Abstract

This thesis concerns fundamental self-organized aspects in π-conjugated polymers. Self-organization is the central issue in nanotechnology of soft condensed matter. The thesis focuses on the design and control of supramolecular hairy-rodlike molecules which are characterized by a thermotropic and preferentially aligned nanoscale structure. The major emphasis is on polypyridine, polyaniline, and polyfluorene. Because of their rodlike chain the formation of supramolecules is nontrivial. The understanding of the structure-property relations of this class of materials is vital in the development of organic high-performance opto-electronic devices. Throughout this work, synchrotron radiation and X-ray diffraction techniques have been extensively used and combined with the photophysical methods.

In the first part, the ways to form hierarchic, highly ordered, and aligned lamellar smectic supramolecules of poly(2,5-pyridinediyl) complexed with dodecylbenzenesulfonic, methanesulfonic or camphorsulfonic acid and pentyl- or hexylresorcinol, octyl gallate, or octyl phenol have been developed and perfected. They have been characterized in the solution, in bulk and – in particular - in aligned films.
Several new phases have been discovered and detailed structural description is given. When side groups are introduced microphase separated phases reveal a regular axial repeat but have different degrees of lateral packing regularity between molecules, varying from crystalline to liquid. Depending on composition they exhibit an order-order and then an order-disorder transition to isotropic phase. Liquid crystallinity allows facile overall alignment and results in the opto-electronic anisotropy as revealed by dichroism and polarized photoluminescence.
In particular, it is shown that the hierarchic supramolecular structure of poly(2,5-pyridinediyl), camphorsulfonic acid and octyl phenol comprises of a higher level head-to-head structure of polymer and lower lamellae, stacked, and monomer related structure levels in normal, equatorial, and meridional directions, respectively. By choosing the exact components and tuning the composition a coherence length as high as 800 Å along the smectic axis has been achieved. By contrast to covalent side chains, the supramolecular side chains can be cleaved from the aligned materials, which render aligned pristine polymer and high photoluminescence quantum yield of pure polymer.
The structure and phase equilibria have been designed between theory and experiment. The compilation of the results has been presented as a phase diagram in the melt state in the high polymer fraction limit. The study shows that the recent theoretical model highlights the most important mechanisms responsible for the observed phenomena and gives trends in which direction the developed system has to be adjusted to achieve the desired effects.

In the second part, the thickness dependent triaxial texturing in poly(9,9-bis(2-ethylhexyl)-fluorene-2,7-diyl) thin film on the rubbed polyimide has been identified, when thermotropic alignment has been applied. The polymer is 5/2 helix as proposed by Lieser and coworkers. It has three chain unit cell and the hexagonal-like cells of helical polymers are flattened in the direction of the surface normal and reveal two kinds of coexistent crystallites, a multiple orientation, where the greater proportion of the crystallites have a crystal axis **a** perpendicular to the substrate surface and where a smaller proportion is aligned with the crystal axis **a** parallel to the surface. This has been found to depend on the temperature and the film thickness.

The overview shows a selection of unpublished results, reviews the trends in the supramolecular science discusses and reviews widely the characterization methods. In addition, a selection of further clarifications of the publications is reported. An unambigous experiment showing a hexagonal (cylindrical) supramolecular hairy-rodlike structure of polyaniline complexed with camphorsulfonic acid and hexylresorcinol is presented. A comb-shaped supramolecule of poly(4-vinylpyridine) complexed with methanesulfonic acid and octyl gallate is found to form a white lamellar self-organized structure. Characteristics in the fluid state are discussed.

# List of Publications

This thesis consists of a review and the following peer reviewed scientific publications. The articles are referred to by Roman numerals throughout the text. The review section introduces the main ideas of the field and provides necessary background for the publications. It is written assuming the reader to be familiar with the listed articles, so their content has not been directly repeated. An assortment of further clarifications and unpublished results is embedded.

**I** M. Knaapila, J. Ruokolainen, M. Torkkeli, R. Serimaa, L. Horsburgh, A. P. Monkman, W. Bras, G. ten Brinke, and O. Ikkala
*Self-Organized Supramolecules of Poly(2,5-pyridinediyl)*
**SYNTHETIC METALS**, **2001**, 121 (1-3), 1257-1258.

**II** M. Knaapila, M. Torkkeli, T. Mäkelä, L. Horsburgh, K. Lindfors, R. Serimaa, M. Kaivola, A. P. Monkman, G. ten Brinke, and O. Ikkala
*Self-Organization of Nitrogen-Containing Polymeric Supramolecules in Thin Films*
**MATERIALS RESEARCH SOCIETY SYMPOSIUM PROCEEDINGS**, **2001**, 660, JJ5.21/1-JJ5.21/6.

**III** M. Knaapila, O. Ikkala, M. Torkkeli, K. Jokela, R. Serimaa, I. P. Dolbnya, W. Bras, G. ten Brinke, L. E. Horsburgh, L-O. Pålsson, and A. P. Monkman
*Polarized Luminescence from Self-Assembled, Aligned, and Cleaved Supramolecules of Highly Ordered Rodlike Polymers*
**APPLIED PHYSICS LETTERS**, **2002**, 81 (8), 1489-1491.

**IV** M. Knaapila, M. Torkkeli, L-O. Pålsson, L. E. Horsburgh, K. Jokela, I. P. Dolbnya, W. Bras, R. Serimaa, G. ten Brinke, A. P. Monkman, and O. Ikkala
*Self-Assembled, Aligned, and Cleaved Supramolecules of Poly(2,5-pyridinediyl)*
**MATERIALS RESEARCH SOCIETY SYMPOSIUM PROCEEDINGS**, **2002**, 725, 237-242.

**V** M. Knaapila, M. Torkkeli, K. Jokela, K. Kisko, L. E. Horsburgh, L-O. Pålsson, O. H. Seeck, I. P. Dolbnya, W. Bras, G. ten Brinke, A. P. Monkman, O. Ikkala, and R. Serimaa
*Diffraction Analysis of Highly Ordered Smectic Supramolecules of Conjugated Rodlike Polymers*
**JOURNAL OF APPLIED CRYSTALLOGRAPHY**, **2003**, 36 (3, Pt. 1), 702-707.

**VI** M. Knaapila, B. P. Lyons, K. Kisko, J. P. Foreman, U. Vainio, M. Mihaylova, O. H. Seeck, L-O. Pålsson, R. Serimaa, M. Torkkeli, and A. P. Monkman
*X-ray Diffraction Studies of Multiple Orientation of Poly(9,9-bis(2-ethylhexyl)-fluorene-2,7-diyl) Thin Films*
**JOURNAL OF PHYSICAL CHEMISTRY B**, **2003**, 107 (45), 12425-12430.

**VII** M. Knaapila, R. Stepanyan, L. E. Horsburgh, A. P. Monkman, R. Serimaa, O. Ikkala, A. Subbotin, M. Torkkeli, and G. ten Brinke
*Structure and Phase Equilibria of Polyelectrolytic Hairy-Rod Supramolecules in the Melt State*
**JOURNAL OF PHYSICAL CHEMISTRY B**, **2003**, 107 (51), 14199-14203.

# Author's contribution

The author has substantially contributed to all the research in papers **I-VII**. He has taken the primary responsibility for all the writing in all the papers **I-VII** and made or crucially co-participated in all the work except the molecular mechanics modeling of paper **VII**. He has made or crucially participated in all the experiments, analysis, and conclusions. In particular, he has optimized ways to form self-assembled nanostructures and complexes using the conjugated polymer polypyridine, discovered their head-to-head hierarchy and the first hexagonal phase of polyaniline, and made new X-ray measurements of polyfluorene. He has solely made the materials experiments in Helsinki University of Technology (papers **I**, **II**, and **VII**) and made or participated in the materials experiments in University of Durham (papers **III-VI**). He has made or participated in the presented X-ray diffraction measurements in University of Helsinki (papers **II-V**, and **VII**), in BM26 of European Synchrotron Radiation Facility (papers **I**, **III-V**), and in W1.1 of Hamburger Synchrotronstrahlungslabor (papers **V** and **VI**), and optical and quantum yield measurements of aligned and/or cleaved materials in University of Durham (papers **III**, **IV**, and **VI**). The optical microscopy figure in the paper **VII** he made in Helsinki University of Technology. The theory discussion (paper **VII**) he has made in close collaboration with Polymer Physics Group of University of Groningen. He primarily wrote the text behind **Appedix**.
An assortment of the results are being patented and all the results have been presented by the author at numerous international conferences in the fields of materials science, physics, chemistry, and X-ray diffraction. Alongside this work the author contributed strongly in the numerous other publications[1] which directly relate to this thesis.

[1] See, for instance,
ADVANCED MATERIALS, **1999**, 11, 1206.
MACROMOLECULES, **2000**, 33, 8671.
SYNTHETIC METALS, **2001**, 121, 1277.
MACROMOLECULES, **2001**, 34, 4917.
POLYMER PREPRINTS, **2002**, 43, 550.
FINNISH PATENT APPLICATION 20020615, 46 PAGES, MARCH 28, **2002**
MACROMOLECULES, **2003**, 36, 3758.
JOURNAL OF APPLIED CRYSTALLOGRAPHY, **2003**, 36, 499.
PCT INTERNATIONAL APPLICATION WO03/082948, 52 PAGES, MARCH 28, **2003**
SYNTHETIC METALS, **2003**, 137, 881.
EUROPEAN PHYSICAL JOURNAL E, **2003**, 12, 333.
FIBRE DIFFRACTION REVIEW, **2004**, 12, 74.
JOURNAL OF PHYSICAL CHEMISTRY B, **2004**.
KFKI REPORT SERIES E - SOLID STATE PHYSICS, **2004**.
PROCEEDINGS OF SPIE -THE INTERNATIONAL SOCIETY FOR OPTICAL ENGINEERING, **2004**.

# Content

# 1 Introduction

## 1.1 Nanotechnology of Soft Condensed Matter

The design of self-organized structures[1,2] and understanding of structure-property relationships[3,4] are key issues in the research of π-conjugated polymers[5-7]. The π-conjugated hairy-rodlike polymers[8] and hairy-rodlike supramolecules[9] represent archetypes of self-organization[7,10,11] and supramolecular concepts[12-16]. They employ the ground rules of the supramolecule[17] and liquid crystal (LC)[18] formation. This topic is a part of the basic research of nanotechnology.

In micro- and nanotechnology pattern formation is achieved using lithography, stamping, and related techniques. They allow preparation of electronic devices like single electron transistors, ultra-small tunnel junctions and optics components like nano-scale gratings. Still, there is an increasing technological demand and scientific interest for achieving even smaller structures than the wavelength of the radiation used in today's optical lithography and etching techniques. In organic materials, self-organization allows materials manipulation down to small structures, generally down to a molecular level. Combined with the existent technology, organic compounds and polymers allow options when smaller structures are targeted. Metal-organic nanostructures working as a Coulomb blockade system at room temperature have been demonstrated[19,20], for instance.

Self-organization is a concept where competing interactions within a molecule yield nanoscale structures. Definite nanoscale domains are formed, if different (functional) chemical groups are chemically attached to the same molecule. In supramolecular assembly the functional groups are mutually connected by molecularly matching physical interactions, such as hydrogen bonding, π-stacking, charge transfer, steric match, interlocked structures etc. Such molecular recognition allows building complexes, supermolecules, which, in turn, are able to form self-organized hierarchy of structures. Such concepts imitate the structure formation in biological materials, the structures are relatively easy to construct and they may eventually provide options to construct simple nanostructures at the 'sub –lithographic' level. Until now the usefulness of these techniques in applications of nanotechnology has not been widespread

In nanotechnology metals and inorganic semiconductors are used due to the stability, superior electronic properties, and suitability for the existing processing techniques. The organic materials are applied mostly as lithographic resists. Block-*co*-polymers have been introduced as litographic templates to transfer patterns onto inorganic semiconductor substrates[21] and Langmuir-Blodgett (LB) techniques to achieve ordered layers of resists[22]. Nevertheless, integrated optoelectronic devices[23,24], organic field-effect transistors[10,11,25-27] and flexible circuit boards[23] can be based on macromolecular materials, too. As a rule they utilise π-conjugated polymers[28,29] whose conductivity is explained by formation of spatially localized non-linear excitations. More importantly, these polymers exhibit high luminescence[6,30]. Self-organization is in turn applied to facilitate their macroscopic properties[7,10,11].

The variety of polymers enables versatile functions. As a consequence, electroactive polymers have been demonstrated to yield various functional nanoscale systems. Among others, self-assembled microactuators[31] or multilayers by consecutive adsorption of polyanions and -cations yielding fuzzy nanoassemblies[32] were constructed early. Two metal electrodes can be connected using a single rigid polyelectrolyte[33]. Molecular-based logic gates have been demonstrated, too[34].

## 1.2 A Scientific Idea

This thesis concerns the fundamental properties of self-organized π-conjugated polymers. The key idea has been to study two material classes, hairy-rodlike and supramolecular hairy-rodlike polymers. The facet of these studies - within the bounds of possibility - is multidisciplinary approach and understanding. The work combines the concepts of π-conjugated polymers, supramolecule formation, and thermotropic alignment. Advanced structural studies using synchrotron radiation integrated with photonics measurements have been carried out. Also, the work has been performed alongside the theoretical framework[8,9].

There are several good reasons to study poly(2,5-pyridinediyl) (PPY), polyaniline (PANI), and poly(9,9-bis(2-ethylhexyl)-fluorene-2,7-diyl (PF2/6). They belong to an interesting class of π-conjugated materials in view of both basic research and suggestive applications. They are good prototype materials for physical studies but *yet al.*low options to the decent and relevant supramolecular chemistry. Their properties are discussed in Chapters 2.1.2, 2.1.3, 2.1.4, and 4.2.2.

The purpose of the work with PPY (papers **I-V** and **VII** ), regioregular PPY (rrPPY)[35], the *m*-coupled counter part poly(2,6-pyridinediyl) (PmPy) (paper **V)**, PANI (paper **II**), and poly(4-vinylpyridine) (P4VP) (paper **II**) was to study whether self-organized supramolecular nanostructures of primarily π-conjugated rodlike polymers can be constructed, how they can be dissolved in amphiphilic molecules, how they can be aligned, and how their phase behaviour can be tailored. The purpose was to investigate the properties and to develop tendencies in supramolecular self-assembly but also a hypothetic connection to technological aspects was kept in mind. PPY was selected for a model compound as a primary work horse. Polypyridines are stable with good electron transport quality and high photoluminescence quantum yield (PLQY). Their well-defined structures allow systematic studies. Nevertheless, their processing is nontrivial due to their rigid backbone, a problem which has here been approached by preparing supramolecular complexes of PPY and amphiphilic molecules.

The work with PF2/6 (paper **VI)** is basic research, too. However, PF2/6 belongs to technologically far more promising π-conjugated polymers and it was studied in aligned thin films, in the realistic application environment. PF2/6 is a characteristic hairy-rodlike polymer but in aligned thin films it shows behavior not seen elsewhere. Like hairy-rodlike PPY, stiff PF2/6 is a polymeric LC (PLC). In contrast, PANI shows organization without LC nature.

There is a need to work with these materials and methods. In general, there is a vast tradition related to the self-assembled supramolecules, LCs, and the hairy-rodlike polymers. However, in the case of the rodlike *π-conjugated* high (molecular weight) polymers the background is much more limited, in particular when concerning their LC supramolecule formation. Although the covalent synthesis of the π-conjugated polymers[36] is well-established, there are still relatively few groups, such as Swager[37] and Meijer[38] groups, working with the supramolecular PPY-type polymers. Furthermore, there are few, such as Winokur[2,4], Samuelsen[1,39], or Sirringhaus[7] groups, investigating conjugated polymers using synchrotron radiation.

# 2 Self-Organization, Supramolecules, and π-Conjugated Polymers

## 2.1 π-Conjugated Polymers

### 2.1.1 Structural Relation to Electronic Properties of π-Conjugated Polymers

Organic semiconductors like π-conjugated polymers[40], see examples in Figure 2, are electronically[41] and optically[6,30] active. Electronically they differ tremendously from crystalline silicon type semiconductors[42]. They are excitonic but can be oxidatively "doped" yielding polaronic mobile charges or frequency dependent dielectric constant. These polymers have a strong dependence between electronic characteristics and structure of the backbone. Their electronic processes, like photoexcitations (Chapter 4.2), charge transfer upon doping or protonation - sometimes incorrectly called doping - may result in structural relaxations that modify their electronic properties[28,29,43,44]. The dynamics of excitations and their optical activity are coupled with the conformation as well[44,45].

It seems intuitively plausible that any efficient electronic and opto-electronic process in organic semiconductors require a well-ordered structure. In chainlike π-conjugated polymers there are few examples where the real polymeric single crystals exist: Hexanediynediyl based materials were reported initially[46] and polydiacetylenes[47] have aroused interest with supramolecules[48,49]. However, their formation is impractical due to the solid state polymerization and almost all π-conjugated single crystals are oligomers - most commonly oligothiophenes and their derivatives[50]. This absence of single crystals is a general starting point of the current work which instead focuses on the formation and characterization of LC materials. Therefore, we find it important to put some attention on the basic electronic nature of π-conjugated chain from structural point of view. We note that this is just one perspective and there are additional viewpoints which are equally valid but omitted here.

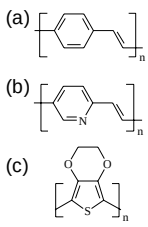


**Figure 2** Chemical structure of some common π-conjugated polymers. **(a)** Poly(*p*-phenylenevinylene) (PPV), **(b)** poly(*p*-pyridylvinylene) (PPyV), and **(c)** poly(3,4-ethylenedioxythiophene) (PEDOT).

Characteristically, 'high' polymers consist of both crystalline, stiff, parts and amorphous domains and therefore, they do not have such exact long-range order as metals and crystalline inorganic semiconductors. This results in the lack of the periodic lattice potential[51] and thus the wave vector $k$ and the band index $n$ (of the periodic Bloch's function) are no longer good quantum numbers. So, the electron states of π-conjugated polymers cannot be described using Bloch functions and the band theory of the crystalline semiconductors is not applicable. Hence, π-conjugated polymers, despite their order, must be treated as amorphous semiconductors. When comparing them to the inorganic semiconductors, the electron density function is (still) a valid concept to describe the electronic structure. In amorphous semiconductor, the tails of the conduction and valence bands reach into the forbidden energy gap. Their density is, however, small, which easily results in the localisation of the states even due to a very small structural disorder of the molecule. If the Fermi-level is near the localised states, the material is an insulator, whereas the opposite case leads to the metallic behaviour. Thus, π-conjugated polymers might be treated as 'inorganic' amorphous semiconductors. However, the character of the charge carriers differs completely. In inorganic materials electrons and holes act as charge carriers, whereas in polymers the charge transport is due to spatially localised non-linear excitations, quasiparticles. Some are illustrated in Figure 3a-c.

In a rigid one-dimensional ideal lattice (say polyacetylene (PA)) the basic cell in reciprocal space (Brillouin zone) is the interval $-\pi/a<k<\pi/a$ where $a$ is the lattice constant. In a π-conjugated lattice[2] π-electron density is not uniformly distributed but is higher in π-bonds than in σ-bonds. Because the electron-lattice interaction is strong compared with the electron-electron interaction, the bond-distances do not remain the same but the lattice is altered so that every second bond becomes shorter. This periodic distrotion of the chain, Peierls distortion, commensurate with the undimerized original lattice reduces the Brillouin zone to $-\pi/na<k<\pi/na$ where $n$ is the number of atoms in the new cell, in simple case $n=2$, see Figure 3d.

[2] This ideal lattice may be discussed using band approach, albeit this is not generally true for conjugated polymers.

Therefore, the edge of the first Brillouin's zone moves towards the Γ-point[3]. This opens the forbidden energy gap on the edge of the new Brillouin's zone and leads thus to semiconducting character of PA. Moreover, in real materials there are relatively strong electron-electron interactions. This means that the electrons can be shifted with respect to the atoms. Also, there are always defects, either spontaneous or intensional (because of doping of intramolecular electronic rearrangement due to protonation of electrochemical doping (voltage pulse) or photogeneration), making the situation exceedingly complex.

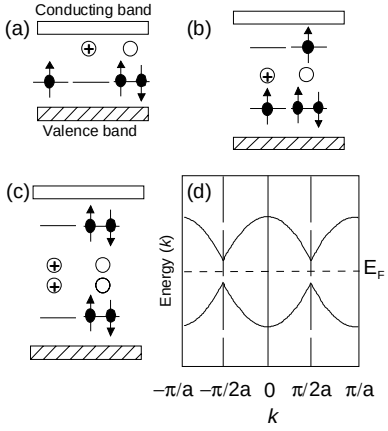


**Figure 3** Energy levels of charge carriers in π-conjugated conducting polymers within the energy gap. Adapted from ref. 29. **(a)** Energy states of the neutral, positive and negative soliton. **(b)** Energy states of the positive and negative charged polaron. **(c)** Energy states of positive or negative bipolaron. A neutral bipolaron does not exist. **(d)** Ideal band structure of the one-dimensional electronic system (lattice) after Peierls distortion.

The *chemical* electron transfer reactions, oxidation and reduction in π-conjugated polymers are termed *n*- and *p*-doping respectively. In practice, the *n*-doping is made by alkali metals in which charge is donated to the polymer, whilst in *p*-doping very electronegative compounds, such as iodine, in which charge is withdrawn from the polymer, are introduced. These concepts are somewhat similar to the corresponding doping concepts of inorganic semiconductors but definitely *not* equivalent: The doping in an inorganic semiconductor means that several atoms in the lattice are replaced by heteroatoms. These sites are virtually electroneutral until they dissociate into free charge carriers and ionised heteroatoms. The doping of π-conjugated polymer means in turn charge transfer of the polymer backbone associated with the insertion of a corresponding number of counter ions into the interstitial spaces. The ion stays near the chain due to Coulombic interaction. The whole system, *i.e.* electron (or hole) and induced lattice polarisation, act as a charge carrier. These objects can further carry either charge or spin or both. Such objects are conveniently regarded as electronic states within the forbidden energy gap, see Figure 3. *E.g.* a soliton may consist of an unbound electron in the gap. We note that the interchain movement of these nonlinear spatially localised excitations can be explained only in a highly nontrivial way. Electrons can tunnel but the transport of the corresponding deformation, the lattice polarisation is the subject which is postponed here.

The structural effects induced by the acid molecules in papers **I-V** and **VII** may be discussed alongside those induced by the dopants. However, it is important to note that, unlike dopants, they maintain the electronic structure of PPY backbone essentially intact. In general, doping of π-conjugated polymers often decreases the degree of crystallinity[52]. It seems plausible that intercalates reduce the order. However, molecularly matching ones can also *improve* it, or lead to completely new structure. Generally speaking, *n*-doping is accompanied with the extension of chain in meridional direction while *p*-doping causes the reduction along the molecular axis (**c** axis)[2]. In contrast, in equatorial direction the doping results in a decrease of the coherence length[2]. Rather complicated further structural effects have been found in *e.g.* K-doped trans-polyacetylenes or in Cs-doped PPV[53]. In self-organized hairy-rodlike polymers (Chapter 2.2.8), like in iodine doped PATs[54-56], the structural variations due to doping are still more complex. The spacing in normal direction is related to the doping but only minimal changes along **b** axis have been found, which loosely relates the observations for CSA protonated (not strictly doped) PPY in paper **V** where the stacking period and the coherence length have been found to be rather independent on the nominal "degree" of protonation within the studied limits while *h*00 reflections change position considerably.

Besides achieving the well-ordered materials, the rodlike conformation related to the π-conjugation, is another aspect of the thesis. Infinite conjugation length results in charge delocalisation, a resonance[57] structure of the whole chain or at least long parts of it. This allows essentially more free charge transport than corresponding coil-like polymer. The π-electron delocalisation itself increases chain stiffening.

Note also that the chains have a finite length and polydispersity. In addition, defects may act as barrier for the charge carriers. In PA, geometrical defects are formed as a result of the changes in the conjugation order[29]. However, polymers consisting of *p*-coupled phenylene groups represent other kinds of defects,

[3] The positions in the Wigner-Seitz primitive cell of the reciprocal lattice (*i.e.* the first Brillouin's zone) are defined so that the Γ-point corresponds to the zero value of the wave vector *k*.

because consequtive rings may be twisted which leads to another type of 'geometric' disorder. In a framework of this thesis, conformation can be planarized using *e.g.* hydrogen bonds between covalently bound side groups[38] or crystalline effects[58] leading to the longer effective conjugation structure which may result in better charge transport. For example, 14 carbon units are needed for a soliton in a trans-PA and about four fully conjugated rings suffice for a polaron or a bipolaron in poly(*p*-phenylene) or polypyrrole. The supramolecule formation might offer a way to influence this ring rotation (*cf.* Chapter 4).

The conductivity of the conducting polymers is anisotropic, a function of the direction of the lattice and not a scalar but a tensor quantity. After alignment this is a macroscopic phenomenon, conveniently studied as AC- and DC-conductivity. The AC-conductivity of the π-conjugated polymers is connected with the electron states that are not lying very near the Fermi-level and depends on the homogeneity of the materials disorder. In contrast, the DC-conductivity of π-conjugated conducting polymers is connected with the electron states near the Fermi-level[28]. These electrons essentially cause the (electronic) conductivity of the polymers. If they are localised, the dominating conducting mechanism is a thermally activated tunnelling between the states whose wavefunctions partially overlap. The energy needed to lift the electron from the occupied state below the Fermi-level to an unoccupied state above the Fermi-level mainly originates from the lattice vibrations. This is denoted as a hopping mechanism. The increasing temperature results in growing energies of the phonons and thus increasing conductivity. This temperature dependence is opposite to one in metals, where the stronger lattice vibrations cause the scattering of the electrons. It is not the same as in the conventional semiconductors either. In polymers, the localised states are randomly distributed, which results in a continuous spectrum of the activation energy. In addition, the tunnelling probability decreases exponentially as a function of distance between the states. When these factors excluding the electron-electron interaction are taken into account, the macroscopic conductivity of the three-dimensional polymeric conductors obeys Mott's formula for the variable range hopping[28,59,60] given as

$$\sigma = \sigma_o \exp\left(-\left(\frac{T_o}{T}\right)^{\frac{1}{4}}\right) \qquad (2.1.1)$$

where $\sigma$ is the conductivity and the $T$ temperature. The interpretation of the other parameters is not straightforward. For polymers they are treated as fitting parameters only. This formula is valid only at a limited temperature range. Conductivity interpolated into zero temperature should differ from zero for a 'metallic-like' polymer. The situation is different if the material consist of randomly distributed metallic and insulating domains and conductivity depends on both of the temperature and the size of the domains. The conductivity of the specimen is in turn a combination of the conductivity of the metallic domains and that due to electron hopping. The latter one is often much lower and determine the macroscopic behaviour.

The transitions in the supramolecular ordering might have possible connections with the metal-insulator transitions. These phenomena are in detail, however, very complicated and beyond this work. Nevertheless, the following general features are pointed out. The conductivity of the π-conjugated conducting polymers depends on the position of the Fermi-level. In the metal-insulator transition it moves through the edge between the localised and delocalised states. In polymeric materials, this transition belongs to the Anderson type being due to the structural disorder. This disorder results in the differences in the energies of the electron states between the lattice sites. If these differences are smaller than the size of the band that corresponds to the density of the electron states, the electrons are mobile between the sites. In the opposite case, they are not able to move and the states become localised. Transitions between these conductivity states are independent on the electron-electron interactions. When dealing with the conductivity between the chains, there might be also Mott type transition. Here the electrons interact with each others and their states can be localised without structural disorder. This happens, if the size of the band decreases below the value of the energy that is needed to move an electron between the lattice sites.

Finally note that the studied supramolecules belong to the *ionically* conducting materials. Ionic conductors are completely different and consist of electrolyte solutions, melts of the salts, or solid electrolytes. In contrast to the crystalline materials and the fluidlike ionic conductors, the solid electrolytes, whether organic or not, contain relatively mobile ions in the solid state. Ion conducting polymeric systems[61,62] are considered to be a random mixture of conductive islands, ions or ionomers or polyelectrolytes, sometimes interconnected by an essentially non-conductive polymer matrix. These systems contain typically more or less free protons whose tunnelling or small ions whose migration between species can occur when they are favourably oriented. The crystalline and chemical environments and especially temperature affect the conductivity of ionically conducting polymeric systems. Amorphous polymers are usually better ionic conductors than crystalline ones, providing more mobility for protons or small ions.

## 2.1.2 Poly(2,5-pyridinediyl)

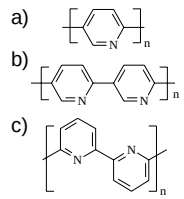


Polypyridines, PPY[35,39,58,63-109][CAS# 67987-55-7], PmPy, and rrPPY, have been comprehensively studied in papers **I-V**, and **VII**. The chemical structures are shown in Figure 4. The polymerization of PPY[69,91] and PmPy[91] and the detailed synthesis of their monomers[68] are well-described and resemble the dehalogenation polycondensation of PPP[110] or PFs[111]. Instead, the preparation of rrPPY is based on 2-bromo-5-iodopyridine and organomagnesium and -nickel chemistry[35].

**Figure 4 (a)** Poly(2,5-pyridinediyl) comprising random mixture of *p*-coupled pyridine units (PPY). **(b)** rrPPY, and **(c)** poly(2,6-pyridinediyl) (PmPy).

Most interestingly, PPY and poly(2,2'-bipyridine-5,5'-diyl) (PBPy) are among the simplest π-conjugated stiff polymers able to form strong physical bonds and thus stable supramolecular structures. Therefore PPY is well suited for the basic research of supramolecular hairy-rodlike polymers. PPY has also a role in the applied research of light emitting diodes (LED)s[78,84,100,104,112]. Photophysical properties of PPY are well-known[108] but in general PPY is not immensely studied. To date there are only around 100 articles dealing with PPY or PBPy[66-69,73,110], their copolymers[37], supramolecular derivatives[37,38], their derivatives containing various bridges[113], or other variations[77] or their protonation[87,95,114,115]. In contrast, there is a large tradition in coordination complexes of pyridine oligomers[116,117] and smaller for polymers[37,118,119].

In comparison to PPP which is practically insoluble except in very strong acids, PPY due to the heteroatom, can be dissolved in formic acid, strong inorganic acids, and *1,1,1,3,3,3*-hexafluoro-*2*-propanol (HFIP). Formic acid can be completely evaporated[120] which was shown using FTIR[121] and it does not protonate PPY, which is important for supramolecule formation. The stronger acids, such as methanesulfonic acid (MSA)[121] or chloroacetic acid cannot be completely evaporated or this is very difficult and they are not chemically inert towards the amphiphiles at all. HFIP provides a good solvent but it is toxic and therefore avoided. Formic acid has been used throughout the papers **I-V**, and **VII**.

Polypyridines can also be protonated with MSA (paper **I** and **VII**) and with CSA[87] to yield PPY(CSA)$_x$ (papers **I-V**). Unlike in PANI (Chapter 2.1.3), doping PPY by CSA does not give rise to conductivity but changes in photophysical properties. Nonetheless, one motivation for work was to learn from analogies of the behaviour of PANI and *vice versa*. PPY can also be protonated by amphiphilic dodecylbenzenesulfonic acid (DBSA) (paper **I**). The DBSA side chains substantially improve the solubility of PPY[95] and it is quite obvious that DBSA leads to the self-assembly and plasticization. Unsurprisingly, recalling the previous studies of intercalates[55,122], bulky CSA alone, too, results in a lamellar structure. This is, however, rather brittle (for small *x*) and less organized than the further complex of PPY(CSA)$_x$ with amphiphiles (paper **V**). Finally note that the removal of the side groups, the cleavage, (papers **III-V**) has been shown using FTIR[123]. See also **Appendix** and ref. 124.

## 2.1.3 Polyaniline

Polyaniline (PANI) is studied in paper **II**. PANI[125,126] (Figure 5) including high molecular weight PANI[127,128] used here are old materials but remain still among the most studied inexpensive conductive polymers. There is an interest in conductive PANI fibres[129-133], for instance. The solubility properties of PANI resemble those of PPY but the solublity in formic acid is nontrivial, if the molecular weight is also high.

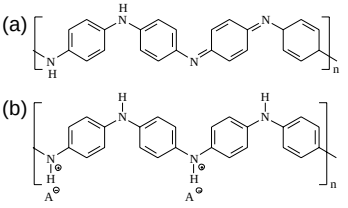


**Figure 5** Polyaniline (PANI): **(a)** Emeraldine base (EB). **(b)** Protonated form, emeraldine salt.

Whilst PPY and PF2/6 consist of identical monomer units, PANI has aromatic rings linked with imine or amine nitrogens so consisting alternating amine and imine parts, ([(-$C_6H_4$-NH-$C_6H_4$-NH-)$_{1-x}$][-$C_6H_4$-N=$C_6H_4$=N-)$_x$])$_n$, where $x$=0, 0.5, or 1.0. These forms are called leucoemeraldine, emeraldine or pernigraniline, respectively. The imine can be protonated using acid-base chemistry and the protonation qualitatively consolidates the present PPY and PANI investigations. However, PANI differs significantly from PPY, and of course from PF2/6, and makes that especially in two ways which focus of interest here.

Firstly, in contrast to the conventional doping, as is well known, PANI is conveniently "doped" by protonation yielding high conductivity. Sulfonic acids, especially CSA and 2-acryloamido-2-methyl-1-propanesulfonic acid (AMPSA) are very suitable for that. PANI-CSA has an intrinsic metallic nature being conductive at normal conditions. The protonation by dodecylbenzenesulfinic acid (DBSA) to form self-

assembled PANI(DBSA)[2] is widely known and has a connection to the PPY(DBSA) work, see paper **I**. Since DBSA is an amphiphilic sulfonic acid (acid form of surfactant) it protonates PANI making it conductive, melt processable and allowing blending with other polymers[134]. Any excess DBSA acts naturally as a solvent. When doped very high metallic conductivity is suggested for PANI, if the entire charge carrier density could participate in the charge transport, see MacDiarmid and Epstein [135], but this is speculative. Rather than the environments where high conductivity or mobility are needed, PANI is a good candidate for semielectronic applications just providing light weight conductive material such as mentioned conductive fibres[136], a fact which is also supported by the stability and inexpensive manufacturing.

Secondly, PANI is not as stiff as PPY. It is, however, rigid enough to form lyotropic solutions[137], which in turn forms guidelines for supramolecular self-organization. The protonated, conducting polyaniline salt is more "rigid" polymer, whereas unprotonated form, emeraldine base, is only "semi-rigid". Polyaniline protonated with CSA in *m*-cresol solvent is an example of material where protonated PANI takes such rigid conformation in solution due to π-electron delocalisation and due to counter ion induced steric extension of the chain which over certain critical concentration may result in lyotropic phases[138,139].

Dissolving PANI was long troublesome due to its small mixing entropy, complex chemical behaviour, and poor quality of the polymer. PANI can be dissolved in strong protic acids and in some selective solvents, such as *N*-methylpyrrolidone (NMP), pyrrolidine of tripropylamine. When PANI is doped with camphorsulfonic acid, it becomes soluble in *m*-cresol[138] potentially due to sterical matching of proton transfer, hydrogen bonding and π-stacking[140]. The interaction of *m*-cresol with PANI gives also large enhancements in conductivity due to 'secondary doping'. Here this means the change in molecular conformation of PANI during the process, as *m*-cresol expands doped PANI chains[141]. PANI$(CSA)_{0.5}$ in *m*-cresol is an example of supramolecular conjugated polymers but even with the *m*-cresol attached to PANI$(CSA)_{0.5}$ it does not provide and nonpolar tail and it is not bulky enough to result in the self-assembly. Instead, further complexation with hexyl resorcinol (HRES) leads to the hexagonal structure.

The PANI networks, a kind of prototypes of self-organized structures, protonated by CSA in the insulating matrixes, such as PMMA, have low percolation threshold in solution cast solid films[142]. Below this volume fraction of the conducting species, the percolation threshold, there are no pathways between 'conducting islands' and the charge transport is prevented. The network or fractallike morphology results in electrical conductivity and optical quality of the blend, where the concentration of PANI is low[143](~ 1 wt-%). PANI-CSA(PMMA) exhibits a continuous increase of conductivity and allow processing of films of by codissolving the PANI-CSA and the matrix or melting the blend.

### 2.1.4 Poly(9,9-bis(2-ethylhexyl)-fluorene-2,7-diyl)

Polyfluorene (PF) has been studied in paper **VI**. Compared to PPY and PANI, PFs[111] represent newer π-conjugated materials. PFs are also called laddertype PPPs (LPPP) in reference to their backbone of fused rings comprising embedded PPP moiety. PFs are regarded related to PPY, because both comprise PPP-type base structure which is bridged in PF. However, PFs are almost always equipped with 9,9-substituents and due to the side chains they are soluble in organic solvents such as toluene or chloroform. Unlike PPP, PFs are also less rigid but still rodlike sufficiently to induce a thermotropic nature after side chain substitution. Further, unlike PPY, PFs reveal systematic changes when aging, which should be taken into account[144].

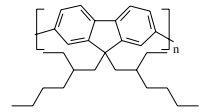

**Figure 6** Poly(9,9-bis (2-ethylhexyl)-fluorene-2,7-diyl) (PF2/6)

Due to their prominent opto-electronic performance (Chapter 4.2.2) poly(9,9-(di-*n*,*n*-octyl)fluorene) (PFO)[10,145-151] (Figure 12, page 21), its copolymers[10,152,153] and PF2/6[111,152,154-157] are of specific interest. Helical PF2/6 (Figure 6) falls well within the purview of this thesis. The structure of PFs have been studied in solid state; PF2/6 in fibres[154], in thin films[149], and in aligned thin films (paper **V**); PFO in fibres[145] and in thin films[151] and their variants in thin film transistors[10,158]. The structure of oligomers[159] and PF2/6 solutions[152] have also been studied.

## 2.2 Self-Organized Supramolecules of π-Conjugated Polymers

### 2.2.1 Physical Bonding

The concept of physical bonding is paramount in the supramolecular self-assembly.

The spatial distribution of valence electrons of individual atoms and their fluctuations affect the spatial electronic distribution of the surrounding atoms, which may lead to the accumulation of the electron density between the nuclei. If the structure where the electron(s) essentially interact with several nuclei is energetically favoured, this results in binding of the atoms due to Coulombic attraction between the charge distributions. This bonding is determined by the degree of the overlap between the electronic wave functions of the atoms involved[57]. Non-directional bonding between highly dissimilar atoms is called ionic while in the covalent bonding the electronic distribution of relatively similar atoms is essentially localized in a certain preferred direction. If the wave functions are distributed over a large distance compared with the atomic separation, the bonding is metallic. Here the packing density of the atoms determines the binding energies. The covalent bonding, connected with the essentially directional valence electrons in molecules, is regarded as a 'chemical interaction'.

*Physical* interactions, instead, are regarded as weak tail contributions of the Coulombic electromagnetic interaction as a consequence of the shape and dynamics of the electron density as well as quantum mechanical character of the molecules and lattices. They are divided in π-π stacking (delocalized electrons), Coulombic forces between charged or multipole species (permanent charges) and van der Waals type interactions arising from atomic dispersion (no permanent charges). They result in physical bonding, such as van der Waals bonding between atoms with closed electron cells or between saturated molecules.

Bonding at hydrogen (papers **I-V**, and **VII**) differs from other bonds since the radius of a bare proton is extremely small and the first ionisation potential is the highest possible and it is difficult to remove an electron completely. Because of only one electron, hydrogen can form only one covalent bond through electron sharing. When taking part in a covalent bond with a strongly electronegative atom, its single electron is almost completely transferred to this atom. The remaining proton exerts an attractive force on a second electronegative atom, which realises the hydrogen bond, if the observed separation of the atoms is smaller than it would be due to dispersion reasons only. The hydrogen bond can be either symmetric A-H-A or non-symmetric A-H…B. The extended electron density of an electronegative atoms and the small size of proton, as well as its strongly reduced electron screening prevent a third atom to be bound to hydrogen. Hydrogen bonds are indicated by the shifts in hydrogen vibrations in infrared region. Hydrogen bonds have multidirectional coordination and possibility to be reversibly controlled.

Self-organized supramolecular architectures are conveniently based on coordination (bonding). Especially, supramolecules of pyridine oligomers and polypyridine modifications are typically based on metal complexes[160]. See an example in Figure 8 on page 18. Organic molecules mainly consist of elements having valence electrons in symmetric *s* and *p* orbitals. Transition metals differ from them. Their bonding electrons behave the same as in lighter elements but their nonbonding valence electrons are *d* electrons. They are divided to the *five d* orbitals becoming stereochemically active, which allows coordination. *E.g.* Pt(II) $4f^{14}5d^{8}6s^{2}$ leads to square, Ni(II) $3d^{8}4s^{2}$ square or tetrahedral, Zn(II) $3d^{10}4s^{2}$, Fe(II) $3d^{6}4s^{2}$ and Fe(III) $3d^{5}4s^{2}$ tetrahedral, and Co(II) $3d^{7}4s^{2}$ square pyramidic coordination polyhedras. The tendencies can be discussed based on valence electron configurations[161]. To see the most stable coordination arrangement requires comparisons with all other possible and hypothetical combinations.

### 2.2.2 Self-Organisation, Self-Assembly, and Microphase Separation

Self-organization and supramolecular concepts have developed for oligomeric and copolymeric as well as LC substances from different background. For this reason, the terminology and tradition differ slightly. Rigid polymers are usually discussed in the context of LCs (Chapter 2.2.4).

Molecules of regular shape form three-dimensionally ordered crystals when the temperature is low enough. If the regularity is broken, or if additional molecules are introduced, the material can still undergo spontaneous aggregation to less ordered intermolecular domains. If this process is energetically favoured, it is denoted as self-organization. It is governed by three principles[160]. First, there is competition between the different interactions and between different molecular sequences. For supramolecular materials this can also be realised because of a favourable molecular shape and physical bonding combined, *i.e. molecular recognition*. Second factors are entropic frustration and topological dereliction. The 'hilly' free energy space of different arrangements is tuned in such a way that different topological states are attainable. Thirdly,

sequences of domains at the different length can be formed spontaneously. These phenomenological principles result in the examples discussed in all the papers **I-VII**.

According to Muthukumar[162] self-organization occurs from microscopic to macroscopic length scales and includes micro phase separation, mesophase formation, and also adsorption, crystallization etc. Essentially the same phenomenon has also been called self-assembly in such a way that a slightly different meaning has been reserved for the self-organization. The definitions vary from author to author. Within this definition, the terms "organization" and "assembly" overlap totally or partially.

According to Lehn[160], the self-assembly concerns the whole evolution of the formation of discrete or extended entities (*e.g.* films or membranes) under all kinds of bonding. Within this terminology, the *supramolecular* self-assembly is regarded as recognition directed strategy for either discrete or extended well-defined arrangements of the limited number of molecular species. Hence, the supramolecular self-assembled moieties are *always* based on supermolecules that are associated by molecular recognition. Such arrangements are due to spontaneous association under the intermolecular control of the non-covalent interactions only. Instead, the ordering covering only multicomponent non-covalent interactions within *structural* and *dynamic* order is called 'self-organisation'. It means that the self-organised system achieve order in space or time or both and can be at equilibrium or at nonequilibrium and exhibit both interactions between parts and integration between the interactions. The broader term 'self-assembly', is often used almost as a synonym to 'self-organisation' and they are discussed loosely and more or less simultaneously keeping in mind that they are not exactly defined.

According to Stepanyan[8,9] self-organization, that is self-organized structure formation can be described in classical statistical mechanics as an interplay between unfavorable repulsive net-interactions (originally due to the even somewhat different electron density distributions) and stretching of the flexible parts of the macromolecule, which result in the microphase separation. This is summarized in paper **VII**.

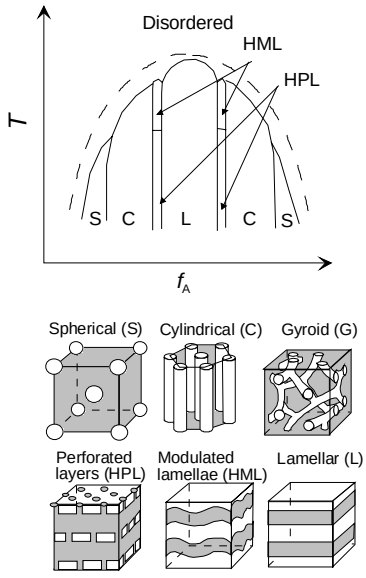


**Figure 7** The microphase separation, morphologies, and corresponding phase diagram in a diblock copolymer A-block-B. *T* equals temperature and *f* equals the macroscopic volume of another block. The segregation degree characterises the organisation. These pictures correspond to the strong segregation limit that is realised by long chains and strong block interaction, inversely proportional to temperature, and that results in sharply microphase separated domains. The gyroid phase is not stable[163].

Self-organization is illustrated by asymmetric materials with multiple length scales. Examples of such materials are *e.g.* different kinds of block-*co*-polymers[164] and other multidomain macromolecules[165] which are polymeric counterparts to surfactants. They contain long blocks of mutually repulsive polymer chains which are covalently connected. These polymers form self-organised, or according to terminology in the block-*co*-polymer literature, *microphase separated* structures in bulk and in many solutions due to the differences in polarity between the domains[163,164,166]. In addition to flexible polymers, there are numerous examples of self-organized rod-coils[167-170]. Block-*co*-polymers are conceptually among the most important self-organized systems which are not based on the supramolecular construction[163,166,171].

At equilibrium the minimum free energy conformations of the amorphous block-*co*-polymers can result either in the disordered state or in the microphase separation, termed *segregation*. This, combined with the small entropy of mixing, for which reason most polymer mixtures tend to phase separate, gives tendency for phase separation between the blocks. Now the *macrophase separation* is, however, prevented due to the covalent linkage. The phase behaviour of undiluted, bulk, $(A\text{-}B)_n$ type copolymer can be controlled by the overall degree of polymerisation *N* and the architectural constraint, *i.e.* by the entropic factors and by the temperature. The copolymer architecture is determined by the number of the block junctions *n* and the composition *i.e.* the overall volume fraction *f* of the first component, say A. The interaction of the distinct blocks arising from their different polarities is in turn characterised by the (energy) parameter $\chi \sim \alpha T^{-1} + \beta$, that is by the enthalpic factors. Here $\alpha > 0$, $\beta$ are constants for *n* and *f*. This, an archetype of self-organization, is illustrated for diblock copolymers, *i.e.* for the case $n=1$, in Figure 7. See also paper **VI**.

## 2.2.3 Supramolecules of Macromolecules

Hierarchical structures of molecules beyond the molecular size, based on synergistic intermolecular interactions without covalent bonds, are called *supramolecular* [17,160,172]. These structures are typical in macromolecular and particularly in multiprotein systems that allow several sites for specific interactions. *Super*molecular chemistry concerns the specific chemistry of supermolecules, well defined discrete oligomolecular species arising from intermolecular association of a few components. *Supra*molecular chemistry includes the chemistry of all kind of supramolecular entities; not only the supermolecules themselves but also supramolecular assemblies, that is polymolecular architectures having multiple length scales. The facet of supramolecular chemistry lies on the idea of the conceptual limits of synthetic chemistry in the convenient preparation of complicated hierarchic structures. *Cf.* the discussion on the present work in Chapter 2.2.8.

The supramolecular architectures are mainly but *not always* constructed by self-organisation. *E.g* polycatenane supermolecules, macrocyclic compounds linked by mechanical bonds, can be synthesized chemically. After this polycatenates can be further self-organized[173]. On the other hand, the self-assembled structures could also be realised because of the non-covalent *intra*molecular interactions.

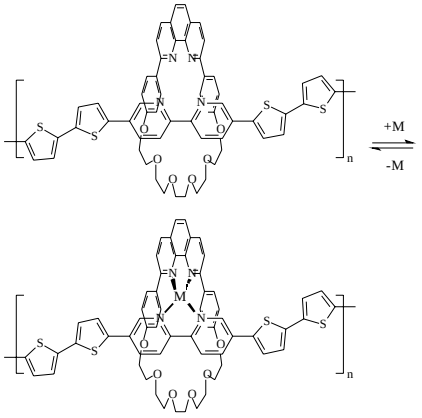


**Figure 8** An archetype of a *functional* supramolecule comprising π-conjugated rodlike polymer. A conductive polymetallorotaxane consists of a polymer, macrocyclic molecule, and a metal cation. The constituents 'molecularly' recognize each other based on the steric match and charge combined. So the physical bond is not based on the binding alone. The cation is reversibly bound or unbound depending on the electrochemical environment, 'initial function' and this is seen as a change of color, 'response function'. Adapted from ref. 37.

The supramolecular structures require molecularly matching interactions, *molecular recognition*. Bare binding of molecules does not fulfill this demand. Molecular recognition and supramolecular catalysis connected with the molecular transport properties form the fundamental functional features of the supramolecular chemistry. Molecular recognition, which is followed by molecular transformation and translocation, is a prerequisite for the supramolecular self-organisation. It is defined by the energy and the information involved in the binding and selection of the parts of the supermolecules, denoted as substrate(s) and receptor(s). The concept concerns all kinds of receptors, whether they are charged or not. It occurs in homogeneous media but it can also take place in the heterogeneous conditions, *i.e.* on phase boundaries. Thus, molecular recognition is characterised by the simultaneous stability of the supermolecule and the selectivity of its entities. If, for instance, a part of the binding energy is used up in the change of molecular formation, the selectivity requirement may not be fulfilled. A classic example of molecular recognition comprising π-conjugated polymer is presented in Figure 8, which shows also an example of functional material. Word for word, *functional* materials, like microactuators[31] reveal a material property realizing "intitial and response function". Functional supramolecules implement this in the intermolecular level. Functional supramolecular systems and procedures are particularly known from the biological machinery, where they reveal enormous complexity.

The present work represents the construction of supramolecular systems, supramolecular *synthesis* but not supramolecular *assistance* to molecular synthesis[17], a second branch of supramolecular chemistry. Another special type of synthetic procedure, the *molecular self-assembly*, is not discussed either. The self-organized inorganic systems, such as self-assembled monolayers (SAMs), typically sulphides onto gold[174], are postponed as well.

Supramolecular *polymers*, see Meijer *et al.*[175] refer to the macromolecule where the monomers are bounded in the supramolecular manner, that is to say by molecular recognition. Some authors use this term also as a common name to all supramolecular systems comprising a polymer[176]. According to Meijer's definition, the systems studied in this thesis are *not* supramolecular polymers.

## 2.2.4 Liquid Crystals

Liquid crystals (LCs)[18,137,177-181] are molecular states intermediate between that of crystalline solids and isotropic liquids. By definition, LCs are ordered in one or in two but not in three dimensions. Not only their organisation but also their physical properties are intermediate. For instance, LCs are fluid-like and optically anisotropic at the same time.

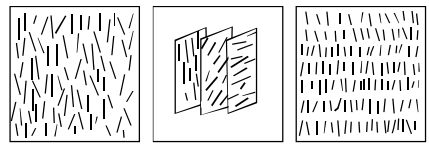


**Figure 9** Schematics of **(a)** nematic, **(b)** cholesteric (chiral nematic), and **(c)** smectic liquid crystals. The structure **(a)** posseses a single direction of preferred orientation and no long range translational order exist. Structure **(b)** has an additional orientational direction twisting along a helix. In addition to local orientational order, structure **(c)** exhibits long range translational order in one or two but not in three dimensions. Adapted from ref. 137.

*Lyotropic* LCPs, introduced in the early 1950s, consist of rigid rodlike polymers in concentrated *solutions*, whereas *thermotropic* LCs are mesophases of the polymers in the *bulk* state[179,180]. The formation of the LC phases is characteristic for the solutions and possible melts of stiff or rodlike polymers as well as for copolymers containing mesogenic fragments. The shape of molecule able to form LC phase can be rodic (1D), discotic (2D), bowlic (3D) or it can be only mass point, hexatic phase (0D) [179,181]. The hexatic phase may not be regarded as LC phase, if it forms three dimensional lattice. The same molecules can naturally consist of several different mesogenic species. The basic forms of 'classical' LCs are illustrated in Figure 9. The formation of lyotropic LCs of the asymmetric particles in solution is not yet evident, because few rigid rodlike polymers are soluble at attainable temperatures. If complete solubility is achieved, the lyotropic phase is however ultimately achieved for concentrations high enough (paper **VII**).

## 2.2.5 Mesomorphic Materials

Alongside LCs the concept of mesomorphic material[182] is discussed. According to de Gennes and Prost[18] mesomorphism is only a more proper term for LC. Elsewhere, mesomorphism is considered to be the general ability of the individual molecule class to form equilibrium phases intermediate between states equipped with the different degree of ordering, between crystalline state and isotropic fluid[183]. This seems to add to the self-organization concept. There are certain self-organized structures, such as inclusion complexes do not need to exhibit any crystallinity or LC in the solid state and may be called mesomorphic. Thermotropic LCs are always mesomorphic but all mesomorphic macromolecules may *not* be LCs. As an example, spherical phases of block-*co*-polymers contain only one kind of molecule. They can include different crystalline degree between spheres and background and still form a correlation in all three dimensions. A three dimensional lattice would in turn not be included in the definition of LCs. The concepts of partially ordered systems -LCs and mesomorphic materials- are fundamental, albeit there may not be any precise definitions.

## 2.2.6 Rodlike Polymers

There are several classical examples of rodlike polymers, like Kevlar® or Nomex®, or helical poly(γ-benzyl-L-glutamate). See the examples in Figure 11. Characteristically, rodlike polymers are infusible and because of limited mixing entropy their dissolving without further modifications is difficult[18,137,177,184,185]. The concept of uniformly stiff molecule is still an idealisation and all real rodlike polymers exhibit equilibrium flexibility and finite persistence length depending on the chemical structure and/or external conditions. As a rule, π-conjugated polymers include a rigid rodlike and/or worm-like conformation.

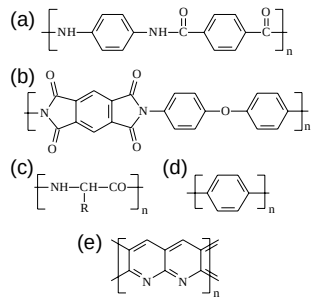


**Figure 10** Rodlike polymers. **(a)** Kevlar®, **(b)** polyimide (PI) (Kapton®), **(c)** poly(γ-benzyl-L-glutamate), **(d)** PPP, and **(e)** pyrolyzed polyacrylonitrile (polypyridinopyridine).

Throughout the present text rigid rodlike polymers will simply be referred to as rigid or rodlike. By contrast, the discussion of the other stiff conformations, such as rigid helix or rigid ladderlike structures is mostly postponed. Helical conformations function as uniaxial rodlike molecules which is typical for chiral polymers[178]. Helical PF2/6 is also denoted "rodlike" in paper **VII**. This is somewhat confusing but the morphology of PF2/6 is apparent from the context. Ladderlike[186] and π-conjugated ladderlike polymers[187] are inherently rigid, too. The rigidity is very strong factor behind the behaviour of these molecules. For instance, it is described elsewhere[188-197] that despite the chemical insimilarity -because of rigidity- the phase behavior of PPY, pyrolyzed polyacrylonitrile (Figure 11e) and paracyanogen[198] coexist.

## 2.2.7 Hairy-Rodlike Polymers

Unlike the most comblike polymers[199], hairy-rodlike polymers[200] consist of rigid backbones equipped with flexible side-chains[201-209]. In supramolecular hairy-rodlike polymer the side chains are connected via physical bonds. These concepts are illustrated in Figure 11.

The hairy rods are classified according to the number of side chains and grafting. *Proper hairy-rodlike polymers* comprise of covalently bonded side chains, high grafting-density of flexible side chains. *Fuzzy rodlike polymers* have low grafting-density or branched flexible side chains and the *bristly rodlike polymers* comprise of fewer flexible side chains with mesogenic parts. This division is somewhat artificial but essentially determines the phase behaviour of hairy rods. There are also several related concepts like *hairy rigid boards*[210].

Flexible comblike polymers tend to microphase separate[185,199] and for hairy-rodlike polymers the tendency for microphase separation is particularly strong[8]. The same is true for supramolecular hairy rods[9] where macrophase separation makes the phase behavior more complicated. Microphase separation of hairy rods is driven by the general materials tendency to fill space uniformly, which results in periodic structures. These domains tend to minimize their interfacial area, which increases the size of these structures. On the other hand they tend to minimize the chain stretching, which in turn decreases the size of the domains. Also the composition dependent tendency to spontaneous curvature ought to be considered (*Cf.* paper **VII**).

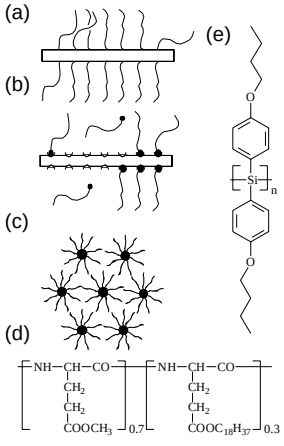


**Figure 11** Hairy-rodlike polymers. **(a)** Hairy-rodlike polymer. **(b)** Supramolecular hairy-rodlike polymer. **(c)** An example of self-organized (microphase separated) domain shown end on. Adapted from paper **VII**. **(d)** Copoly(glutamate), adapted from ref. 209. **(e)** Polysilane with bis(butoxyphenyl) substituent, adapted from ref. 200.

Hairy rods are characteristically LCs[200] and they form layered mesophases[203]. Polyglutamates, aromatic polyesters or polyamides are typical examples of hairy rod backbones embedded in high-density side chains capable of intermolecular interaction. They are mainly LCs above the melting point of the side chains. In contrast to bare rodlike polymers, they also reveal order-disorder transition (ODT) into a disordered phase upon heating. Near the ODT the fluctuations are large and the density coupling related to the orientation process dominant. This fact is applied in papers **III-VI**.

Besides hairy rods with a carbon backbone, phthalocyanito-polysiloxanes or -polygermoxanes with unsymmetrical short and long alkyl chain substitutions. See an example in Figure 11. Hemiporphyrazine-polygermoxans are typical fuzzy rods (Figure 12 in Chapter 2.2.8 on page 21) where the side chain crystallization is prevented by branched chains or partial substitution with long alkyl chains. It is also possible to attach polysiloxane side chains to the rigid aromatic skeleton[211]. Moreover, besides usual synthetic hairy rods, cellulose derivatives, such as cellulose ethers and cellulose and amylose esters, are regarded as fuzzy rods due to the stiffness and hydrophilic sites of cellulose.

The assemblies of the hairy rods are conveniently further manipulated by Langmuir-Blodgett (LB) and related techniques[209] where pinholes and channels are ultimately prevented. Polysiloxanes provide particularly homogeneous and stable LB films and hemiporphyrazines also a biaxial orientation in the film. They have NLO activity and *e.g.* polysilanes with branched alkyl side chains or side chains consisting of alkoxyaryl groups offer fuzzy rods with NLO character due to delocalized σ-orbitals of Si.

## 2.2.8 Hairy-Rodlike π-Conjugated Polymers

Side chains are routinely used to modify the solubility and tractability of π-conjugated polymers to achieve self-organized structures and LCs. Upon substitution the solubility or melting temperature depression may be achieved without loss of rigidity of the backbone: PPP type hairy rods that form an analogy to PPY have worm-like conformation in both concentrated[212-215] or dilute solutions[216]. PF2/6[152] reflects the same.

The early types of π-conjugated hairy-rodlike polymers are based on PPP, PANI[217] or PATs[218,219] or combinations of phenyl rings and unsaturated chains[220] and were prepared quite same time ago. Instead, 9,9-disubstituted PFs, like PFO are of more recent interest. There are also some hairy-rodlike PPY analogies, like ladderlike PPY[38,88]. See these examples in Figure 12.

PATs[1,2,10,221] form the best studied prototype of a self-organized π-conjugated hairy-rodlike polymer. There are numerous up-to-date reports on their synthesis[222], general photophysics and PLQY[223], alignment and consecutive linear polarization[224,225], circular dichroism and circular polarization[226], on the structural details behind that[227], detailed description of the interchain interactions[228], and their self-organization[1,54-56,218,229-237]. Oligothiophenes[50] and derivatisized PTs like PEDOT[238] (Figure 2) have a particular role as charge transfer materials in organic electronics. There are numerous variants of PTs, like end-functionalized by dendrons[239], bent LCs[240], poly(3-thienylmethylacrylate) [241], or supramolecular complexes with oligopyridines[37] to mention a few.

Because of π-conjugated backbone, the sidegroups affect not only solubility and structure but also the electronic behaviour. An archetype is PANI equipped with covalently bonded sulphonic acid containing sidegroups leading to 'self-doping'. The side groups of π-conjugated backbone result generally in thermo- and solvatochroism as well as thermotropic and lyotropic character and self-organization. All this has been seen earlier in PATs[229-231]. Further, the specific alkyl, alkoxy, or phenylalkyl side groups have significant effects on the photophysical properties of π-conjugated hairyrods, such as PATs[223].

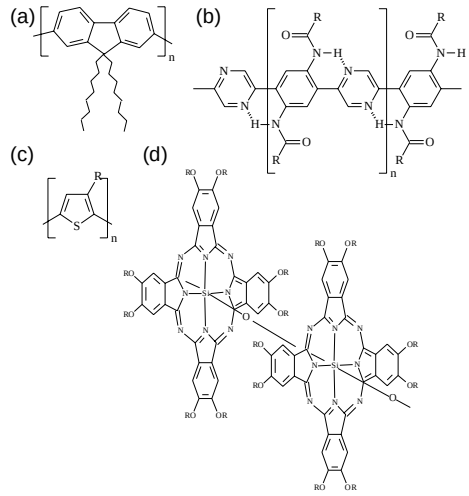


**Figure 12** Hairy-rodlike π-conjugated polymers: **(a)** Poly(9,9-dioctylfluorene) (PFO). **(b)** Ladderlike PPY analogy. Adapted from ref. 38. **(c)** Poly(*3*-alkylthiophene) (PAT). **(d)** Phthalocyanitopolysiloxane (*Cf.* Chapter 2.2.9)

Paper **VI** deals with one π-conjugated covalent hairy-rodlike polymer. In many respects, they resemble the supramolecular hairy-rodlike polymers studied in papers **I-V** and **VII**. However, in the current work, the covalent side groups (paper **VI**) belong to the archetypes, branched long alkyl chains. In contrast, the supramolecular side chains used in this work (papers **I-V**, and **VII**) are very short and therefore the supramolecules may *not* be completely described in the terms of prototype hairyrods. This is discussed in theoretical part of the paper **VII**.

One important motive of supramolecular chemistry is to build systems almost or completely inaccessible through covalent synthesis. Of course, the present work does not aim at the preparation of complicated systems just for the sake of complexity but to outline general tendencies. Also, the idea of the limits of covalent chemistry refers to very complex materials like interlocked molecular machines[17,242-244].

There are examples of covalent hairyrods made of PPY[69] or PANI[245]. These covalent analogies are not structurally much studied and not studied here either. Instead, it turned out that the structure of PATs provides very good analogy to work which has been made here. The structure and phase behavior of P3HT has been characterized at length using XRD as early as 1989 by Winokur *et al.*[229] and later in thin films by Sirringhaus[7], and Aasmundtveit *et al.*[235]. The general PLC phase behaviour was studied by Tashiro *et al.*[230,231] already in 1991. An interesting and important result in papers **I-V**, and **VII** is that the self-organized PLC structure of PATs, especially P3HT[2,7,229,235], has surprisingly similar structure and structure characteristics, and phase behaviour. Unfortunately, this point is not sufficiently stressed in the papers. The supramolecular and covalent hairy rods resemble each other but XRD patterns of P3HT and those of $PPY(CSA)_x(amphiphile)_y$ are almost identical.

## 2.2.9 Hairy-Rodlike Structures of Stacked π-Conjugated Molecules

Besides the high hairy-rodlike polymers, there is another important class of self-organized π-conjugated molecules which cannot be ignored, that of stacked π-conjugated molecules[246], by example hexabenzocoronene derivatives[247-249]. When substituted they form cylindrical assemblies resembling hairy rods. Their properties have clear analogies and *e.g.* thermotropic alignment can be used[248].

A prime of these are phthalocyanines (PC) (Figure 13) which were invented over 60 years ago[250-254] but only quite recently have their electronic and supramolecular features been utilized. PCs have aromatic structure of four inter connected pyrrole units forming π-electron cloud delocalized over an array of 18 carbon and nitrogen atoms and they form self-organised stiff architectures, the general interest of the present text. It is somewhat controversial, in which cases their structures can be called supramolecular or self-organized or both. Here we follow Nolte[255] and Hanack[256]. PCs form columnar stacks and layered structures and metal cations can be embedded in the centre of the molecule upon coordination[256] leading to bridged main-group phthalometal complexes. Their construction techniques are at an advanced state to an extent of achieving defect-free copper pthalocyanine single crystals on an atomically flat Au surface. They can be constructed growing first Au surface using molecular beam epitaxy (MBE) and then PC single crystal layer using organic MBE[257].

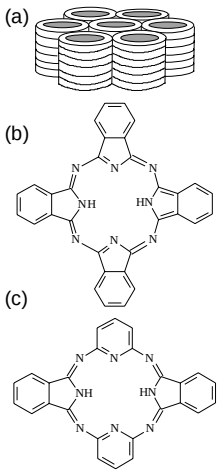


**Figure 13 (a)** A schematics of stacked π-conjugated molecules. Adapted from ref. 255. **(b)** Phthalocyanine (PC). **(c)** Hemi-porphyrazine (HP)

The supramolecular stacks can be formed in solution or in liquid phase[258]. The stacking can give rise to semiconductivity or conductivity in the stacking direction[259]. NLO activity exists in helical structures[258,260]. Depending on preparation, there are four main classes of self-organized or supramolecular self-organized PC systems with various substituents.

In the first procedure LC PC systems consist of PCs peripherally substituted with alkyl or alkoxy chains forming self-organized but not necessarily supramolecular discs[255]. The mesophases contain typically hexagonally arranged ordered columns due to van der Waals forces. They consist of PC molecules closely packed with their planes perpendicular to the column axis due to π-stacking[255]. Side chains tune solubility and phase behavior and structures are typically soluble in organic solvents or water[261]. Depending on the nature of the chain and possible metals, the discotic LCs are found for alkyl substituted PCs equipped with side chains longer than $C_4$ or $C_6$[256]. The phase transitions of LC heterocyclic PCs can be tailored by changing the substituents. The transition from the solid to the LC phase corresponds to the melting of the side chains. The extension or branching decreases the degree of crystallinity and therefore the transition temperature. Characteristically, PCs equipped with the linear chains exhibit phase transitions from crystalline to mesophase at lower temperatures compared with the PCs substituted with branched chains with smaller crystallizing tendency[255]. Interestingly, this is not always true. Branching near the core of PC may decrease the clearing point[256]. Transition temperature can also be lowered by substitution of benzene by thiophene, whereas metalation many times raises it[262]. In contrast to alkyl chains, the second procedure is based on the crown ether substituted PCs that create supramolecular structures and improve solubility. There are crown ether substituted PC which are even *too* soluble in water to form LB films[255].

The third case is the proper polymeric PCs such as polygermoxanes and polysiloxanes containing a linear chain of stacked PCs. These columns equipped with alkyl substituents are considered as hairy rods (Figure 12). There are also *coordination* polymers compared with the covalent bound polysiloxanes and related compounds, called proper supramolecular polymers (*Cf.* last paragraph in Chapter 2.2.3). In contrast to these polymeric PCs, bridged transition metal complexes with macrocyclic ligands, 'shish-kebab' polymers, consist of alternating metal PC and ligand species. The case comprises bridged ligands which are either π-electron containing molecules, like pyrazine, or negatively charged ligands, such as $CN^-$ or SCN, if the oxidation state of the central metal is +III, like in $Co^{3+}$ or $Fe^{3+}$ [256].

In contrast to PCs, another stacked archetype material, hemiporphyrazines (HP)[263] contain a 20 π-electron macrocycle including two pyridine and two pyrrole moieties instead of four pyrrole units (Figure 13) In spite of the closely related structure compared with the PCs, HP:s have different properties. HP:s are thermally stable and after, *e.g.* iodine, doping they show moderate electric conductivity. The feature of HPs compared with PCs is their Schiff base nature and they exhibit lability in aqueous acidic media.

# 3 X-ray Scattering and Diffraction in the Studies of Soft Nanoscale Condensed Matter

## 3.1 X-ray Diffraction of Soft Condensed Matter

### 3.1.1 The Kinematic Approximation

X-ray diffraction (XRD)[264,265] has been extensively used in all the papers **I-VII**. The XRD results from the scattering of X-ray photons by individual core electrons and interference among the waves scattered by these events. Electrons that take part in the chemical bonds (of heavy atoms) are not seen. The scattering refers to the first phenomenon, whilst the diffraction refers the combination of both. In materials science diffraction refers to crystalline or otherwise relatively well-ordered samples inducing regular diffraction peaks, while the term scattering is employed for diffuse-like diffraction patterns.

In this thesis we deal with elastic X-ray scattering of hard X-rays within the classical kinematic approximation or the first Born approximation which term may best relate to the particle scattering. So there is no energy transfer from photon to electron. We consider only monochromatic and coherent radiation, so the phase relationships between the incident and scattered photon hold and the interference phenomena, say diffraction, among the scattered photons occur. We have made the following assumptions, which make sense from the analysis point of view: We assume scattering weak enough to occur only once in the sample. However, multiple scattering is generally present in small-angle scattering (SAS) due to the weak single scattering because of small scattering angles and long scattering path in the transmission geometry (papers **I**, **III-V**, and **VII**). It occurs also in grazing-incidence geometry due to the very long scattering path (papers **II**, **V**, and **VI**). If the diffracted photons were essentially rediffracted within the specimen, the dynamic theory should be applied. Further, we do not consider inelastic Compton scattering or Compton modified scattering thought these phenomena are always physically present, especially at wider scattering angles. We do not consider other related topics such as soft X-rays or extreme ultraviolet radiation[266], Rayleigh scattering from individual atoms, or coherent scattering from phonons either.

XRD may be termed Bragg diffraction. It defines two plane waves scattered from the two point-like particles located at O and P with the distance $r$ defining the vector $\bar{r}$ drawn from O to P. The direction of incident and scattered waves are defined by the unit vectors $\bar{S}_o$ and $\bar{S}$, respectively, at a distance far from the O and P. The scattering vector is given by $\bar{s} = \left(\bar{S} - \bar{S}_o\right)/\lambda = \bar{q}/2\pi = \left(\bar{k} - \bar{k}_o\right)/2\pi$, where $\lambda$ is the wavelength of the radiation and $\bar{k}_o$ and $\bar{k}$, the wave vectors of the incident and scattered radiation, respectively. When the scattering is coherent and there is no phase change on scattering, the phase difference between two waves scattered at O and P, depends only on the path length difference between two rays. This distance is known form the distance between the scatterers and the phase difference is $\Delta\varphi = \left(2\pi/\lambda\right)\left(\bar{S}_0 \cdot \bar{r} - \bar{S} \cdot \bar{r}\right) = -2\pi\bar{s} \cdot \bar{r}$.

No proper crystals but LCPs are considered. In the case of solutions (paper **V**) or melts (papers **V** and **VII**) SAS of (almost) independent or dense scatterers, respectively, are dealt with. Hencefort we refer SAS when feasible. Besides the text books of XRD of π-conjugated polymers[1,2] and general XRD[264,265,267], the used concepts and symbols are adapted from the references of the XRD of soft condensed matter[266,268-277].

*Scattering from an Electron*

XRD is produced by the interference of X-ray waves scattered from the electrons which behave essentially if they were free, because the energy of X-ray photons is much larger than that of the binding energy of light atoms. For the elastic scattering, the secondary waves, "the classical scattering from an electron" have thus the same intensity by the Thompson formula

$$I_e(\theta) = I_o r_e^2 \frac{1}{R^2} \frac{1+\cos^2 2\theta}{2} = I_o r_e^2 \frac{P(\theta)}{R^2}, \qquad (3.1.1)$$

where $I_o$ is the primary intensity of the probe beam, $r_e = e^2/mc^2$ is the classical radius of electron, $m$ its mass, $e$ its charge, and $c$ the speed of light. $R$ is the distance from the object to the point of registration, $2\theta$ the scattering angle, and $P$ the polarization factor. The polarization factor in Equation (3.1.1) is valid for

unpolarized X-rays only (papers **II** and **VII** and partially papers **III** and **V**). It approaches unity for low angles *also* when polarized synchrotron radiation is used (papers **I**, **III-VI**) but fails otherwise. If the unpolarized radiation of X-ray tube is polarized by the crystal monochromator, the Bragg angle of the monochoromator ($\alpha$) has to be accounted, and the polarization factor takes the form[278]

$$P(\theta) = \frac{1 + K(\alpha)\cos^2 2\theta}{1 + K(\alpha)}, \tag{3.1.2}$$

where $K(\alpha) = \cos^2 2\alpha$ for a mosaic crystal and $K(\alpha) = \cos 2\alpha$ for a single crystal[279]. *E.g.* for quartz and $CuK_\alpha$, $\alpha[1011]=13.3489^o$. The polarization factor of synchtrotron radiation takes the form[264]

$$P(\theta) = f_\perp + (1 - f_\perp)\cos^2 2\theta, \tag{3.1.3}$$

where $f_\perp = I_\perp / (I_\perp + I_{II})$ is the fraction of the perpendicular polarization of the incident beam with respect to the given diffraction plane. The components refer to the incident beam perpendicular and parallel to the diffraction plane.

The flux of the scattered X-rays is

$$J_e(\theta) = J_o r_e^2 \frac{1 + \cos^2 2\theta}{2}, \tag{3.1.4}$$

where $J_o$ is the flux of incident beam. The differential cross section of unpolarized X-rays

$$\left(\frac{d\sigma}{d\Omega}\right)_e = \frac{J_e}{J_o} = \frac{I_e}{I_o} R^2 = r_e^2 \frac{1 + \cos^2 2\theta}{2}, \tag{3.1.5}$$

where subindices refer to the electron and primary beam. The first one is hencefort dropped out.

The term intensity *I* may be used to denote both flux *J* and the differential cross section $J/J_o$ but we may also make a distinction between them. The flux is what is experimentally measured and the differential cross section is determined when the flux of incident beam is known. The flux is measured as the amount of energy transmitted per unit area per second describing the strength of a beam of radiation. The differential scattering cross section express the energy transmitted per second through the unit angle $d\Omega$ instead of unit area and allows the consideration independent on the distance of the observation. It yields the cross section when integrated over a given angle. The absolute intensity is given in the square of electrons.

Although the measured quantity is the probability of finding a scattered photon in a given angle, the term intensity is used in the formulas of the kinematic diffraction theory. The quantum mechanical counter part of Equation (3.1.5) is used for inelastic scattering.

The flux (or the intensity) of the scattered X-rays is the square of the amplitude *A*

$$J = AA^*, \tag{3.1.6}$$

where the amplitude is of the oscillating wave field of the frequency $\nu$ and wavelength $\lambda$ propagating in a given, say, *x*-direction in time *t* given by

$$A(x,t) = \mathrm{A}\cos(2\pi(\nu t - x/\lambda)) = \mathrm{A}\exp(i2\pi(\nu t - x/\lambda)) = A_o b \exp(i2\pi(\nu t - x/\lambda)), \tag{3.1.7}$$

where A is the modulus (the absolute value) of $A(x,t)$, $A_o$ is the amplitude of the incident beam, and *b* is the scattering length describing the efficiency of the scattering and depending on the radiation and particle. For unpolarized X-rays

$$b_e = r_e \left(\frac{1 + \cos^2 2\theta}{2}\right)^{1/2}, \tag{3.1.8}$$

having the dimension of length and approaching $r_e$ for small scattering angles[4]. This is used in the expression of the intensity in electron units, $I_{eu} = I / b_e^2$, which is dimensionless and which depends only on the structure of the matter corresponding to the observed flux divided by the scattering of the single electron at the sample position.

[4] Since $b_e \approx 1$ for $2\theta \to 0$, the scattering length density and electron density are equal in the context of SAS.

Finally note that the arbitrary or relative intensity units have mostly applied in this thesis. The measurement of the intensity of the (reduced) primary beam allows the determination in absolute units that are employed for the solutions (paper **V**). In practice, the scattering can be measured using a material whose scattering power can be theoretically estimated. In our studies a standard sample, *e.g.* polyethylene (LUPOLEN) that is calibrated using the primary methods was used. The primary determination of absolute units is difficult, because the primary beam is so intense that the detector cannot measure it and the scattered beam under similar conditions, although the image plate may be used to measure direct beam without damage of the detector. The use of filter of known absorption coefficient is difficult, because even small differences in energy of the spectral components result in large differences in the absorption coefficient. Therefore, the primary beam should be strictly monochromatized. There are a few methods to reduce the primary beam, such as choppers, for instance. Nickel can be used as a calibration standard for WAXS[280] but there is no such good material for SAXS. The scattering arising from the density fluctuations of an amorphous material can be utilized. Water is a good choice, because of well-tabulated properties.

*Scattering from Atoms*

*Amplitude, Atomic Scattering Factor, and Scattering Intensity*

Scattering amplitude and intensity are the essence of XRD. We continue considering Bragg scatterering for which the amplitude of $N$ identical scatterers[5] is

$$A(\bar{s}) = A_o b \sum_{j=1}^{N} \exp(-i2\pi \bar{s} \cdot \bar{r}_j) \, . \tag{3.1.9}$$

An atomic scattering factor $f(\bar{s})$ is another fundament. This is amplitude of the X-ray scattering from an atom in the units of $A_o b_e$ given by

$$f(\bar{s}) = \int n(\bar{r}) \exp(-i2\pi \bar{s} \cdot \bar{r}) d\bar{r} \, , \tag{3.1.10}$$

where $n(\bar{r})$ is the time averaged electron density distribution of the atom . $\bar{r}$ is measured from its center. The atomic scattering factor describes the scattering arising from the oscillation of the electrons coupled to the oscillation of the incident photons[281-283]. This was formerly called anomalous scattering and afterwards the X-ray dispersion. When the incident photons have high enough energy, part of them scatter normally and part of them are absorbed. The absorbed photons excite electrons and re-emit at either lower energy or at the initial energy. This results in fluorescence or strong coupling to absorption edge energy, respectively. The scattered photons show phase delay and are thus retarded compared with the normally scattered photons. Also, the absorption must be taken into account in the scattering geometry (Chapter 3.2.1). The absorption of X-rays (in soft condensed matter) is mainly due to photoionization, equivalent to photoelectric effect, of atoms with the ejection of the electrons, *i.e.* photoelectrons, from the inner atomic shells. This means that the energy of the X-ray photons is larger than the binding energies of the electrons in an atom of molecule. If it was considerably larger, the electrons would be considered as free and the (inelastic) Compton scattering would be more probable absorption process than photoelectric effect. Photoionization results in other secondary processes depending on the available final states of photoelectrons.

Subsequent decay of electrons to the initial state yields fluorescence that depends on the difference between two energy levels and the transition rules. When the atom is bound in solid state, there may be considerable increase in unoccupied states (due to excitons, plasmons, surface plasmons etc.), which result in increased absorption. These processes are significant for sufficiently heavy atoms containing tightly bound electrons. When the binding energies become larger, as in the case of core electrons in heavier atoms, the oscillation of the electrons may be coupled to the oscillation of the incident photons and electrons are absorbed and re-emitted either at the lower energy or at the initial energy, which result in sharp increase in fluorescence or in absorption. The dispersion and absorption are interrelated and both factors are studied as a function of energy.

The quantum mechanical interpretation of $f$ is subtle and related with the change in the transition probabilities of bound electrons[264,265]. The form factor approximations for practical use[284] and SAS[285] are also complex vehicles. Rather, in our simple discussion, the X-ray dispersion may be understood as follows:

---

[5] The amplitude of a large number of scatterers, $n(\bar{r})dr$ , where $d\bar{r}$ is the volume element $dxdydz$ around $\bar{r}$ (which now is a general position vector) . This is proportional to the Fourier transform of the local number density of the scattering centres in the sample volume, is given by $A(\bar{s}) = A_o b \int_V n(\bar{r}) \exp(-i2\pi \bar{s} \cdot \bar{r}) d\bar{r}$ . The integral is over the (illuminated) scattering volume.

The hard X-ray photons of wavelength 2-0.5 Å interact with the *internal* electromagnetic fields arising from electrons of heavier atoms moving in the material. The electrons are not treated as free as in XRD above but as bound and their response to the incident X-rays differs from that of matrix atoms.

The X-ray beam is described as an oscillating electromagnetic field for its amplitude written as

$$A = A_0 \exp(i(\omega t + \varphi)), \tag{3.1.11}$$

where $A_0$ is the modulus of the absolute value of $A$, $\omega = 2\pi\nu = 2\pi c/\lambda$ an angular oscillation velocity, ν the wave frequency, λ the wavelength, c speed of light, and $\varphi = 2\pi x/\lambda$ the phase of the amplitude at a given time. Equation (3.1.10), is defined by the ratio of maximum scattered X-ray field $A_s$ to the incident field $A$ by

$$f = \frac{A_s^{\max}}{A^{\max}}. \tag{3.1.12}$$

The atomic scattering factor, $f = f(q,E)$, depends on the magnitude of the scattering vector $q$ and on the energy of the photons. The dispersion effects become noteworthy, when the energy of photons, $E = \hbar\omega$, approaches the ionization energy of the atom, the energy needed to remove an electron from its ground state. Bound electrons are then approximated as classical dipole oscillators, an oscillating mass with a natural oscillation frequency $\omega_0$ and damping constant $\gamma$. The behavior under an oscillating field are treated using classical equation of motion[6] from which the position of an electron, $x$, is deduced. The maximum amplitude of the electric field at a distance $r$ from the atom is then

$$A^{\max} \propto \frac{\omega^2}{r(\omega_0^2 - \omega^2 + i\gamma\omega)}. \tag{3.1.13}$$

The scattering factor of the single electron is deduced from Equations (3.1.12) and (3.1.13) implying

$$f_e \approx 1 - \frac{\omega_0^4}{(\omega^2 - \omega_0^2)^2 + \gamma^2\omega^2} + i\frac{\gamma\omega^3}{(\omega^2 - \omega_0^2)^2 + \gamma^2\omega^2}. \tag{3.1.14}$$

The parts of Equation (3.1.14) are a different function of energy. Consequently, the X-ray scattering response of the components is different in different energies and the atomic scattering factor is conventionally expressed as a sum of three different terms,

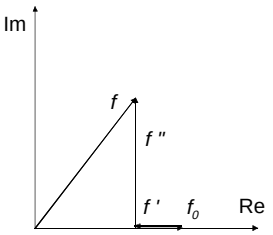


**Figure 14** Components of the atomic scattering factor

$$f = f_0 + f'(\omega) + if''(\omega). \tag{3.1.15}$$

The real dispersive term, $f'$, is in phase and negative with respect to the elastic component $f_0$. It takes its minimum, when $\omega=\omega_0$. At this energy the electron is oscillating in phase. The imaginary absorptive term, $f''$, introduces 90° phase shift in the total scattering factor and takes its maximum, when $\omega \geq \omega_0$. At these energies, the electron absorbs from the field to abandon the atom. In general, the real and imaginary parts of (3.1.15) are related by the Kramers-Kroning relation

$$f'(\omega) = \frac{2}{\pi}\int_0^\infty \frac{\omega' f''(\omega')d\omega'}{\omega^2 - \omega'^2}. \tag{3.1.16}$$

Once the $f''$ spectrum is obtained experimentally from the sample via fluorescence measurements, the corresponding $f'$ spectrum can readily be calculated by numerical integration using this relation.

The corrections to the scattering factor can be ignored, when $\omega_0/\omega$ and $\gamma$ are small. Then $f_e$ approaches unity and the electrons can be treated as free, which is the case of XRD from light atoms. Our XRD experiments of macromolecules are based on scattering from light atoms and low energies of X-ray photons that may be scattered from the electrons of material but that mainly are not absorbed due to insufficient energy to excite the available electronic transitions. (We do not consider Compton scattering.)

---

[6] $\frac{e}{m}A = \frac{d^2}{dt^2}x + \gamma\frac{d}{dt}x + \omega_0^2 x$ yields $x = \frac{e}{m}\frac{A_0}{(\omega_0^2 - \omega^2 + i\gamma\omega)}\exp(i\omega t)$

There the binding energies of their electrons are order of magnitude higher (~ 100 keV) than energies of incident X-ray photons (~ 10 keV). The photons do not excite the electrons and the scattering properties more or less approach those of free electrons. Correspondingly, when the energy of X-ray photons is far from the ionization energy, the atomic scattering factor approaches $f_0$ and practically equals $Z$. The incident and scattered angles are related with the X-ray wavelength comparable to the atom size, however. The atomic scattering factor varies between the elements (and bonding between the elements) but is the same for each atom of same element. When plotted against $s = 2(\sin\theta)/\lambda$ the scattered waves from the all parts of its electron cloud are in phase and add up in the forward direction yielding $f(s=0) = Z$, where $Z$ is the corresponding atomic number, and start to differ from the phase for increasing $s$ resulting in decreasing $f$ and the overall amplitude $A$. The shape of the overall curve is directly related to the shape of the electron density distribution of the atom.

As a whole[7], the amplitude of the scattered X-rays for $N$ atoms is

$$A(\bar{s}) = A_o b_e \sum_{k=1}^{N} f_k(s) \exp(-i2\pi \bar{s} \cdot \bar{r}_k) . \tag{3.1.17}$$

In paper **VI** we use the amplitde for similar atoms given by

$$A(\bar{q}) = A_o b_e f(\bar{q}) \sum_j \exp(-i\bar{q} \cdot \bar{r}_j) . \tag{3.1.18}$$

We note that in paper **VI** only carbon and hydrogen were considered. Carbons dominate the scattering intensity so the approximation makes sense.

To the distinguishable particles, the general amplitude is expressed using the generalized (valid also for particles) scattering length $b$ and denoting/redefining the amplitude by the normalized amplitude

$$A(\bar{q}) \equiv A(\bar{q}) / A_o = \sum_j b_j \exp(-i\bar{q} \cdot \bar{r}_j) \text{ [8]}. \tag{3.1.19}$$

Recalling $\rho(\bar{r}) = b_e n(\bar{r})$ this leads to the fundamental equation of the scattering intensity

$$I(\bar{q}) = \left|A(\bar{q})\right|^2 = \left| \int_V \rho(\bar{r}) \exp(-i\bar{q} \cdot \bar{r}) d\bar{r} \right|^2 . \tag{3.1.20}$$

This is the complex square of the Fourier transform of the scattering length density; more accurately, an integral over the (finite) illuminated volume approximating the Fourier transform; and equally valid for X-rays and neutrons. The normalized amplitude, Equation (3.1.19) is used here, which means, that the intensity in Equation (3.1.20) actually denotes the differential scattering cross section, see Equations (3.1.4) and (3.1.5). Due to the thermal motion, rather than the amplitude, it is the ensemble average of amplitude

$$I(\bar{q}) = \left\langle A(\bar{q}) \right\rangle^2 = \left\langle \int_V \rho(\bar{r}) \exp(-i\bar{q} \cdot \bar{r}) d\bar{r} \right\rangle^2 , \tag{3.1.21}$$

which is treated.

*Autocorrelation*

The illustration of the electron and scattering length density distribution in the real space requires distribution functions. We can use the electron density distribution function which is the most illustrative or the correlation function which can be determined from the experimental intensity pattern. There is a wide selection on correlation functions with differences in normalization or constant terms (Chapter 3.6.3). In particular, the autocorrelation function (Patterson function in crystallography), is given by

---

[7] For the atoms (of the same kind) this is given by $A(\bar{s}) = A_o b_e f(s) \int n_{at}(r) \exp(-i2\pi \bar{s} \cdot \bar{r}) d\bar{r}$, where $n_{at}(\bar{r})$ express the density distribution of the atomic centres.

[8] The generalized amplitude in the terms of density distributions of the electrons, $n(\bar{r})$, is given by $A(\bar{q}) = b \int_V n(\bar{r}) \exp(-i\bar{q} \cdot \bar{r}_j) d\bar{r} = \int_V \rho(\bar{r}) \exp(-i\bar{q} \cdot \bar{r}_j) d\bar{r}$, where $\rho(\bar{r}) = \sum_\alpha b_\alpha n_\alpha(\bar{r})$ is the general scattering length density distribution. Subindices refer to the atomic species.

$$\Gamma_p(\bar{r}) = \tilde{\rho}^2 = \int \rho(\bar{u})\rho(\bar{u}+\bar{r})d\bar{u} = \langle \rho(\bar{u})\rho(\bar{u}')\rangle V = \int I(\bar{s})\exp(-i\bar{s}\cdot\bar{r})d\bar{s}\ ^{9} \qquad (3.1.22)$$

where $\Gamma_p(0) = \langle \rho^2 \rangle V$, and $\Gamma_p(\bar{r}\to\infty) = \langle \rho(\bar{u})\rangle\langle \rho(\bar{u}')\rangle V = \langle \rho \rangle^2 V$. The scattering volume is $V = \int d\bar{u}$. The autocorrelation function is related to the average of the product of the given scattering length density distributions $\rho(\bar{u})\rho(\bar{u}')$ and can be deduced from the intensity as an inverse Fourier transform. It describes how the considered scattering length densities in the neighbouring regions are correlated to each other on average: When the domains equal, there is a nominally perfect correlation and for the separation long enough there is none.

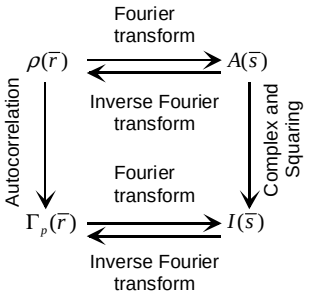


**Figure 15** Relations between the scattering length density, $\rho(\bar{r})$ (the electron density $n(\bar{r})$ multiplied by the scattering length of the electron $b_e$) the autocorrelation function, $\Gamma_p(\bar{r})$, the amplitude $A(\bar{s})$, and the scattering intensity $I(\bar{s})$.

Figure 15 shows the relations between the discussed quantities. The scattering intensity can be deduced from the structure in two alternative ways. The first way utilizes the determination of the amplitude from the electron density distribution and it is employed in the structure determination of the well-ordered crystalline structure (Chapter 3.1.2). The amorphous or liquid like matter may be in turn best treated via pair correlation function (Chapters 3.3.3 and 3.6.3). Both aspects are important for PLCs.

*Invariant*

An invariant, *Q*, is the overall scattering power of the specimen taking into account the intensity of the scattering which appears from it under all possible scattering geometries as

$$Q = \int I(\bar{s})d\bar{s} = \frac{1}{(2\pi)^3}\int I(\bar{q})d\bar{q} \qquad (3.1.23)$$

*Q* was first introduced by Porod[271] for SAS (Chapter 3.6) but it can be applied to the overall scattering as well and may be introduced here, too. An invariant is related to the aurocorrelation so that when Equation (3.1.22) is substituted in Equation (3.1.23) we get

$$Q = \int \Gamma_p(\bar{r})\left[\int \exp(-i2\pi\bar{s}\cdot\bar{r})d\bar{s}\right]d\bar{r} = \int \Gamma_p(\bar{r})\delta(\bar{r})d\bar{r} = \Gamma_p(0)\,. \qquad (3.1.24)$$

Since *Q* depends only on the mean square fluctuation of the scattering length density in the sample, and not how the fluctuations are distributed, its value remains the same "invariant" so far as the constitution of the material remains the same, too. This is also true when the structure is disturbed and the positions of the atoms are altered.

## 3.1.2 Structure Determination in Soft Condensed Matter

The structure factor $F_{hkl}$ defines the structure of the unit cell, while the amplitude of the scattered photons is product of the lattice factor and the structure factor. $F_{hkl}$ is the integral over the product of the scattering length distribution of the unit cell and the complex phase factor. It is not self evident when the concepts of crystallography are valid for less ordered LCPs. LCPs do not form single crystals but they contain crystalline phases. Their aligned frozen-in structures still consist of large number of unit cells regularly arranged in three-dimensional space and the unit cell vectors $\bar{a}$, $\bar{b}$, and $\bar{c}$ define their unit cell edges[10]. Together with the angles $\alpha$, $\beta$, and $\gamma$ between the $\bar{b}$ and $\bar{c}$ axes, $\bar{c}$ and $\bar{a}$ axes, and $\bar{a}$ and $\bar{b}$ axes,

[9] Equation (3.1.20) rewritten by considering two points represented by the vectors, $\bar{u}'$ and $\bar{u}$, and defining their separation by $\bar{r} = \bar{u}' - \bar{u}$, which implyes $I(\bar{q}) = A(\bar{q})A(\bar{q})^* = \left[\int \rho(\bar{u}')\exp(-i\bar{q}\cdot\bar{u}')d\bar{u}'\right]\left[\int \rho(\bar{u})\exp(-i\bar{q}\cdot\bar{u})d\bar{u}\right] =$ $\int\left[\int \rho(\bar{u})\rho(\bar{u}+\bar{r})du\right]\exp(-i\bar{q}\cdot\bar{r})d\bar{r} = \int \Gamma_p(\bar{r})\exp(-i\bar{q}\cdot\bar{r})dr$ . $\tilde{\rho}^2$ represents a common symbol used in SAS[271].

[10] In the papers **III-VI**, the lattice vectors are marked by the bold **a**, **b**, and **c**.

respectively, they form the lattice parameters. The origin of the unit cell in a lattice point defined by $\bar{r}_{uvw} = u\bar{a} + v\bar{b} + w\bar{c}$ , where *u*,*v*,*w* are integers. The seven crystal systems depending on the parameter selection is a valid concept, too. Monoclinic ( $\bar{a} \neq \bar{b} \neq \bar{c}$ , $\alpha$=$\gamma$=90°) and hexagonal ( $\bar{a} = \bar{b} \neq \bar{c}$ , $\alpha$=$\beta$=90°, $\gamma$=120°) systems are studied in papers **V** and **VI**. The lattice of all these lattice points is defined by

$$z(\bar{r}) = \sum_{u=-\infty}^{\infty} \sum_{v=-\infty}^{\infty} \sum_{w=-\infty}^{\infty} \delta(\bar{r} - \bar{r}_{uvw}) , \tag{3.1.25}$$

and the unit cell content is specified using the distribution of the scattering length density $\rho_u$ by

$$\rho(\bar{r}) = \rho_u(\bar{r}) * z(\bar{r}) , \tag{3.1.26}$$

where $\rho(\bar{r})$ is the scattering length density of the whole crystal containing the information of the structure in real space. The Fourier transform of this Equation yields the amplitude of the scattered wave as

$$A(\bar{s}) = F(\bar{s})Z(\bar{s}) , \tag{3.1.27}$$

a function in reciprocal space. The Fourier transform of $\rho$, is the structure factor $F(\bar{s})$ and that of $z(\bar{r})$ the lattice factor $Z(\bar{s})$ . The lattice factor itself is a lattice in reciprocal space and its lattice points are given by $\bar{r}^*_{hkl} = h\bar{a}^* + k\bar{b}^* + l\bar{c}^*$ , where the indices (*hkl*) are integers or zero. These Miller indices and the vectors $\bar{a}^*, \bar{b}^*, \bar{c}^*$ define the reciprocal lattice similar to Equation (3.1.25). The information contents of these functions are still equivalent. If the unit cell parameters are known, the indexation of XRD peaks consists of deciding on the set of Miller indices so that the observed diffraction angles $2\theta$ are consistent with those calculated from the Bragg law[11].

The structure factor $F(\bar{s})$ is a smoothly varying function defined over the whole reciprocal space, while the lattice function $Z(\bar{s})$ and thus the amplitude $A(\bar{s})$ is nonzero at the reciprocal lattice points only. Measured intensity is in turn the absolute square of the amplitude (Equation (3.1.20)) and the structure factor observable and meaningful only in the discrete points corresponding the reciprocal lattice points and can be replaced by the expression

$$F_{hkl} \equiv F(\bar{r}^*_{hkl}) = \int \rho_u(\bar{r}) \exp(-i2\pi \bar{r}^*_{hkl} \cdot \bar{r}) d\bar{r} , \tag{3.1.28}$$

where integration is over the unit cell. Traditionally, this diffraction condition is visualized using Ewald sphere of radius $1/\lambda$ by drawing a line in the direction of the incident beam to cut the sphere at a point which is selected as the origin of the reciprocal space. The diffraction occurs, when a reciprocal lattice point, the terminus of a reciprocal lattice vector $\bar{s}$ (Chapter 3.1.1) meets the surface of the sphere. When crystal is rotated, all the reciprocal lattice points within the distance $2/\lambda$ from the origin are obtained.

The intensity can be treated as an expression

$$I_{hkl} = \left|F_{hkl}\right|^2 \quad \text{for } \bar{s} = \bar{r}^*_{hkl} . \tag{3.1.29}$$

So the observed intensity occurs at the scattering angles determined by the lattice factor and is "modulated" by the structure factor. The diffraction directions give the information about the lattice structure, whereas the measured intensities contain the information of the arrangement of atoms in the unit cell. When $F_{hkl}$ is known for the desired *hkl* reflections, the positions of atoms in the unit cell can be derived using Equation (3.1.28).

When the positions and intensities of the X-ray reflections of single crystal are already known we turn to the phase problem: The absolute value of the structure factor $F_{hkl}$ deduced taking square root of Equation (3.1.29) does not provide information about the phase angle of $F_{hkl}$ and thus the content of the unit cell. There are a few possibilities to solve the phase problem for soft matter.

(i) Direct methods are based on the comparison of the magnitudes of the structure factors among different reflections. The electron density is nonnegative and it is concentrated on the atomic centers. The phase angles cannot get arbitrary values but they must obey these requirements. When doing so the phase angles with regard to structure factors produce inequality relationships and statistical distributions that can

[11] $2d_{hkl}\sin(2\theta/2) = \lambda$ ,where $d_{hkl}$ is the interplanar spacing between the parallel crystallographic planes so that $1/d_{hkl} = \left|\bar{r}^*_{hkl}\right|$ .

be utilized to solve the phase problem. This method was described early[286,287] and the required physical constraints are carefully tabulated[288].

(ii) The phase can be estimated based on the appropriate model or reasonable initial guess built using different molecular modelling treatments. Then the density distribution can be calculated by combining the phase information and experimentally measured amplitudes and the scattering pattern can be recalculated for comparison. This iterative process has been used in paper **VI**.

(iii) The isomorphous replacement used for the biological matter is based on isomorphous crystals having almost similar structure except for one or more heavy enough atoms replaced by chemically similar atoms with different scattering power. If the replaced atoms are located at the Patterson map the structure factors for given Bragg reflection of two crystals are $F_1=F_{M1}+F_C$ and $F_2=F_{M2}+F_C$, where $F_C$ is the contribution of the common part of the crystal. $F_1$-$F_2$=$F_{M1}$-$F_{M2}$ is obtained from the knowledge of the positions of M1 and M2. The calculated difference is then compared with the possible differences of the square roots of measured intensities and the best match yields the signs for these square roots.

(iv) The anomalous scattering affect both the intensity of crystalline reflections at different wavelengths and the intensity of certain symmetry related reflections at the same wavelengths. Both effects are used to solve the phase problem in crystals containing heavy atoms before and after crystallization requiring that $Z$ is much larger than those of the rest of the atoms. This comprises conventionally multiwavelength anomalous dispersion (MAD) phasing, a standard technique in protein crystallography, utilising changes in the diffraction properties at different wavelengths near the absorption edge of these atoms[281-283]. The anomalous scattering and the amplitude of the total structure factor are collected at two or several wavelengths, which allows detection of additional anomalous differences and differences between the symmetry equivalent reflections at measured at the two wavelengths.

## 3.2 Data Treatment

### 3.2.1 Corrections to the Measured Scattering Intensity

The concepts above are valid for the "pure" scattering intensity. Before it can be treated, the experimental and instrumental effects and broadening must be taken into account. They are due to nonideal monochromatization, collimation, and focusing, and finite resolution of the detector. Besides the noninstrumental structure factor (Chapter 3.1.2), the factors addressed in crystallography with symmetric (parafocusing Bragg-Brentano) reflection geometry include the polarization factor (Chapter 3.1.1), the Lorentz factor, the absorption, the multiple scattering (Chapter 3.1.1), the multiplicity factor accounting the different planes with the same spacing, and the temperature. The situation is dependent on the geometry and the required accuracy in the given conditions. In grazing-incidence geometry, when integrated intensity is collected the following corrections are required: Normalization vs. a constant incident flux, a correction for the Lorentz factor, a correction for the size of the irradiated area, absorption correction from the windows, and correction due to the anisotropy of the resolution function of the instrument. When the irradiated area is not determined by the slits but the sample edges, further correction are needed. In addition, there are systematic errors due to the inadequacy of the scattering theory[289]. Several factors are usually negligible, when working at a rather small and limited scattering angle region, when the peak broadening due to the small crystallite size dominates, or when relatively qualitative information is enough to the conclusions needed. For a recent review in the case of π-conjugated polymes, see the text of Breiby and Samuelsen[290].

Here we consider symmetric parafocusing Bragg-Brentano reflection geometry and refer to symmetric transmission, or grazing-incidence geometry (Chapter 3.4) when applicable. Five aspects can be mentioned.

(i) The scattering due to the air background (also when the sample is in vacuum or in helium atm) has to be subtracted. In transmission mode the sample holder is to be taken into account too.

(ii) In all geometries the measured scattering intensity has to be divided by the polarization factor $P(\theta)$. The form of the factor depends on the used radiation, see Chapter 3.1.1.

(iii) The absorption correction due to the scattering angle dependent scattering path is to be considered. This correction is not significant for small angles in transmission geometry but for wider angles, when scattered rays travel longer path inside the sample. The corresponding absorption correction is given by[275]

$$I(\theta)=\frac{I_{meas}(\theta)}{\mu\left(1-\frac{\cos\alpha}{\cos(2\theta-\alpha)}\right)}\left[\exp\left(\frac{-\mu T}{\cos(2\theta-\alpha)}\right)-\exp\left(\frac{\mu T}{\cos\alpha}\right)\right], \qquad (3.2.1)$$

where $\mu$ is the linear absorption coefficient and $T$ the thickness of the flat sample. $\alpha = \theta$ for symmetric transmission geometry, and $\alpha = 0$ for the transmission geometry for SAS.

(iv) The detector related geometrical corrections have to be calculated for the different purposes separately. For instance, for the flat HISTAR® detector and SAS used at our laboratory the following approximate correction is presented by Ulla Vainio[291]:

$$I(l) = I_{meas}(l)\frac{d\theta_o}{d\theta_l} \approx I_{meas}(l)\frac{\arctan\left(\frac{x_o}{R}\right)}{\arctan\left((l+1)\frac{x_o}{R}\right) - \arctan\left(l\frac{x_o}{R}\right)}, \qquad (3.2.2)$$

where $l$ is the running number of the pixel (from the origin at the virtual position of the primary beam) and where $(x_o / R) = \tan 2\theta$ is the wideness of the pixel nearest to the origin divided by the distance between the sample and the detector.

(v) Apart from corrections for polarization, absorption and instrumental broadening, there is a group of other correction factors commonly known as Lorenz-factor. We may describe how Lorentz correction applies in particular to Papers **I-VI**. First one should account for the changes in the scattering volume with the scattering angle. When usual scanning measurement is made, both incident and excident angle change. The change due to incident angle is, however, taken care of by the absorption factor and one needs only to consider the changes in the the part of the illuminated volume which is "seen" by the detector through the receiving slits. When we use position sensitive detector or slits that are wide enough to allow the whole sample to be observed at any angle, this correction reduces to unity. This is the case for example in all the experiments herewith. A second component arises from the random orientation of sample, that is a given structure takes up all orientations in space with equal propability. Thus, given any scattering vector $q$ it becomes increasing unlikely that $q$ resides in a particular volume element of the reciprocal space. Due to this "powder-averaging" the intensity contained in this volume element is spread evenly on a spherical shell and is therefore diluted by the factor inversely proportional to the surface area $4\pi q^2 = \sin^2\theta$.

Moreover we should also consider how the intensity is detected and presented. By definition, a unit intensity within the previously mentioned shell whose area is $4\pi q^2$ and thickness $\delta q$ should produce a unit intensity per pixel on an ideal detector (a detector where each pixel has the same solid angle to the sample). However, if we have a flat detector, which is a general case in this thesis, the distance to the detector changes as $R/\cos 2\theta$. Thus intensity per pixel diminishes as $\cos 2\theta$. Combining this with the powder averaging term gives the total Lorenz correction factor $\sin^2\theta/\cos 2\theta$ to multiply the experimental intensity curves. Note that we have not included the radial speading of the intensity pattern $\delta q = \cos\theta\delta\theta$ nor the angle between detector plane and scattered beam (s.c. parallax). The reason is that these two do not reduce the average number of counts per pixel (when using the type of detectors as in here, *i.e.* gas filled position sensitive detector or image plate) but merely redistribute them radially. Therefore they belong to section "instrumental broadening", Chapter 3.2.2.

Finally note that the Lorentz factor varies depending on sample conditions and experimental practise. Originally Lorentz correction referred corrections to account the Bragg angle dependence of integrated intensity[12] whatever the case[270]. For randomly oriented powder crystallites it is given by

$$\frac{1}{2\sin^2\theta\cos\theta} = \frac{1}{\sin 2\theta\sin\theta} \sim \frac{1}{q^2}, \qquad (3.2.3)$$

where $2\theta$ is the scattering angle So the factor is reduced to $q^2$, which is valid at small angles. It is applied for obtaining integrated intensities (structure factors) of Bragg reflections[13]. After the Lorenz correction (and other applicable corrections) these are obtained from the peak areas in the radial intensity curves, which are azimuthal averages (intensity per pixel as a function of radius) from the 2D XRD patterns.

---

[12] The integrated intensity is the characteristic of the specimen. Instead, the maximum intensity is easily altered by slight variation of experimental conditions. Lorentz correction describes how the integrated intensity corresponding a small volume contributes to the whole scattering when it is oriented randomly. This does not account how the intensity (or, more accurately, flux) is detected but assumes that the whole integrated intensity is detected.

[13] For perfectly parallel and monochromatic incident beam the diffraction condition (Chapter (3.1.2)) is satisfied whenever the Evald sphere of reflection cuts the reciprocal lattice point. The detected beam may not be perfectly parallel and the incident beam not strictly monochromatized and a flat detector may be applied. Then the Lorentz correction allows the geometry of the Ewald sphere crossing by the reciprocal node to be taken into account.

## 3.2.2 Instrumental Broadening

The further treatment besides those mentioned in Chapter 3.2.1 is to get an idea of a pure diffraction line from the measured profile, extract this contribution and then interpret the pure line profile in terms of lattice imperfections. The latter topic is discussed in Chapter 3.5.2. The first issue depends much on the working conditions but here we discuss about typical issues still considering an archetype, Bragg-Brentano geometry, and referring to the other cases when necessary.

In general, the instrumental broadening, *G*, smears the pure intensity pattern approximately as

$$I_{meas}(\bar{s}) = I(\bar{s}) * G(\bar{s}) , \tag{3.2.4}$$

where $I_{meas}$, and $I$ are the measured and the pure scattering intensity, respectively[14]. Based on the convolution theorem the "pure" intensity is obtained as

$$I(\bar{s}) = F^{-1}\left\{ \frac{F\{I_{meas}(\bar{s})\}}{F\{G(\bar{s})\}} \right\} . \tag{3.2.5}$$

Although the instrumental profile may be obtained using Fourier transforms, a careful subtraction of instrumental effects is considerably time-consuming. Several aspects such as eigen system analysis[292], iterative folding[270], or even maximum entropy method[293] for solving the double-inverse problem of removing instrument broadening from XRD profiles are discussed. The shape, size and the intensity distribution of the primary beam are to be directly measured, too.

Classically there are six standard instrumental weight functions dedicated to the Bragg-Brentano geometry[294] introduced originally by Alexander[295]. These functions are partly valid for the geometries used in the present work as well and with comments they can be discussed in the more general context. The order in many of materials discussed in the Chapter 2 is so poor that the instrumental weight functions are small compared to the materials distortions and further approximations can be safely done.

The basic instrumental weight functions are due to (i) source (primary beam), (ii) flat specimen, (iii) axial divergence, (iv) specimen transparency, (v) receiving slit, and (v) misalignment[295].

The *approximative* total instrumental profile $g(\varepsilon)$ is in turn the convolution of the distinct functions:

$$g(\varepsilon) = g_i * g_{ii} * g_{iii} * g_{iv} * g_v * g_{vi} \tag{3.2.6}$$

(i) The source weight function may be approximated by a Gaussian intensity function as

$$g_i = \exp(-k_i^2 \varepsilon^2) , \tag{3.2.7}$$

where $k_i = 1.67 / FWHM$ of the primary beam. The synchrotron sources have more exact distributions available. This effect broadens diffraction peaks *symmetrically*. It takes the deviation from the spot-like focus into account, a thing which may be included in the source function too. This effect is important both in the transmission and grazing-incidence geometry. The source is the most important instrumental function and is illustrated in Figure 16a.

(ii) The effect of flat specimen surface[296] arises from the varying displacements of different portions of the flat specimen surface from the focusing circle to which the specimen surface is tangent. The ideal sample should be curved. The corresponding weight function is

$$g_{ii} = |\varepsilon|^{-\frac{1}{2}} , \tag{3.2.8}$$

where the angular limits are from $\varepsilon = 0$ to $\varepsilon = -(\gamma^2 \cot\theta / 14.6)\,\mathrm{deg}$ , where $\gamma$ is the horizontal beam divergence. This effect is small except for small Bragg angles $\theta$ or when the beam divergence $\gamma$ is large. The effect of flat specimen is present also in grazing-indicence geometry. Because it is not focusing in papers **II**, **V**, and **VI**, (unlike in Seeman-Bohlin geometry) it can be disregarded safely.

(iii) Vertical divergence weight function may take the form

---

[14] $h(\varepsilon) = f(\varepsilon) * g(\varepsilon) = \int_{-\infty}^{\infty} f(\varepsilon') g(\varepsilon - \varepsilon') d\varepsilon'$ , where $h(\varepsilon)$ so represents the measured and $f(\varepsilon)$ pure diffraction line for which the diffraction theory is valid. The variable $\varepsilon$ measures the angular deviation of any point from the theoretical scattering angle $2\theta$. The auxiliary variable $\varepsilon'$ has the same dimension.

$$g_{iii} = \left|2\varepsilon \cot\theta\right|^{-\frac{1}{2}} \approx \left|\varepsilon\right|^{-\frac{1}{2}}, \qquad (3.2.9)$$

where the axial limits are from $\varepsilon = 0$ to $\varepsilon = -(\delta^2 \cot\theta / 4 \cdot 57.3)\,\mathrm{deg}$ [15]. This term is appreciated for a diffractometer without soller slits. The important aspect is that the vertical divergence of the beam has generally *asymmetric* effect on the measured intensity. This is illustrated in Figure 16b.

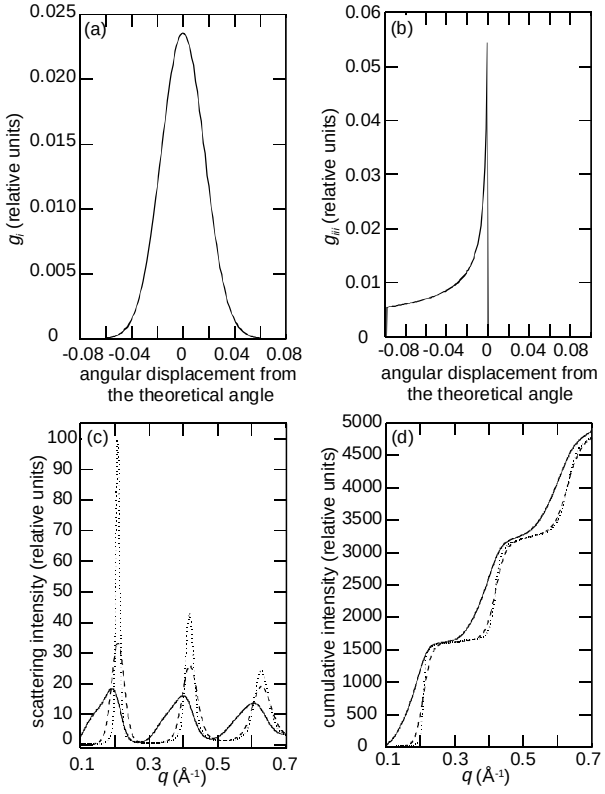


**Figure 16** A calculation of the peak broadening due to the instrumental effect in the scattering intensity curve in transmission geometry. **(a)** Source weight function according to Equation (3.2.7). **(b)** Vertical divergence weight function, Equation (3.2.9). **(c)** Calculated scattering curves: Pure scattering intensity curve according to Equation (3.5.3) in relative units representing Bragg reflections of lamellar structure, when $\varepsilon_d$ and $\varepsilon_e$ 5% and 2% and $N$=40 $a$=20, without an instrumental effect (dotted line), the same pure scattering convoluted by the source function presented in the point **(a)** (dashed line), and the same convoluted by both the source and the vertical divergence functions presented in the points **(a)**-**(b)** (solid line). The curves are normalized with respect to the integrated intensity. **(d)** Corresponding cumulative scattering intensities.

(iv) Specimen transparency [297] weight function is because of the penetration of the specimen of the finite linear absorption coefficient $\mu$ (of the solid material) by the beam. This can be presented by

$$g_{iv} = \exp(k_{iv}\varepsilon), \qquad (3.2.10)$$

where $k_{iv} = (4\mu R/114.6)\sin 2\theta$, where the limits vary from $\varepsilon = 0$ to $\varepsilon = -\infty$, and where the thickness of the specimen is assumed to be $t \geq (3.2/\mu)(\rho/\rho')\sin\theta$. Here $\rho$ and $\rho'$ are the densities of the solid material composing the powder and that of the powder including interstices, respectively. This effect is present for grazing incidence geometry making the depth profiling difficult. It is larger for thick samples with small absorption coefficient in Bragg-Brentano geometry, which was basically the case in our earlier studies before the present work[298]. For transmission the absorption is also addressed in the background subtraction.

(v) Receiving slit weight function is present in GIXD setup and it is a rectangle in profile with a width $w_s$ which equals the angle subtended by a receiving slit at the centre of the coniometer arc. It covers the angular limits from $\varepsilon - w_s/2$ to $\varepsilon + w_s/2$ for any angular position. Besides the source function, this is another effect which widen peaks symmetrically, whilst all the others listed functions make the line profile asymmetric and shift the peaks from their theoretical positions.

(vi) The misalignment function arises from the residual misalignment of the specimen. Again according to Alexander, is found to take the form

[15] The profile corresponds to uniformly divergent beam, where $\delta$ is the vertical divergence. In practice the form of $g_{iii}$ would vary depending on experimental technique. There are no general profiles concerning of wide-range of experimental conditions.

$$g_{vi} = \frac{1}{1 + k_{vi}^2 \varepsilon^2}, \qquad (3.2.11)$$

which is an empirical formula where $k_{vi} = 2/w_{vi}$, where $w_{vi}$ is *FWHM* of the spectral profile. Since $w_{vi} \approx \tan\theta$ is small for low angles, this function is peaked at wide angles. In grazing-incidence geometry the misalignment is obviously most prominent.

Besides the functions above there are at least two additional factors which should be kept in mind.

(vii) Spectral impurity may appear because of the improper adjusting of the monochromator. Nonetheless, when the beamline optics works as defined to work, the spectral impurity is rarely a problem, at least when the higher harmonics are cut.

(viii) Detector resolution (when using position sensitive detector) may be the bottleneck when considering very sharp peaks or, on the other hand, when low scattering angles are treated and the distance between the sample and the detector is not large enough.

The coherence length is discussed in papers **III-V**. In these cases a synchrotron beamline with high quality optics were employed and the instrumental effects due to the beam divergence and the spatial resolution of the detector are taken into account both by measuring the width of the beam using a narrow slit and calculating them based on the beam line drawings.

## 3.3 Crystalline and Amorphous Polymers

### 3.3.1 Crystalline Polymers

This thesis focuses on the long chain polymer molecules with a regular axial repeat but with the different degrees of lateral packing regularity between molecules, varying from crystalline to LC and to isotropic liquid melt. Here both the distinction and the difference between the ordered (partially) crystalline and amorphous weakly ordered matter is somewhat blurred and these characters coexist.

When LCPs are studied, the lack of single crystalline oligomers may be marked. LCP:s are studied because of their polymeric and LC nature that practically prevents the formation of single crystals. On the other hand, π-conjugated polymers are studied because of their opto-electronic properties or/and their combination with LCP character and stability. The combination of these properties is hardly or never present in oligomers. Thus, LCPs represent wholly own field of study and single crystals of "corresponding" oligomers are fully different material not a more sophisticated versions of the present work

The unsubstituted rodlike polymers are mostly crystalline and also their variants induce Bragg type peaks (papers **I-VII**). The concept of crystal is applicable, when not oversimplified. *E.g.* crystallite is a convenient description but in system where the order exists at different length scales it has limited utility. For hairy-rodlike polymers, due to their tendency to form fibres, the lattice parameters are obtained from the fibre XRD patterns by investigating Bragg reflections. The analysis of which way atoms are packed in the unit cell is based on the collected integrated intensities of XRD peaks subjecting them to the sequence of analysis, see particular example for PF2/6[154]. The lattice parameters are introduced for the frozen-in LCs in papers **III-VII**. Their variations due to the external effects, like temperature, reflect the structural freedoms (paper **V**) and order-order transition (OOT). The disappearance of sharp reflections is directly related to the ODT (papers **V** and **VII**). In the papers **I-V**, and **VII** the supramolecular matter is rather disordered at the atomic level so that only the effective period results in the WAXS peaks (paper **V**). The structure analysis based on a priori information and the GIXD data of PF2/6 in thin films is discussed in Chapter 5.4.2.

The XRD line broadening related to the crystal imperfections (Chapter 3.5) plays a crucial role when working with π-conjugated polymers. According to Scherf and List[111] the avoiding of chemical imperfections related to the crystalline defects is an issue of the work with PF. Despite the locally induced disorder, the high mesomorphic order was obtained in papers **III-V**, which in turn illustrates the fact that the order in the different length scales can be *independently* tailored. This is one important result of this thesis.

For determination of the degree of crystallinity of semi-crystalline material, the intensity of the crystalline component is separated from the total intensity of the sample. This separation (for the lamellae material) is dealt detail in refs. 299 and 300. It is delicate, because the coexistence of aligned and nonaligned amorphous component in the *data* of rodlike polymers. The subtraction of the amorphous part has been done in paper **V** by using the nonaligned amorphous component of the exactly *same* image plate data, which ensures the exactly same measuring and sample preparation conditions and neglecting the aligned amorphous component, which is small. We consider ordered system revealing an amorphous character, too, but the distinct crystalline and amporphous *domains* are neither expected nor seen in SAXS data.

The other options would be to prepare a corresponding wholly amorphous sample, which would be here impossible because the self-organized structure is always present, measure that identically and subtract that data from the data of crystalline matter or, on the other hand, prepare an independent model and calculate the amorphous data from that, a method whose reliability is difficult to test. The current case is advantageous because there is no overlapping of the XRD peaks and because the background is very low. The determination would be then made using *e.g.* Ruland's method or by comparison between model and experimental data. In paper **V**, however, the purpose was to present a correlation function without the amorphous part (Chapter 3.6.3).

Interesting question on the role of crystalline vs. amorphous part remains regarding the fine details of the correlation function along the normal (**x**) direction: The thickness of the first layer, $l_1$ = 4 Å, is estimated from the first minimum of the correlation function and the thickness rest is $d_{100}^c$-$l_1$ = 12 Å. It is not clear which one describes the thickness of the polymeric, stacked part, and which one the less ordered, side chain rich part, of lamellae. The linear crystallinity which is the ratio of $l_1$ to $d_{100}^c$ (~ 0.17), was calculated. After that, the volume fraction of stacks could be determined as a ratio of the absolute crystallinity calculated by WAXS. It could be estimated if the reflections are separated from the amorphous background in absolute units using amorphous sample which cannot be prepared for current system. Absolute intensity would not be required if the data reach up to large $q$-values (8 Å$^{-1}$). Samples were not isotropic either and the orientation distribution (Chapter 3.3.2) for texture correction was unknown and somewhat meaningless to measure, because it varied from case to case and samples were not evenly oriented. Comparison of the experimental data between amorphous and crystalline models would be also difficult, because both models would be difficult to construct due to charges and the relatively large size of the system. Again, unlike coiled polymers, rodlike PPY is *not* expected to form irregular matrix of large crystalline and amorphous domains but uniformly ordered paracrystalline or LC material.

## 3.3.2 Aligned Polymers

The preferred orientation manifests in XRD data as short arcs or spots instead of Debye circles which arise from macroscopically isotropic, locally ordered matter. In general, XRD provides a straightforward method to determine the orientation of the crystallites. Further, unlike standard polarized absorption spectroscopy, XRD probes the preferred orientation of crystalline and amorphous domains separately, *cf.* Chapter 4.1.

The XRD patterns give the orientation distribution of a reciprocal lattice vector $r^*_{hkl}$ or the normal of a crystallographic plane (*hkl*). Conveniently, vector **w** is considered so that Θ and Φ are the azimuthal angles, between **z** and **w**, and between **x** and the projection of **w** on the (*xy*0) plane, respectively, commonly used in the spherical polar coordinates. The plane normals are called *poles* and the pole distribution (function) $T(\Theta)$ differs from the orientation distribution itself which is explained only when the orientation distribution of the sufficient number of plane-normals is realized through the XRD measurement. The orientation parameter, a single number, may be a more desirable illustration of the orientation instead of the whole pole distribution. The form of one of the most common orientation parameter, Hermans orientation parameter, analogous to that in the physics of LCs[18,277] is given by

$$f = \langle P_2(\cos\Theta)\rangle = \frac{3}{2}\langle \cos^2\Theta\rangle - \frac{1}{2}, \qquad (3.3.1)$$

where $P_2$ is the second order Legendre function of cosΘ and where $f$ gets the values 1, 0, or -½ when the pole is parallel, random, or perpendicular to **z**. The degree of orientation is discussed in the terms of pole figures[270], which is the stereographic projection of the pole distribution, in the context of fibre diffraction.

The considered supramolecular materials show a biaxial texture in a place of a typical uniaxial one (papers **III**-**V**). Then, highly interestingly, PF2/6 shows a “triaxial” texture in thin films, discussed in detail in Chapter 5.4.1 (paper **VI**). The degree of orientation[270] of the aligned samples may be deduced from the widths of the XRD arcs or poles (Chapter 3.3.2). Though the orientation of LCs can be determined using birefringence or fluorescence polarization (Chapter 4.4), XRD provides information which may be deduced from the *bare* crystalline part, not from a sample as a whole. The degree of alignment is quantitatively treated in the present work. Because of the crude alignment method (shearing) in the papers **III**-**V**, the degrees of axial and in-plane orientation in each sample were different even in the different parts of the sample, which would have made the accurate determination pointless. Further work based on the results of paper **VI** was already started during the course of this work but is not any longer included in this thesis. There are now significantly better aligned samples (ref. 369), and therefore the interest was shifted to them. An example, the degree of orientation for type I of PF2/6 (paper **V**) is determined in the Chapter 5.4.1.

### 3.3.3 Amorphous Polymers

Amorphous polymers and polymers in the melt state generate diffuse scattering. This is either due to local intra- and intermolecular short-range order (extending over a few atomic radii) or larger scale density fluctuations of nonparticulate matter, like a polymer dispersion[301]. Here we discuss about the amorphous short range order, while larger scale fluctuations are discussed in the context of SAS in Chapter 3.6.

Besides completely amorphous matter, both semi-crystalline polymers, such as PANI which consist of distinct crystalline and amorphous domains, and crystalline polymers, such as PPY, reveal secondary diffuse scattering background and a broad amophous halo at $2\theta \sim 22^{o}$ corresponding the average atomic distance 4 Å. The amorphous scattering does not arise from the distinct completely amorphous domains only, but from local intra- and interchain order, whether there is long-range order present or not. The diffuse scattering contains the superposition of local inter- and intrachain order.

The amorphous halo is seen in papers **III-V**, too. Because of the dense packing and very stiff nature of PPY the material is not expected to contain distinct crystalline and amorphous mesodomains and we point out that no evidences of them were seen at low scattering angle either.

The discussion on the amorphous component serves to highlight a dispersion[301] character of the crystalline part (distinct regions) in an amorphous host matrix or *vice versa*. This is an idealization which ought to be evaluated on a case-to-case basis. The rigid polymers can be more accurately thought to reveal oriented crystalline, oriented noncrystalline, unoriented crystalline, and unoriented noncrystalline phase. Compared to the flexible polymers, the rigid polymers exhibit much higher intrachain order and thus meridional Bragg reflections (papers **III-VI**).

The local structure, where the intrachain aspect plays a role, is probed by the radial distribution function (RDF) analysis[268,270,302]. This approach reflects the nature of noncrystalline matter illustrating the behavior of LCPs. As is well-known, the RDF for a polymer is fundamentally the same as that for liquid where the environment of an atom is not the same as that of the next one but can be described as a statistical way using pair disribution or pair correlation function, the normalized pair density. For the system consisting of the atoms of one kind it is given by

$$g(\bar{r}) = \frac{n_2(\bar{r})}{\langle n \rangle}, \tag{3.3.2}$$

where $n_2(\bar{r})$ is the atom density at point $\bar{r}$ around an arbitrarily chosen atom (from the center of atom). The average number of atoms found is equal to $n_2(\bar{r})d\bar{r}$, where $d\bar{r}$ is the volume element separated from the arbitrary atom by $\bar{r}$ and $\langle n \rangle$ the average number density of atoms.

The term RDF originates from the fact that in the first approximation the value of the function of the isotropic material depends only on the distance, not on the direction, from an arbitrary atom. For uniaxially oriented polymers with cylindrical symmetry, the cylindrical distribution function is often used. Function $n_2(\bar{r})$ is zero for $r$=0 and has its first maximum at the distance which corresponds to the first coordination shell and subsequent minima and maxima with gradually diminishing values related to further shells. So $g(\bar{r})$ approaches unity for large distances. Several atoms are further addressed by further redefinitions and for the isotropic polymer RDF is obtained from the interference function

$$i(\bar{q}) = \langle n \rangle \int_0^{\infty} [\hat{g}(\bar{r}) - 1] 4\pi r^2 \frac{\sin qr}{qr} dr \,. \tag{3.3.3}$$

A problem in the studies of amorphism is the infinite integration limit in $q$, which leads to the truncation error due to the finite experimental $q$-range. Therefore the measurements should be performed using as wide region of scattering angle as possible. Practically this means the use of shorter wave length, *e.g.* Mo-tube instead of Cu-tube. Mo $K_\alpha$ reaches up to 15 $Å^{-1}$[303].

For the aligned polymers this consideration must be done with respect to the orientation axes. The alignment direction related enhancement in the amorphous scattering indicates whether this arises primarily from intra- or interchain correlation. In papers **III-V** the amorphous scattering is not only uniaxially but biaxially distributed, which suggests the different nature of amorphism not only originated from the interplay and uniaxial distribution of inter- and intrachain correlation but also from the side groups. It is *very* important to notice that the introduction of the latter is the clue which makes the developed materials free floating due to its amorphous nature but simultaneously highly ordered due to the self-organization phenomenon of competing interactions.

The scattering discussed so far originates from the short range, crystalline (Chapter 3.3.1) or other particular or nonparticular order (Chapter 3.6). Moreover, there is also always a scattering at all $q$ because of the thermal density fluctuations. This arises from the random motion of the atomic, molecular, and microphase domains which momentarily coverage and create density fluctuations. Unlike the other contributions, the thermal density fluctuation occurs at *all* length scales. When the number of atoms existing in the certain volume is bigger than that in the same volume at some other place the scattering is generated no matter what the size of the volume is.

The microphase separated polymers (Chapter 2.2.2) show strong inhomogenities in their melt state driven by the interchain segment correlation, s.c. correlation hole, which results in the broad SAS peak at finite nonzero angle[304]. These concentration fluctuations above the ODT are seen in the hydrogen bonded comblike supramolecules[305]. The hairy-rodlike polymers resemble block-*co*-polymers[8,9] and in this thesis the correlation hole was indeed observed above the ODT and described in papers **V** and **VII**.

The probing of the amorphous nature is the second pillar of the LCPs and design of opto-electronic phenomena requires structural understanding at the short length scales. Usually experimental interference function is compared to that obtained from molecular modelling and then the RFD is calculated from both functions with similar truncation conditions. For π-conjugated materials these studies are rather scarce. However, Winokur *et al.*[306] compared RFDs instead of interference functions and use exceptionally high maximum $q$-value (20 $Å^{-1}$). Unfortunately, the rigorous RDF approach has not been used here because the emphasis of larger structures. This would be difficult, because, as pointed out by Winokur[302], physically correct models for comparison with the RDF data are difficult to apply to polymers with shallow torsional potential, like LCPs, π-conjugated polymers, and polyelectrolytes. The studied supramolecules apply to all these classes. Also compared to the pure polymers, an additional effect, the concentration fluctuation is present in the mixtures making the interpretation even more challenging.

## 3.4 Surfaces and Interfaces

Thin films are studied in papers **II**, **V** and **VI**. Because the applications of π-conjugated polymers require thin films, the XRD studies of films, surfaces, and interfaces are decisive[16]. In this respect, paper **VI** represents a work where numerous X-ray reflections were able to be detected. Also, like the earlier reports[7,11,307], paper **VI** shows differences in film and fibre morphology due to the surface confinement.

In this thesis, the films are investigated by grazing-incidence X-ray diffraction (GIXD) (paper **II**, **V**, and **VI**), by glancing angle diffraction[17] (paper **II**) and by X-ray reflection (paper **VI**). When SAS is considered, the term grazing-incidence small-angle X-ray scattering (GISAXS)[308,309] is used. Rather small angles but primarily Bragg peaks are discussed in paper **II** and technique may be denoted as GIXD, rather than GISAXS as it is called there. The basic geometry used in these studies is depicted in Figure 17.

The incident, reflected, refracted, and scattered beams are characterized by the wave vectors $\bar{k}_o$, $\bar{k}$, $\bar{k}_1$, and $\bar{k}_2$ respectively. In glancing incidence, the scattering vector equals to $\bar{k}_2 - \bar{k}_o$. Any variation in the scattering length density results in proper GIXD reflections. Like XRD, the X-ray *reflection* arises from scattering of the photons by electrons in the material followed by the interference of the scattered photons. Therefore, there is no fundamental difference between XRD and X-ray reflection. The reflection is denoted as "grazing" when the angle of incidence is at or below the critical angle of the substrate or any scattering planes in the film. Correspondingly, using the notation of Figure 17, then the scattering vector equals to $\bar{k}_2 - \bar{k}_1$. The wave vector of the incident beam, $\bar{k}_o$, equals to the direction of the beam and the plane of incidence is defined by this vector and the surface normal. This is vector **x** in papers **V** and **VI** and ($x$0$z$) plane in Figure 17. The reflected beam is not necessarily in the plane of incidence. If the surface is not perfectly flat, or, if it contains inhomogenities, the off-specular reflection or diffuse scattering comes into existence off the specular direction typically a few degrees

In GIXD, a point-focused incident beam impinges on the flat surface of the film specimen at or below a critical angle of surface of the specimen or its substrate below the film. The primary beam penetrates into the bulk but is almost totally reflected from the surface of the specimen or from the surface of the substrate. It is still pierced though the film assuming the critical angle of the film is smaller than that of the substrate and the used incidence angle between them. The maximum gain is ideally received at the critical angle of

[16] The only reason to work first with shear aligned bulky films instead of aligned thin films was limited experimental opportunities.

[17] In glancing angle XRD the incident angle is larger than that used in GIXD. This increases the scattering path but does not reduce the background. Note that in Figure 2 in paper **II** the reflected wave is consequently at the wider angles than the proper XRD reflection.

the substrate. Therefore, it is most advantageous to work at the critical angle and keep the incident angle strictly constant during the experiments[18].

The detection in GIXD is performed in the upper half (practically at quarter) space in the exit direction. Because of the used geometry, (i) the direct beam spillover (in the case where the sample is smaller than the beam so that the sample edges limit the beam), (ii) evanescent wave along the surface, and (iii) the total reflection of the primary beam are observed. (iv) The displaced (by the amount of the incident angle) origin of the scattering is seen. Still, some (v) background may appear at wider angles due to the roughness of the surface, which result in the local deviations in the incident angle. Finally (vi) the proper GIXD reflections arising from the proper microscopic scattering planes are seen at wider angles. The variations in the larger scale morphology are reflected at smaller angles for which the term GISAXS is used.

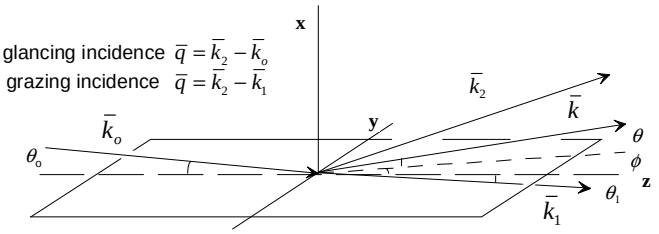


**Figure 17** Geometry of the reflection and scattering at the surface of the studied *sample*. The angles are much exaggerated. The symbols and the selection of axes (**x**, **y**, and **z** perpendicular to each others) correspond to that applied in papers **V** and **VI**, where **x** is the surface normal and the axis **y** on the surface is perpendicular to the incident beam. $\theta_o$ is the incidence angle of the incident beam, $\theta$ is that of the reflected beam, and $\theta_1$ that of the refracted beam. $\phi$ is the angle between the reflected beam and ($x0z$) plane. In the specular case $\phi = 0$.

The advantage of the grazing-incidence and/or exit angle is to substantially reduce the background (thermal, diffuse, defect, Compton etc.) contribution due to the bulk/bulky substrate with respect to the elastic contribution of the surface/film onto the substrate. The advantage is also to significantly lengthen the X-ray path and thus the scattering volume inside the film and so to enhance the detected signal. However, both the position and energy resolution at the reciprocal space is worse than in the other XRD techniques.

GIXD is generally used in order to study microstructures[310] or strains[311] or interfaces[312] in thin films and unlike microscopies, XRD at surfaces allows the detection of large macroscopic areas[19]. The requirement of flat surfaces and films limits the use of the method. On the other hand to be useful in thin film devices, π-conjugated polymer has to meet this requirement so the applicability of GIXD already itself is a certain indirect indication of the feasiblity of the polymer.

A kinematic approach may be mostly sufficient to analyze the data. It is valid for weak photon-electron interactions, when the scattered wave amplitude is relatively small so that the interaction between the incident and scattered waves can be neglected. This fails for the regime of total reflection where radiation field within the surface is the superposition of the incident and outgoing waves. When regarding the region outside this part of reflectivity curve -which is usually the most important part of the study- or when considering GIXD, where the scattering angle region is generally much larger than the angle of incidence, the kinematic theory may be employed[313], assuming that the interaction of hard X-rays with the matter is weak enough. The dynamical theory has to be utilized for perfect crystals near Bragg scattering[264,265], which refers to the glancing angles, too. In article **VI**, we have assumed that when at least one of the angles in consideration, like scattering angle, is much bigger than the incident angle, the kinematic approximation does not crucially fail[313].

The X-ray reflectivity is employed to characterize films and interfaces, especially diffuse interfaces by probing the deviation of the intensity curves from the simulated ones. The specular reflection gives information on the depth dependent scattering length density, while the off-specular about the surface topology and in-plane inhomogenities.The specular X-ray reflectivity is measured in paper **VI**. Incident and (detected) exident angles is changed and kept equal, part of the energy is reflected at each interface of the substrate and the sample, and the rest is transmitted. Material is described by the refractive index $n$

$$n = 1 - \delta + i\beta = 1 - \frac{\lambda^2 \rho}{2\pi} + i\frac{\lambda \rho_{abs}}{4\pi}, \qquad (3.4.1)$$

[18] Due to the quasi-2D character the normal direction is unattainable and some information may be lost. Therefore, the sample should be slightly rocked.
[19] In the GIXD experiments of this thesis, the area of the beam is mostly not limited by the slits but the sample edges.

where $\rho$ is the scattering length density and $\rho_{abs}$ the linear absorption coefficient of the matter. The imaginary part is responsible for the absorbed radiation[20]. Above the critical angle the reflectivity decreases rapidly and plays a major role at small angles of incidence in the vicinity of the critical angle.

The rest of the energy, which is transmitted at the boundary, corresponds to the Fresnel's coefficient of the transmitted beam and T=1-R. The reflectivity is unity when the incident angle equals that of the critical angle of the substrate. By analogy with SAS measurements, for *one* interface, the reflectivity curve can be imagined as an extension of the Porod's law (Chapter 3.6) applied to the flat surface and parallel interfaces. For $k_{xo} >> k_{xc}$ the reflectivity implies

$$R = |r|^2 = \left| \frac{k_{xo} - k_{x1}}{k_{xo} + k_{x1}} \right|^2 \cong \frac{1}{16} \left( \frac{k_{xc}}{k_{xo}} \right)^4 \sim k_{xo}^{-4} \sim q^{-4}, \tag{3.4.2}$$

where $k_{xo}$ and $k_{x1}$ are the normal components of the incident and refracted X-rays, whereas $k_{xc}$ is the value of $k_{xo}$ for critical angle of the substrate and where $r$, Fresnel's coefficient, is the fraction of the amplitude that is reflected.

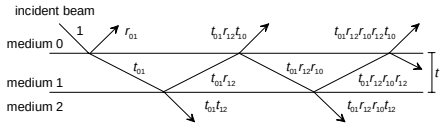


**Figure 18** The schematics of two interfaces showing the changes in magnitude of the amplitude of the X-ray when it is reflected or refracted at the given interface. "1" is the magnitude of the incident beam and $t$ means the thickness of the films but $t_{jk}$ is the transmission coefficient. See paper **VI**.

The overall Fresnel's coefficient for three materials marked respectively by 0, 1, and 2 and two parallel interfaces indexed by 01 and 12 (Figure 18) is in turn a sum of all amplitudes of all the beam contributions emerging from the 10 interface given by

$$r = r_{01} + t_{01}r_{12}t_{10}\exp(-i2\phi_1) + ... + t_{01}r_{12}(r_{10}r_{12})^{m-1}t_{10}\exp(-i2m\phi_1) + ... =$$

$$r_{01} + \frac{t_{01}t_{10}r_{12}\exp(-i2\phi_1)}{1 - r_{10}r_{12}\exp(-i2\phi_1)} = \frac{r_{01} + r_{12}\exp(-i2\phi_1)}{1 + r_{01}r_{12}\exp(-i2\phi_1)}, \tag{3.4.3}$$

where $m$ is the number of times the beam has been reflected at 12 interface and where $4\phi_1$ is a phase shift of the beam at the interface 12 with respect to the beam which is reflected at the first interface 01. Note that $r_{10} = -r_{01}$ and $t_{01}t_{10} = 1 - r_{01}^2$ which represents the conservation of energy. The reflectivity reaches its maxima when the rays which emerge from the 10 interface have been reflected at the 12 interface one or more times. These rays differ in phases by a factor $2\pi$ from each other and interfere constructively. The consideration of multilayers follows the same principles. Compututional difficulties arise, when the interfaces become fuzzy and the number of layers large. In our studies the difficulty was in turn that the chemical nature and the density of PF2/6 and PI are close to each other and therefore these two layers contribute almost as one bulky layer in the reflectivity data.

In general, the obtained well-defined reflectivity curves (paper **VI** and ref. 396) indicate a good macroscopic quality of the PF2/6 films. This was expected, because a nonuniform film would lead to short circuits in LEDs, which is not a problem for PF. Instead, the supramolecular counter part does not show similar quality but the reflectivity curves are fuzzier and not shown in paper **V**. The local quality was studied using scanning near-field optical microscope (SNOM) in paper **II** but short-circuits are observed when PPY$(CSA)_{0.5}(HRES)_y$ is used as an electron transport layer in OLED. The test use in PLEDs has been reported in ref. 123 (**Appendix**) but this detail has been disclosed. Our experimantal arrangement (paper **VI**) contained an ITO layer, too. There are detailed previous studies of multilayers reflectivity of uniform and patterned indium tin oxide[314]. ITO had a strong contribution also in our studies, *cf.* the discussion in ref. 396.

[20] The critical angle of the radiation is $\theta_{cr} \cong \sqrt{2\delta} = \lambda\sqrt{\rho/\pi} \approx (1.61/mrad)(\lambda/\text{Å})(\sqrt{\rho}/\sqrt{g/cm^3})$. For polymers $\delta$ is the order of $10^{-6}$, whether X-rays or neutrons are used, and therefore the critical angle is of the order of milliradians.

# 3.5 Lattice Imperfections

## 3.5.1 Peak Broadening due to Finite Crystallites

All the articles, **I-VII** deal with the periodic system (*cf.* Chapter 3.6) where the order varies between the levels of organization and where the effects of the lattice imperfections on the reflection widths are a focus of interest. This is not only because of similarities between small and wide-angle scattering analysis of periodic materials but also because of the interest to build soft material where the interplay between order and disorder are controlled. The lattice imperfections influence the widths of the reflection orders and this is illustrated for the lamellae below. LCPs differ from crystals and these concepts have to be modified. Especially, a crystallite cannot be understood as a tiny single crystal as is the case of the crystalline materials but rather as an effective size of the ordered domain with smooth boundaries or order within wholly continuous LC. Note that there are shear aligned block-*co*-polymers that are called 'single crystals'[315], which is somewhat confusing. For a perfect crystal without the lattice distortions the widths of all reflection orders in reciprocal phase are equal and of the form[273]

$$\Delta q \sim \frac{2\pi}{D}, \tag{3.5.1}$$

where $D$ is the size of crystallite and where the exact prefactor depends on the form of the crystal. The heights of the XRD peaks are reduced due to the lattice imperfections of the first kind characterized by the Debye-Weller factor $\tilde{D}$

$$\tilde{D} = \exp(-2M), \tag{3.5.2}$$

where $M$ is proportional to $s^2$. Since this effect refers to the *thermal* imperfection of the first kind - which reduces the height but does not change the form of the Bragg peaks - and not to the increasing disorder of LCPs in the thermal transitions, it is postponed in the following discussion.

For comparison, the scattering intensity is directly calculated using a simplified expression

$$I(q) = 1 + 2\sum_{m=1}^{N-1} \frac{N-m}{N} \exp\left(-\frac{q^2\left(\sigma_d^2 m + \sigma_e^2 m^2\right)}{2}\right)\cos(qma), \tag{3.5.3}$$

where the first factor $(N-m)/N$ describe the crystallite size and the latter parts the distortion and the lattice parameter fluctuations. $N$ is the number of lamellae and $a$ is the lamellae period, $\sigma_d$ is the standard deviation of the interplanar separation vector measuring the variation in the lattice vectors, *i.e.* the distortions of the second kind, and $\sigma_e$ that of each lattice parameter in each crystal. *Cf.* Chapter 1 in ref. 273.

We continue to consider lamellae and the peak broadening in intensities in the phenomenological terms: Here crystallite size and paracrystallity and strain in Chapter 3.5.2. The effect of crystallite size itself is the most obvious and important factor behind the peak broadening. Here we assume that the radiated scattering volume comprises a large number of tiny single crystals, crystallites. As described in Equation (3.5.1), there is an inverse relation between the ideal reflection width and the size of the crystallite. In the lamellae case (papers **I-V**, and **VI**), the reflection width due to the crystallite size is given by

$$(\Delta q)_s \approx \frac{5.6}{aN}, \tag{3.5.4}$$

where $a$ is the lamellar period, and $N$ their number. Note that this relation holds for all the diffraction orders, which is illustrated in Figure 19 (page 42). Obviously, the coherence length of a crystal ($L$) estimated by Scherrer's formula is related to Equation 3.5.4 by

$$L_{hkl} = aN \cong \frac{5.6}{(\Delta q)_s} \cong \frac{K\lambda}{\Delta 2\theta \cos\theta}, \tag{3.5.5}$$

where $\lambda$ is the wavelength, $2\theta$ a scattering angle so that $\Delta 2\theta$ is the breadth at half-maximum intensity. This is the general form of any reflection but the prefactor takes different values for different reflections unless crystals are spherical. The prefactor $K$ of unity is used thorough the articles **III-V** and represents the case of

infinite lamellae comprising of a crystal which is flat in the direction of reflection. Prefactor 5.6/ $2\pi$ (0.89[270] or 0.9[2]) is applied for lamellae elsewhere. For cubics the value of 0.94 is to be used[270].

Originally Sherrer formula was derived with the Gaussian line profile for the isotropic mixture of cubic perfect crystal crystallites of uniform size consisting of parallel platelets. The basic assumptions of the derivation are Gaussian line profiles and small cubic crystals of uniform size[270]. Then and *only* then, $L$ equals exactly the number times the spacing of the layers. Otherwise, its predictions become somewhat blurred and definition for the size of crystallites, $L_{hkl}$, an effective crystallite dimension which is the volume average of the crystallite dimension normal to the reflecting planes. Therefore, $L_{hkl}$ ought to be called *an effective crystallite dimension*, as pointed out by Klug and Alexander[270] and not the size of crystallite. Nonetheless, it can be employed in comparable studies, for instance between articles **III-V** and the work of Trondheim group[235,236], if the conditions are otherwise comparable. Even more accurately, $L_{hkl}$ can be denoted as the volume ($V$) average of the crystallite dimension $T$ normal to the reflecting plane

$$L_{hkl} = \frac{1}{V}\int T dV = \frac{1}{A\langle T\rangle}\int T dV = \frac{\langle T^2\rangle}{\langle T\rangle}, \tag{3.5.6}$$

where $A$ is the projected cross-sectional area of the crystal parallel to the reflecting planes.

## 3.5.2 Peak Broadening due to Lattice Imperfections

The peak broadening is discussed in papers **III-VI**. When the data is corrected for polarization, absorption, and background (mostly air scattering) and when the Lorentz correction and appropriate other factors are accounted for, the peak broadening of the pure XRD line may be treated. In practice, the peak broadening is reliably evaluated only when the instrumental broadening is substantially smaller than the broadening due to the sample itself. Besides effect of crystallite size (Chapter 3.5.1) two appropriate though idealized lattice imperfection types which usually occur in polymers to varying degree.

(1) There are two types of lattice imperfections called the displacement disorder.

The thermal vibrations realise the crystal imperfection of the first kind, *cf.* Equation (3.5.2). The ideal or an ideal average lattice is imagined to exist throughout the crystal but the actual positions of the atoms are slightly displaced from these ideal positions. The displacements of the first kind are usually small compared to the interatomic positions. The crystal imperfection of the first kind may also be a substitutional disorder where some atoms or molecules are replaced by the foreign constituents but this issue is omitted here.

Paracrystallinity represents the second effect of displacement disorder and distortions of the second kind. Originally the paracrystals are introduced by von Hosemann[316], and they are understood as a kind of crystallike objects where unit cell edges and an electron density distribution vary from cell to cell. Self-organized macromolecules, like block-*co*-polymers are often regarded as paracrystals[317]. There is no statistical average of the regular lattice and the long-range order is lost. Paracrystals have, however, a spherically symmetric *a priori* distance statistics of the centres of the smallest units. By comparison the true amorphous matter (see Chapter 3.3.3) shows neither the long ranger order nor three dimensional lattice nor a spherical a priori probability of nearest neighbours. There are no sharp interfaces between the definitions: In the case of the imperfections of first kind the distance between the nearest neighbour atoms fluctuates moderately and the semblance of crystalline order persists to longer distances, *i.e.* the average position of the atoms follow long range crystalline order, while in the paracrystals there is no average lattice present and when the fluctuation is large enough the system is termed liquid instead of paracrystal. Crystals, of course, may also have only a slight perturbation in long range order - the concept is rarely pure. There are several variations of paracrystals, too.

The gaussian displacement disorder reflects a decay of the Ornstein-Zernike type correlation function.

$$\Gamma(r) \sim \exp\left(-\frac{r}{\xi}\right), \tag{3.5.7}$$

where $\xi \approx a/2\pi^2\varepsilon_d^2$. Note that the form of the distribution function is not relevant, however. *Cf.* the formulas of the correlation length, Equations (3.6.6) and (3.6.15).

The line broadening due to the paracrystals has a characteristic dependence on the diffraction order. Here we rely on the concepts of Baltá-Calleja & Vonk[273]. When the distances between the lamellae are assumed to be normal distributed and when $a$ is taken as an average period, the lattice or displacement disorder within the crystals is given by

$$(\Delta q)_d \approx \frac{4\pi^2 \varepsilon_d^2 n^2}{a}, \qquad (3.5.8)$$

where $n$ is the order of a reflection and where a dimensionless parameter $\varepsilon_d \equiv \sigma_d / a$ is the reduced variance of the interplanar separation vector ($\sigma_d$ is the standard deviation) measuring the percential variation in the lattice vectors, see Figure 19.

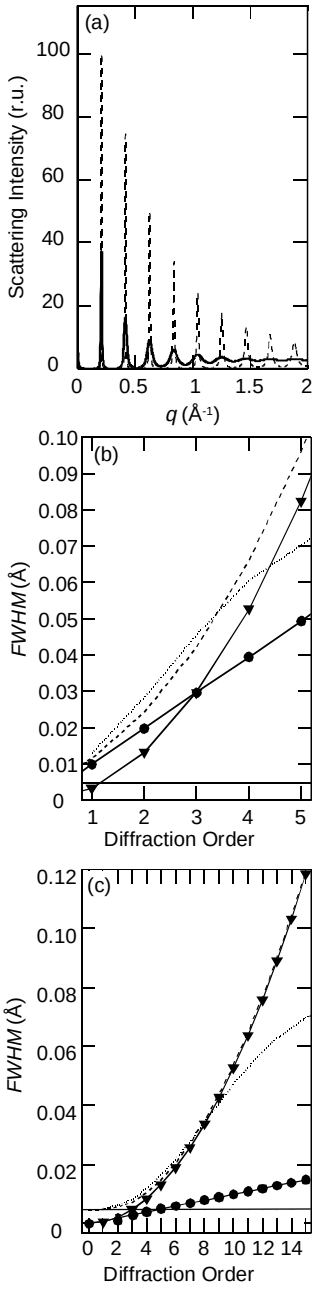


**Figure 19** A calculation of the peak broadening due to the defects in the scattering intensity curve. **(a)** Scattering intensity curve according to Equation (3.5.3) in relative units representing Bragg reflections of lamellar structure, when $\varepsilon_d$ and $\varepsilon_e$ are 5% and 2% (solid line) or 2% and 0.2% (dashed line), respectively. $N$=40, $a$=20. The first selection gives five well-defined diffraction order and more linear reflection full width half maximum (*FWHM*) dependence, as in the case discussed in papers **III-V**, whilst the latter selection is corresponds to that of a model compound, polyethylene[316]. As is the case in peak width analysis, no amorphous component is taken into account. **(b)-(c)** Reflection *FWHM* as a function of diffraction order presenting independent contributions, the effect of crystal size, Equation (3.5.4) $(\Delta q)_s$, (solid line), the effect of paracrystallinity, $(\Delta q)_d$, Equation (3.5.8) (dots), and the effect of microstrains, $(\Delta q)_e$, Equation (3.5.9) (triangles) as well as their combinations, the square root of their sum of squares, $(\Delta q)_t$ Equation (3.5.10) (dashed line) and the *FWHM* of the Gaussian fitting of the each calculated Bragg peak presented at the point (dotted line). Case **(b)** corresponds to that presented as a straight line in the point **(a)** and case **(c)** that presented as a dashed line. The microstrains are dominant in the case **(b**) (*Cf.* papers **III-V**) and paracrystallinity in the case **(c)**. Note that the sum of square of the distinct components is a good approximation for small $n$ yielding slightly smaller values than those of calculated from the intensity curve. This should be case for every $n$. However, as seen in point **(a)** for larger $n$, the Bragg reflections become somewhat blurred because of the tails of the neighbour peaks and the simply determination of *FWHM* for every peak without subtracting the contribution of the tails yield too small *FWHM* values. This error may be treated using Warren Averbach method.

(2) The effect of lattice parameter fluctuations are realized in the microstrains. Microstrains may be caused by rapid cooling of the specimen. This is discussed in the papers **III-VI**. Instead of paracrystals, microstrains do not perturb the long range order.

Ideally the line broadening due to the microstrains has linear dependence on the diffraction order. The fluctuation of lattice parameters from crystals to crystals is

$$(\Delta q)_e \approx \frac{4\pi\sqrt{2\ln 2}\,\varepsilon_e n}{a}, \qquad (3.5.9)$$

where $\varepsilon_e$ is the reduced variance of each lattice parameter in each crystal, see Figure 19.

(3) Combination of the effects. The discussed effects naturally coexist and the combination of their effect on the line broadening may be in the first instance approximated by the sum of square rule

$$(\Delta q)_t^2 = (\Delta q)_s^2 + (\Delta q)_d^2 + (\Delta q)_e^2, \qquad (3.5.10)$$

which is illustrated in Figure 19. This is a good estimation if the fluctuations are small and when nothing but a few first diffraction orders are considered. There are generally few works, like that of Prosa *et al.*[234], where *e.g.* PATs show as many as 5 diffraction orders. Papers **III** and **V** present 5 diffraction orders, too.

The discussion above gives the qualitative understanding to the peak broadening for mesomorphic lamellae. Moreover, state-of-the-art peak analysis of synthetic high polymers[273] and self-organized hairy-rodlike polymers[234] is discussed in the terms of Warren-Averbach method used for metal alloys[318], based on Fourier transformation or Fourier series expansion of the reflections. The peak broadening due to the dislocations that is indistinguishable from paracrystallinity can be dealt with.

There are several variations of Warren-Averbach method. In short, the "basic form" of the method takes each reflection separately having the origin at the reflection center and assumes that each profile is a convolution of the crystal size and the distortion contribution. This assumption is valid for small $q$ when the zeroth order reflection is approximated by disregarding the exponent term in $S(q)$ which leads to the peak broadening for large $q$, *cf.* Equation (3.5.3). When the function is considered near to the each reflection order $q = 2\pi n/a + q'$ the exponential term containing $q'$ is left out resulting in a series expansion of the $n$:th (sufficiently sharp) reflection

$$I(q') = 1 + 2\sum_{m=1}^{N-1} \frac{N-m}{N} \exp\left(-2\pi^2 n^2 \left(\sigma_d^2 m + \sigma_e^2 m^2\right)\right) \cos\left(q' m a\right). \tag{3.5.11}$$

The first factor $(N-m)/N \equiv A_m^o$ is related to the crystallite size, whilst the latter part, the exponent factor, describes the distortion and lattice parameter fluctuations. Although this form of the first factor is directly related to the lamellar model and $N$ lamellar planes, the term is generally the overlap volume for the crystal and its ghost shifted by $m$ Bragg distances (of the lowest order reflection) in the normal direction to the Bragg planes. The $m$:th Fourier coefficient of $n$:th reflection is

$$A_m(n) = A_m^o \exp\left(-2\pi^2 n^2 \left(\sigma_d^2 m + \sigma_e^2 m^2\right)\right), \tag{3.5.12}$$

and the logarithms of coefficients are plotted against the square of the diffraction order $n^2$

$$\ln A_m(n) = \ln A_m^o - 2\pi^2 n^2 \left(\sigma_d^2 m + \sigma_e^2 m^2\right). \tag{3.5.13}$$

The slope of the curve, Equation (3.5.13), is determined for every Fourier coefficient $m$ and the slopes are plotted as a function of $m$ in order to distinguish the contributions from paracrystallinity and microstrains. The crystal size is obtained from the intercepts of the plots by extrapolating $A_m^o$ or from the slope of the curve at small values[268]

$$\frac{dA_m^o}{dm} = -\frac{1}{N}. \tag{3.5.14}$$

The Fourier coefficients are obtained from the integral

$$A_m(n) = \int_{-\pi/a}^{\pi/a} dq' I(q') \cos\left(q' m a\right). \tag{3.5.15}$$

Before the use of method the background is subtracted and the tails are added to the reflections and the tails of the other reflections are removed, which can be done using preliminary fitting of s.c. pseudo-Voigt functions, for example, to describe both the peaks and the background[234]. Since the integrated intensities of the diffraction peaks are dependent on the structure factor and conditions, the Fourier coefficients for different diffraction orders are normalized to be comparable by scaling the coefficients of each reflection so that the zeroth order coefficient is unity $A_0(n) = 1$.

# 3.6 Small-Angle Scattering

## 3.6.1 Applicability of Small-Angle Scattering

Small-angle X-ray scattering (SAXS) combined with wide-angle X-ray scattering (WAXS) is the primary investigation method of this thesis. Small-angle scattering (SAS)[271,272,275] is used to study relatively large structures and noncrystalline materials. The size of these objects is of the order of 10 Å or larger and information is obtained using either X-rays or neutrons at low detection angles, typically $2\theta$ less than $2^{o}$. In practice, X-ray scattering studies are divided into two categories. There are studies of the short range order accomplished via the determination of the radial distribution function (RDF) [268,270,302] (Chapter 3.3.3) and the studies of the larger density fluctuations[21]. Amorphous materials, such as liquids, glasses, or glassy polymers barely reveal sharp diffraction maxima, while the stronger scattering effects are present in multicomponent materials, such as polymer blends, or single-component materials with well-defined molecular segments, such as block-*co* -polymers. On the other hand, while X-rays give high intensity and high energy and angular resolution, neutrons provide advantages based on the scattering event from the nuclei instead of core electrons, the lower kinetic energy of particles (~10 meV) compared with the energy of hard X-ray photons (~10 keV), and the magnetic moment of the neutron. Due to the time associated with the wave period being of the order of time period of atomic movements, neutrons give information on atomic and molecular motions and unpaired electrons of certain atoms.

This work is limited to SAXS, which requires both specific experimental method of measuring and that of analysis: First, the standard arrangement of SAXS utilizes transmission geometry, whilst grazing-incidence, GISAXS, is used for thin films. The first geometry is used in the papers **I**, **III-V**, and **VII**, while the latter geometry but GIXD, rather than GISAXS, is utilized partly in the paper **V** and solely in the papers **II** and **VI**. Secondly, since the intensity of the primary beam is much higher than that of scattered beam even a minor tail can seriously disturb the detection of the observed scattering. This is particularly realized for SAXS, because neither the tail of the primary beam nor the considered reflections extend out to wider angles. Also, due to the low order of the typical samples, the SAS reflections are inherently weak. Thirdly, the high angle-resolution needed distinguishes SAXS from the most diffraction studies. For these reasons careful collimation and large distance between sample and detector are essential requirements.

There are four prototype systems that are widely studied using SAXS.

(i) In dilute particulate system polymers, colloids etc. are uniformly dispersed in the second material. The system is assumed to be sufficiently dilute so the positions of the particles are uncorrelated. There is no difference between classical particle-solvent pairs and particle-solvent pairs with supramolecular interactions but the scaling laws and the treatment of SAS are generally valid.

(ii) In the nonparticulate two-phase system two materials are also randomly mixed but neither of them is considered the host or dispersed matrix. An archetype of such system is a blend of two immicible polymers. Also, typical semiflexible and semicrystalline polymers form irregular matrix of crystalline and amorphous domains. Hence, such two-phase system can actually contain only one kind of molecules. The crystallinity distribution of semicrystalline polymers has an effect on SAXS[320] provided that the size of the crystallites corresponds to the *q*-range measured by SAS.

(iii) In a soluble blend two components are dissolved molecularly in the thermodynamic sense. Here misciple polymer blends or isotropic disordered block-*co*-polymers are illustrative examples. The boundary between a dilute particulate system and a soluble blend is not well-defined. If the shape and size of the particle is the main interest, the theory of the dilute particular system is appropriate, whereas the approach of the soluble blend is convenient for discussion of the thermodynamic properties. Resembling system is discussed in the paper **VII**.

(iv) In a periodic system the macromolecules form well-defined microstructures of the order of nanometers. The prototypes are hierarchical biological molecules, such as collagen, or amphiphiles, such as silver behenate, both used as calibration samples for SAS. This case is dealt with in all the papers **I-VII**. In such case the usual XRD analysis (WAXS) is more or less applicable, even if the standard experimental arrangement is very different. The degree of the order is often much below that of crystals and the effects of the lattice imperfections (Chapter 3.5.2) are a particular focus of interest. Some additional assumptions of the sample or the problem are usually made, too. The details of the size of less than 10 Å are many times ignored, for instance. Hierarchical systems, like those in the present work, are important exceptions.

[21] Using high energy (80 keV) flux it is also possible to use transmission geometry in order to study the local structure of amorphous materials and reach an atomic level resolution but this is rather unusual. See *e.g.* ref. 319.

WAXS, too, is important in the papers **III-V**. The periods of interests are small compared to those of *e.g.* block-*co*-polymers studied using 'pure' SAXS. Although the size of the discussed structures is clearly over 10 Å, the reflections distributed over large *q*-range give decisive information. The distinction between the considered scattering angles is blurred and may also be unnecessary. SAXS/WAXS just forms one tool in the context, where the hierarchy is probed from intramolecular to several intermolecular levels and finally to the level of the macroscopic alignment. Also experimentally, SAXS/WAXS[321-324] used in this thesis form a sole facility where one sample and one transmission geometry though two detectors *in-situ* were used. This justifies the used approach in many instances and makes the combined use a powerful tool.

## 3.6.2 The Assumptions of Small-Angle Scattering

The two basic assumptions of the general treatment of the SAS, not bound to the existence of well-defined objects occur for all heterogeneities in the colloidal range.

(i) The statistical isotropy in the system arising from the structure itself or some change, like rotation of the particles, in time. This means that the autocorrelation, Equation (3.1.22), in reciprocal space depends only on the magnitude of the distance albeit this does not hold for the electron density or the scattering length density in ordinary space. Consequently, the phase factor can be replaced by its average as stated in the fundamental formula by Debye[325]

$$\left\langle e^{-i\bar{q}\cdot\bar{r}} \right\rangle = \frac{\sin qr}{qr} . \tag{3.6.1}$$

The Debye formula is not restricted to any scattering angle region but is valid for all isotropic scatterers. Accordingly, the scattering intensity, Equation (3.1.20), for the continuous 2-phase "polymer and matrix" system is

$$I(q) = \int_{V_1}\int_{V_2} \rho(\bar{r}_1)\rho(\bar{r}_2)\frac{\sin qr}{qr} dV_1 dV_2 , \tag{3.6.2}$$

where $r = |\bar{r}_1 - \bar{r}_2|$ is the distance between the scatterers.

(ii) The lack of long-range order that is to say no correlation between two points separated far enough. This requirement has a connection to the treatment of correlation function (Chapter 3.6.3).

## 3.6.3 Correlation Functions in Small/Wide-Angle Scattering

As most of physical experiments, the scattering experiments, especially those at low scattering angle, are mostly discussed in the terms of correlation or response functions, of one kind or another. They afford the convenient vehicle to bridge the gap between the local and macroscopic description.

The common correlation function of the form of Ornstein and Zernike[326], Γ, is thought to be a (order) parameter which measures the persistence of memory without strict physical interpretation. In real space the correlation function is related to the order parameter density *m* as

$$\Gamma(\bar{r}) = \langle m(\bar{r})m(0)\rangle - \langle m(\bar{r})\rangle\langle m(0)\rangle , \tag{3.6.3}$$

where the parentheses denote ensemble average. A translationally invariant system with isotropic fluctuations (no intrinsic direction) is considered. The lowest order approximation of the series form of the free energy of the system may be given by

$$G = \int d^3r \left[ c_1 |\nabla m(\bar{r})|^2 + c_2 m^2(\bar{r}) \right] = \int \frac{d^3k}{(2\pi)^3} \left( c_1 k^2 + c_2 \right) |m(\bar{k})|^2 = \int \frac{d^3k}{(2\pi)^3} G(\bar{k}) , \tag{3.6.4}$$

where the latter part is the Fourier transform of the first part and where $m(\bar{r})$ and $m(\bar{k})$ form a Fourier pair. If the average value of the free energy residing in the Fourier mode is $k_B T$, the correlation function in the reciprocal space, a Fourier pair of $\Gamma(\bar{r})$ is

$$\Gamma(\bar{k}) = \left\langle |m(\bar{k})|^2 \right\rangle = \frac{k_B T}{c_1 k^2 + c_2} , \tag{3.6.5}$$

where $k_B$ is the Boltzmann constant, $T$ temperature, and $c_1$, $c_2$ parameters which may depend on temperature. The correlation function in the real space is obtained as

$$\Gamma(\bar{r}) = r^{-P} \exp\left(-\frac{r}{\xi}\right), \tag{3.6.6}$$

where $\xi = \sqrt{c_1 / c_2}$ is the correlation length and $P = d - 2$, where $d$ is the dimension of the system.

It is too simple to talk about just correlation length but it may be related to density, conformation, or orientation, for instance. The form above, however, may be a kind of generic start[327] to describe various electronic or liquid crystalline systems related to the scalable phenomena in matter in the first instance. In principle, characteristic decay of Equation (3.6.6) is seen in the papers **III-V**, too.

For practical purposes we may start from the assumption (ii) presented in the previous Chapter. Since the auto-correlation, Equation (3.1.22), tends from its initial value (maximum) toward a constant and because of the requirement of no long-range order this constant is achieved for a finite distance, the structure is described by a finite region only. The rest contains no information. This means that a constant value through the total volume makes on contribution (except at zero angle not accessible by the experiments). For this reason it is convenient to consider (electron) and scattering density fluctuations rather than the density itself and redefine the auto-correlation[22] as

$$\Gamma_\eta(\bar{r}) = \Gamma_p(\bar{r}) - V\bar{\rho}^2 = V\gamma(\bar{r}). \tag{3.6.7}$$

The average of the product of two fluctuations is the correlation function (of small-angle scattering) $\gamma$ so defined and with the following general property:

$$\gamma(\bar{r}) = \langle \eta(r_1)\eta(r_2) \rangle, \tag{3.6.8}$$

where $\gamma(0) = \overline{\eta^2}$, and $\gamma = 0$ for larger $r$. The assumption (ii) (Chapter 3.6.2) requires that $\gamma$ is zero for the finite, colloidal $r$. This does not fail even for the prototype (iv) of Chapter 3.6.1.

By the help of Debye form of the phase factor (Equation (3.6.1)) and Equation (3.6.7) related to the Equation (3.1.22) the scattering intensity can be written in the form of Debye and Bueche[328]

$$I(q) = V\int_0^\infty 4\pi r^2 \gamma(r) \frac{\sin qr}{qr} dr. \tag{3.6.9}$$

The intensity is then an extrapolated rather than measurable value corresponding to the square of the total number of the irradiated electrons in the scattering volume $V$. In other words, it is interpreted in the case where each electron in the volume $V$ acts in coherence in the region defined by $\gamma$ yielding

$$I(0) = V\int_0^\infty 4\pi r^2 \gamma(r) dr \quad \text{for } q \to 0. \tag{3.6.10}$$

The correlation function is obtained by the inverse Fourier transform of that

$$\gamma(r) = \frac{1}{V}\frac{1}{2\pi^2}\int_0^\infty q^2 I(q) \frac{\sin qr}{qr} dq. \tag{3.6.11}$$

This corresponds to the invariant concept, Equation (3.1.23) in its original formulation. This means that though the intensity pattern is altered upon the shift of the system the mean square fluctuation of the electron density directly related to $\gamma(0)$ remains unchanged implying

$$\gamma(0) = \frac{1}{V}\frac{1}{2\pi^2}\int_0^\infty q^2 I(q) dq = \overline{\eta^2} = \frac{1}{V}Q \quad \text{for } r \to 0, \tag{3.6.12}$$

when the Debye formula is unity.

The general feature of the autocorrelation is that the scattering length density is twice included in the integral. If we consider the case of two phase regions (like in paper **V**) with different $\rho$ it does not matter

---

[22] Porod's original notation[271] is $\tilde{\eta}^2 = \tilde{\rho}^2 - V\bar{\rho}^2 = V\gamma(\bar{r})$ while the presented one is widely used in XRD context[277].

which one of the particular domains has which $\rho$, but the autocorrelation and thus the scattered intensity takes the same form. This feature corresponds to the Babinet's principle in optical diffraction. The fractions of the components do not matter either. If we denote them by $\varphi_1$ $\varphi_2$, the average (scattering length density) electron density is $\bar{\rho} = \varphi_1\rho_1 + \varphi_2\rho_2$, which is directly related to the mean square fluctuation and thus the invariant of the system so that

$$\overline{\eta^2} \equiv \left\langle (\rho - \bar{\rho})^2 \right\rangle = (\rho_1 - \rho_2)^2 \varphi_1\varphi_2 = \frac{1}{V} Q \,. \tag{3.6.13}$$

Hence, the Babinet's principle holds and also it is true that a constant $\bar{\rho}$ throughout the volume has no effect on scattering features and, as discussed earlier, may be subtracted. This fact makes it difficult to say, for instance, whether the substructure in lamellae seen in the fluctuation of $\gamma$ along the **x** axis (paper **V**) originates from the PPY part or side chain part of the matter. On the other hand, if the scattering length densities of the fractions are known, for instance based on the chemical composition, and if the scattering measurements are made in absolute units, the invariant can provide the relative amounts of the two phases.

There are several alternative formulations for the correlation function concepts for SAS and instead of the introduced Porod's original notation, a somewhat different formulation introduced by Baltá-Calleja and Vonk[273] was utilized in papers **III-V**. We still continue to denote autocorrelation using capital lambda while in their reference it refers to the three-dimensional correlation function and gamma to the one-dimensional one.

The correlation function is defined as the quotient of the autocorrelation and that for $\bar{r} = 0$ as

$$\gamma(\bar{r}) = \frac{\Gamma_p(\bar{r})}{\Gamma_p(0)} = \frac{\int \rho(\bar{u})\rho(\bar{u} + \bar{r})d\bar{u}}{\int \rho^2(\bar{r})d\bar{u}} = \frac{\langle \rho(\bar{u})\rho(\bar{u}') \rangle V}{\langle \rho^2 \rangle V} \,, \tag{3.6.14}$$

where $\gamma(0) = 1$. The correlation length is the integral breadth of the correlation function as

$$\xi = 2\int_0^\infty \gamma(r)dr \,. \tag{3.6.15}$$

Although the correlation function by itself does not provide any new physics (after the intensity), it is particularly useful when illustrating the relative and directional order of microphase separated matter giving such good tool to make the LC interplay between ordered crystal and disordered liquid - which is just one of the essences of this thesis - more concrete. In particular, as pointed out by Baltá-Calleja and Vonk[273] it has a number of applications in the cases, like lamellae stacks that realize electron density variations in one direction. Usually the order in such systems is so poor that the correlation function dies rapidly and its resolution is not good enough to make the detailed *three*-dimensional interpretation possible.

For the system considered in papers **III-V**, the one-dimensional linear normalized correlation function of ref. 273, defined as

$$\gamma(r) = \frac{\int dq q^2 I(q)\cos(qr)}{\int dq q^2 I(q)} \,, \tag{3.6.16}$$

where the decay of Equation (3.6.6) is seen, is being used in a form

$$\gamma_j(r) = \frac{\int dq_j q_j^2 I_j(q_j)\cos(q_j r)}{\int dq_j q_j^2 I_j(q_j)} \,, \tag{3.6.17}$$

where *j*=x, y, or z, where this has the value 1 at the origin, and where the intensity is

$$I_j = I(q_j) - I_{iso}(q_j) \,, \tag{3.6.18}$$

where $I_{Iso}(q_j)$ is in turn the isotropic intensity due to the amorphous matter and *r* is the (scalar) distance. Mesomorphic material may contain aligned and nonaligned crystalline component and amorphous isotropic but also amorphous aligned component.

As described in the theoretical background in the paper **VII**, the self-organization in the supramolecular hairy rods are treated as if they are rod-coil block-*co*-polymers. On the other hand, we consider the correlation function of Equation (3.6.17) in paper **V** and it differs from those calculated to block-*co*-polymers. Even the strong segregated materials of sharp two-domain interface may not allow such ideality in the triangular shape which is seen in papers **III-IV** and paper **V**. In short, the order in microphase separated domains -a coherence length with respect to the period- is considerably better, a fact which is also seen in the high number of the repeat distances obtained from the peak-width/position ratio.

A good resolution allows us to recognize the impact of the suggestive features in *three* dimensions: Lamellae with long range order as well as shorter range order due to the components of the layers in normal direction; well-ordered stacks in equatorial direction; and finally, in the meridional direction. The meridional component of less ordered (with respect to the other chains) and monomer units are 'modulated' by component suggestively arising from two monomer units and one CSA, which is plausible, because nominally every second monomer was protonated. This shows a combination of three-dimensional local and overall order of hairy-rodlike supramolecule of π-conjugated polymer which is fluidlike also at low temperatures and consequently less ordered in the direction of the rodlike polymer backbone.

## 3.6.4 Scattering Intensity Curve

When employing broader angle region, ultimately SAXS/WAXS (papers **III-V**) it is the asymptotic power law- behaviour of the scattering intensity not only the magnitude and direction of the scattering vector of Bragg peaks which contain the information. Simultaneously, the scattering arises both from the well-defined and less ordered objects and in very different length scales so the characteristics of the entire scattering curve are worth strictly keeping in mind.

An archetype is illustrated in Figure 20. A plateau, Guinier characteristics (*cf.* page 50) is observed when approaching the infinite particle size region near the zero angle. At very wide angles the contribution of individual atoms are seen and the intensity, again, barely depends on the scattering angle.

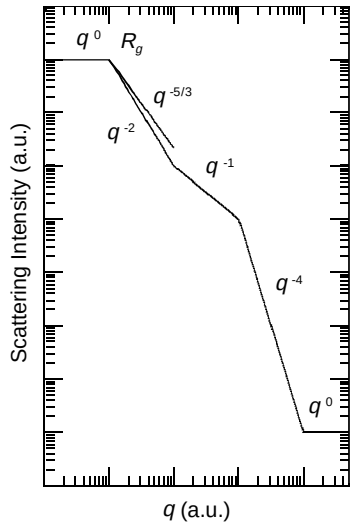


**Figure 20** The schematics of asymptotic behavior of the scattering intensity. The power laws for a polymer system appear as straight segments in a double-logarithmic plot. The different regions are related to the molecular mass (power zero), Gaussian chain (power minus two), expanded chain (power minus five to three), rodlike molecule (power minus one), thickness of the molecule (power minus four), and single atoms (power zero), respectively. $R_g$ refers to the region where the radius of gyration may be determined.

When the thickness of the polymer dominates a characteristic $q^{-4}$ of three dimensional objects is seen. Besides SAS, this is seen in reflectivity curves in paper **VI** and in Chapter 3.4. The one-dimensional rod leads to the minus one characteristic. The increasing size leads ultimately to the bending and for example Gaussian distributed (monomers and) chain[137,185] with power minus two curve. Excluded volume effect is related to the minus five to three curve.

The asymptotic behaviour (Figure 20) is an idealisation related to the shape and number of the different levels of organization. The transition points between the regions are not as clear cut as in the schematics. Nonetheless, when successful they probe the fundamental scaling of the less defined regions in polymeric matter[185]. *E.g.* the differences from $q^{-4}$ behavor are directly related to the dimension (euclidian or fractal) in matter. The scaling of the well-defined structures, like a long period as function of the number of the monomers is in turn based on the magnitudes of the scattering vector of the well-defined peaks. An example related to the present work is performed in ref. 199.

*First Part of the Scattering Curve*

The first part of the SAS curve concerns particle scattering of a dilute particulate system. This is important for π-conjugated polymers: As discussed in paper **V**, the strict dissolution of rodlike polymers is a subtle and the visually clear solution[137,329] can actually reveal an effect of dense packing. The stiffness of the chain and the excitations may be studied in the different forms of solutions (Chapter 4.2.3).

The particles are thought to be embedded in a continuous matrix and assumed to lack all internal structure. Therefore, (Chapter 3.6.3) the scattering length density $\rho(r)$ can be replaced by the *excess* of the scattering length density $\eta$(r) in the particle over the average $\langle\rho\rangle = \rho(r) - \eta(r)$. The average $\langle\rho\rangle$ is essentially same as the scattering length density of the background. For vacuum, $\eta$(r) equals to $\rho(r)$ and is here denoted in that way, *i.e.* $\rho(r)$ stands for the excess scattering length density in the particle.

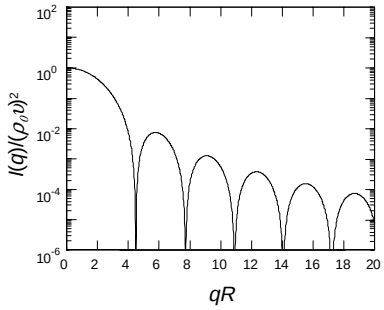


**Figure 21** Calculated single particle scattering intensity for a solid sphere calculated from Equation (3.6.19). The minima occur, when $qR = \tan(qR)$, which corresponds to the values $qR$ = 4.49, 7.73, 10.9, 14.1 …≅ (2$k$+1)π/2. The maxima correspond to the values $qR$ = 5.76, 9.10, 12.32, 15.51 …≅ $k\pi$ ; $k$ are integers. $\rho_0\upsilon$ is the total scattering length of the particle, i.e. the sum of the scattering length of all segments (atoms etc.) in the particle. Scattering intensity is proportional to its square.

For a solid sphere of radius $R$ with a uniform density $\rho_0$ [ $\rho(r) = \rho_0$ for $R \geq$ r, and $\rho(r) = 0$ otherwise] Fourier transform, the assumption of the isotropic sample, the intensity is

$$I(q) = \rho_0^2 \upsilon^2 \frac{9(\sin qR - qR\cos(qR))^2}{(qR)^6}, \qquad (3.6.19)$$

where $\upsilon = (4/3)\pi R^3$ is the volume of the sample. This result, the scattering intensity of independent scatterers in an uniform matrix introduced by Rayleigh[330], is one of the fundamental curves of SAS, illustrated in Figure 21. According to Porod[271] even Equation (3.6.19) illustrates all the common features of the SAS pattern arising from not too anisotropic particles. The oscillatory character, zero points, is due to the specific symmetry. The central peak is due to the all secondary waves in phase and simply added at $q \to 0$. Therefore, the amplitude equals the number of the excess electrons ($\Delta n_e$)

$$\text{single particle } I_1(0) = (\Delta\rho)^2 V^2 = (\Delta n_e)^2, \qquad (3.6.20)$$

and the subsequent maxima implement the periodic variation of the intensity[23]. However, in paper **V** we study anisotropic material and the spherical approximation fails. In contrast, for thin rod of length $L$ and cross-sectional area $a$ the intensity is given as

$$I(q) = \rho_0^2 \upsilon^2 \left( \frac{2}{qL\cos\Theta} \right)^2 \sin^2\left( \frac{qL}{2}\cos\Theta \right), \qquad (3.6.21)$$

where $a$ is assumed to be very small compared with to $L$. The rod is considered a thin line with a scattering length density $\rho_0\upsilon$ per unit length concentrated on the axis. The origin is located at the center of the rod and the angle between its axis and vector $q$ is Θ and $q \cdot r = qr\cos\Theta$ .The average of Equation (3.6.21) for all orientations, originally given by Neugebauer and discussed by Kirste and Oberthür[331], is given by

$$I(q) = \rho_0^2 \upsilon^2 \frac{1}{2}\int_0^\pi \left( \frac{2}{qL\cos\Theta} \right)^2 \sin^2\left( \frac{qL}{2}\cos\Theta \right)\sin\Theta d\Theta = \rho_0^2 \upsilon^2 \frac{2}{qL}\left[ Si(qL) - \frac{1-\cos qL}{qL} \right], \qquad (3.6.22)$$

where $Si(x) = \int_0^x \frac{\sin u}{u} du$ . Furthermore, Kratky and Porod derived similar expression for a circular disc[332]

[23] The intensity of a sphere is not strictly periodic, because $I(q+T) = I(q)$ , where $T$ is the period, does not hold.

$$I(q) = \rho_o^2 \upsilon^2 \frac{2}{q^2 R^2}\left[1 - \frac{J_1(2qR)}{qR}\right], \quad (3.6.23)$$

where $J_1(x)$ is the First order Bessel function. A modification of Equation (3.6.22) has been employed in paper **V.** Note that the disc does not necessarily mean a proper disk but rather a 2-D object. As shown in paper **V** *e.g.* PPY(CSA) reveals disklike behaviour in solution.

*Guinier Law*

The first part of the scattering curve, also known as Guinier region, realizes the Guinier law given by

$$I(q) = \rho_o^2 \upsilon^2 \exp\left(-\frac{1}{3} q^2 R_g^2\right), \quad (3.6.24)$$

where *Rg* is the radius of the gyration of particle[24] and where $\upsilon$ is the volume of the particle. The Guinier law[275] holds when $q << 1/R_g$, the system is dilute, *i.e.* the particles in the system scatters independently of each other, the system is isotropic, *i.e.* the particles reveal random orientations, and the internal structure of the matrix can be ignored, its density is constant giving no effect in considered *q* range. The Guinier law is universal on these conditions. It is valid even if the shape of the particle is unknown, irregular or complex. When the logarithm of $I(q)$ is plotted agains $q^2$ the initial slope yields $(1/3)R_g^2$. The intensity in Equation (3.6.24) is the average intensity per particle, whereas it is the intensity of all particles is measured. Since the particles are assumed to be independent in uniform matrix without an internal structure, the measured intensity is the sum over all particles

$$I_{measured}(q) = NI(q), \quad (3.6.25)$$

where $N=cV/N_AM$; $c$ is the concentration, total mass of particles per total volume of solution, $V$ the volume of the sample in beam, $N_A$ the Avogadro number, and $M$ the molar mass, typically known from the GPC. If the intensity is known in relative units (in practice counts per second), the radius of gyration is directly determined using the slope of and the first term in the right part of the equation is simply regarded to meaningless constant. The radius of the gyration is then related with the physical radius. Moreover, the use of absolute units makes the determination of $\rho_0 \upsilon$ possible, becasue $I_{measured}(0)/N = I(0) = \rho_0^2 \upsilon^2$ where scattering length density in the particle $\rho_0$ is known from the chemical structure of the simple polymers in common solvents[333]. When the intensity is determined in absolute units, the concentration of the particles in the scattering volume and thus $N$ has to be taken into account.

The intensity is regarded as independent *i.e.* the particles in the system scatter independently. In practice, this means very dilute liquid solution of particles dissolved to the solvent matrix. The concentration is dependent on the molecular character. PPY, rrPPY, and PmPy, and that of the CSA doped PPY were studied in solution down to the concentration of 5 mg/ml. The experimental problem was the weak and noisy signal arising from the more dilute solutions and it may be that the polymers do not form system of independent scatterers even at the lowest measurable concentration. Therefore, the measurements reflect guiding tendencies. See further discussion in paper **V**. The consideration of the transition point between the Guinier region seen as a plateau at smallest angles in the double-logarithmic plots was done.

The matrix is assumed to be devoid of any internal structure revealing uniform randomly distributed background. In real dispersions, there are always some inhomogeneities based on atomic and molecular clusters, which yield some phase coherence of the waves scattered from the solvent molecules. These inhomogenities can be ignored, when their size scale is much smaller than $1/q$ and they do not result in effects at the discussed *q*-range. In addition, it is assumed that the solvent is not only uniform but also its different molecular orientations are randomly distributed.

When the sample fulfills the discussed conditions, the size of the particle can be determined from the measured intensity curve that is function of the radius of gyration and the particle volume. Real material consists of nonidentical particles and the Guinier law can be modified, if the particle density is not dependent on the particle size. The scattering from the different particles is still assumed to be uncorrelated and the expression for the intensity is given as

---

[24] $R_g^2 = \frac{\int r^2 \rho(r) dr}{\int \rho(r) dr}$ When the particle length density is constant, $R_g^2 = \frac{1}{\upsilon}\int r^2 \sigma(r) dr$ so that $\sigma(r)$ equal to 1 in particle, 0 otherwise.

$$I(q) = \frac{1}{N}\rho_0^2 \sum_j N_j v_j^2 \left[1 - \frac{1}{3}q^2 R_{gj}^2 + ...\right] = \frac{1}{N}\rho_0^2 \left(\sum_j N_j v_j^2\right)\left[1 - \frac{1}{3}q^2 \frac{\sum_j N_j v_{j2}^2 R_{gj}^2}{\sum_j N_j v_j^2} + ...\right], \quad (3.6.26)$$

where *Wj* is the mass of *j*:th size particle. Because particles are assumed to be uniform, *Wj* is proportional to the particle volume of *j*:th size particle. Recognizing the number average of the square of the particle volume and the *z*-average of square of the radius of gyration, the Guinier law for nonidentical particles is

$$I(q) = \rho_0^2 \left\langle v^2 \right\rangle_n \exp\left(-\frac{1}{3}q^2 \left\langle R_g^2 \right\rangle_z\right), \quad (3.6.27)$$

where the density of the particle is assumed to be constant. Nevertheless, end-to-end distance of an Gaussian coil scales as $N1^{/2}$ and volume as $N^{3/2}$ and the density as $N/V \sim N^{-1/2}$, and thus the average scattering length density depends on the particle size. Volume and solvent interactions make the situation more complicated and the validity of this approximation must be thought in care.

*Central Parts of the Scattering Curve*

The central part of the scattering curve (Figure 20) is related to the character of the macromolecule and it is distinguished from the both other regions giving important parameters.

The discussion on the regions in the middle utilizes the correlation function $\gamma(\bar{r})$ (Chapter 3.6.3) and equations therein. The scattering length (electron) density is assumed to be a constant and the correlation function is separated as $\gamma(r) = (\Delta\rho)^2 \gamma_o(r)$, where $\gamma_o(0) = 1$ is a normalization and $\gamma_o(r \geq D) = 0$. *D* is the largest dimension of the particles[271]. The correlation function $\gamma_o(r)$ is related to the geometry of particle only and vanishes for $r \geq D$. The physical meaning of $\gamma_o$ is described intuitively by the particle shifted by a vector *r* and illustrated in Figure 26. The volume $\hat{V}$ in common with the particle and its "ghost" comprises all the points that give a contribution to $\gamma_o(r)$. An average over all direction of *r* yieds

$$\gamma_o(r) = \left\langle \hat{V}(r) \right\rangle / V . \quad (3.6.28)$$

Then the particle is cut into rods of varying length, *l*, called chords along the lines of equal spacing. The group of chords for all directions is described by a distribution function $G(l)$ where $G(l)dl$ is the probability of a random chord to be between *l* and *l+dl*. Each chord with $l > r$ has a piece *l-r* which is included in $\hat{V}$. The chord distribution $G(l)$ is equivalent to the correlation function $\gamma_o(r)$ implying the relations

$$\gamma_o(r) = \frac{1}{\bar{l}} \int_r^D (l - r) G(l) dl \text{ , where } \bar{l} = \int_0^D l G(l) dl \text{ , and} \quad (3.6.29)$$

$$G(r) = \bar{l} \int_r^D \frac{d^2 \gamma_o(r)}{dr^2} . \quad (3.6.30)$$

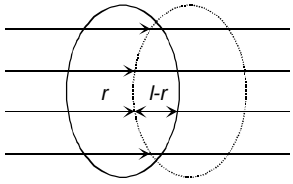


**Figure 22** Particle and ghost. The lines are of equal spacing and the rods of varying length *l* are called chords or intersection lengths.

Then Equations (3.6.9) and (3.6.30) yield the scattering intensity and the correlation function as

$$I_1(q) = (\Delta\rho)^2 V \int_0^D 4\pi r^2 \gamma_o(r) \frac{\sin qr}{qr} dr , \quad (3.6.31)$$

$$\gamma_o(r) = \frac{1}{(\Delta\rho)^2 V} \frac{1}{2\pi^2} \int_0^\infty q^2 I_1(q) \frac{\sin qr}{qr} dq . \quad (3.6.32)$$

The normalized correlation function $\gamma_o(r)$ equals the volume of the particle as

$$V = \int_0^D 4\pi r^2 \gamma_o(r) dr . \quad (3.6.33)$$

Given the invariant *Q*, Equation (3.6.12), the volume takes the form $V = 2\pi^2 I_1(0)/Q_1$, so the volume of the particle can be derived from the diffraction pattern alone. The correlation length, on the other hand, is

$$\xi \equiv 2\int_0^D \gamma_o(r)dr = \frac{\overline{l^2}}{\overline{l}} = \frac{1}{Q_1}\pi\int_0^\infty I_1(q)qdq\,, \tag{3.6.34}$$

being the weight average of a chord. If the lines are drawn in all directions, the number average $\overline{r_1}$ of the chords equals the correlation length and it can be derived from the intensity. The scattering intensity of the central part is in turn deduced from a power series of Debye factor as

$$I_1(q) = \underbrace{(\Delta\rho)^2 V}_{(\Delta n_e)^2}\int_0^D 4\pi r^2 dr\gamma_o\left(1-\frac{q^2r^2}{3!}+\frac{q^4r^4}{5!}-...\right) = (\Delta n_e)^2\left(1-\frac{q^2\overline{r^2}}{3!}+\frac{q^4\overline{r^4}}{5!}-...\right), \tag{3.6.35}$$

where $\overline{r^n}$ describes the average differences between the points independently within the particle volume. *E.g.* when the center of mass is taken as a reference point for two random particles, $\overline{r^n} = \overline{(r_1 - r_2)^2} = \overline{r_1^2} + \overline{r_2^2} = 2R^2$ and the relation to the radiuses of gyration is $\overline{r_1^2} = \overline{r_2^2} = R_g^2$.

*Final Slope*

The asymptotic behaviour of the scattering curve at larger *q* is

$$I(q) \sim q^{-\alpha}\,, \tag{3.6.36}$$

which can be shown, because sine, cosine, sine integral, and Bessel function in the intensity Equations 3.6.19, 3.6.21, and 3.6.23 are finite for large *q*. This s.c. Porod's law is an asymptotic form of Equation (3.6.19) for large *q* and it does not hold for a sphere with a uniform density when $\langle\cos 2qR\rangle \neq 0$. It is *independent* on the particle size of randomly oriented particles, when *qd* >> 1, where *d* is an arbitrary dimension. It can be deduced starting from Equation (3.6.9) in spherical coordinates. The application of Porod's law is to determine the surface area of the mass unit[25] but is also gives information about dimensionality. The exponent $\alpha$ is four for three-dimensional (spheres), two for the two dimensional (disks), and one for one-dimensional (rods). For ideal two phase system Porod's law is given by

$$I(q) \to \frac{2\pi(\Delta\rho)^2 S}{q^4}\,, \tag{3.6.37}$$

where *S* is the total interface area of the phases. The 2D objects realize the law

$$I(q) \to \frac{2\pi\sigma_o^2 S}{q^2}\,, \tag{3.6.38}$$

where $\sigma_o$ is the electron density per unit area. Correspondingly, the 1D case is

$$I(q) \to \frac{\pi(\rho_o L)^2}{qL}\,, \tag{3.6.39}$$

where we consider a rod of length *L* and uniform electron density $\rho_o$. Unsurprisingly, the Equations (3.6.38) and (3.6.39), respectively, correspond to scattering curves of PPY(CSA) and PPY in paper **V**.

[25] For the determination of the specific surface Equation (3.1.23) can be employed instead of the measurements of absolute intensity: $S/V = \pi\lim I(q)q^4/Q$.

# 4 Polarized Photoluminescence in the Studies of Soft Nanoscale Condensed Matter

## 4.1 Polarized Light from Aligned Polymers

Polarized PL has been studied in papers **III-IV**, and **VI**. The purpose has been to use optical anisotropy as a probe of axial alignment (and *vice versa*) together with XRD. In principle, every polymer in the material contributes to PL, whether amorphous or crystalline or LC. In contrast, amorphous domains of the same material do not give rise to XRD reflections in the first instance. This makes discussion complicated.

Polarized PL has a conceptual technological importance, too. Polarized light is conventionally formed using isotropic light source and a separate polarized filter. The disadvantage is the reduced intensity due to the filter. Instead, aligned polymeric semiconductors produce polarized light due to aligned transition dipole moments and no additional filters are needed, which increases power efficiency. The lack of filters also itself reduces costs and weight. Organic materials are also light and their preparation is easy. The EL polymers can also be deposited from solution by simple spin-coating and they have usually good thermal and mechanical stability. They allow the full color spectrum due to chemical tuning. The use of PLEDs was first demonstrated in 1990[334], whilst the first polarized PLED made from a stretch-oriented PAT was reported more recently[224].

Aligned π-conjugated molecules show also other anisotropic opto-electronic properties, such as optical dichroism or directional differences in charge carrier mobility[10], independently of the emission. When PPY is blended with a viscoelastic polymer, such as polyvinylalcohol (PVA), this blend can be stretched resulting in optical dichroism[335], which is observed in stretch-oriented PPY/PVA films[105], too, and ascribed to a larger delocalization length of the ordered chains, which lie in the alignment direction.

The rubbed PI layers, prepared using cloth rubbing, polarized ultraviolet light, or hot air, have long been used as standard alignment layers in LCDs[336] where low molecular weight liquid crystals (LMWLCs) are utilized. However, throughout the thesis only the LCPs are dealt with. There are four main methods to aligned polymers for polarized light. (i) Mechanical alignment, (ii) alignment on pretreated substrates (paper **VI**), (iii) LB techniques, and (iv) LC self-assembly and the alignment of LCs (papers **III-IV**). The results of the same alignment are studied in paper **V** and in Chapter 5.4 but using XRD. Also in the case (ii) LCPs are usually required[225]. Two related concepts are (v) luminescent quest molecules in an aligned host matrix and polarizing excitonic energy transfer (EET) [337-340] and (vi) circularly polarized (CP) emission[226,341].

(i) In mechanical stretching or rubbing, a polymer is blended into the viscoelastic host polymer. When the blend is stretched, the rigid polymers are aligned. The soft films tend to relax into an unoriented equilibrium state. Strong rubbing also degrades the polymer. One concept for the fabrication of polarized PLEDs[342] uses PE-MEH-PPV blends prepared by mixing MEH-PPV with UHMW polyethylene in xylene. The solution is poured onto a glass surface where it forms a gel. Films are then tensile drawn, which results in alignment and polarized EL, when the substrate is a hole injector and when these layers have an electron injector deposited on top. It is claimed that this is valid for any solution or gel processing.

(ii) Rubbing of the substrate of the polymer film results in aligned structures[342]. The rubbing substrate cannot be removed after alignment but this is usually not needed. The degree of alignment can reach very high values. PI (paper **VI**) and PTFE are typical choices. PI can be further doped to tune the transport properties. A process for fabricating polarized PLED:s[343] using the friction transfer method is known and this method itself has been patented[344]. In the friction transfer method crystalline materials are grown on a highly oriented PTFE substrate deposited with a second layer. The third, grown layer becomes oriented, *i.e*. the overlayer does not eliminate the orienting ability of the aligned PTFE chains. In polarized PLED, the third layer is an aligned luminant polymer, such as PPP or PPV, and the second layer conducting polymer, such as PEDOT or PANI, used as a charge transport layer. This construction is then deposited with another charge transport layer.

(iii) Some shish-kebab-type polymers align in LB deposition[345]. Due to instability, the films should be cross-linked after deposition, which is generally difficult to combine with alignment, and no such films are reported yet.

(iv) In contrast to the stretched blended materials, the aligned state of LCs represents their thermodynamic equilibrium. LMW LCs can be aligned using flow, electric or magnetic field. Despite the fact that LMW LCs are polarizers in LCDs there are few examples, where they are used as a light source.

In LCPs, the flexible side chains are introduced to the π-conjugated backbone resulting in an LC phase (Chapter 2.2.8, papers **I-VII**). Light emitting LCPs can be aligned using *e.g*. mechanical methods. This methodology has been developed for LC PF[146]. A method of manufacturing polarized polymeric EL

materials is demonstrated for LCPs[346]. This method comprises the use of rubbed PI and LCP, and it is used in paper **VI**. In the prior method, a luminant LCP material with hole and/or electron injecting materials, can be mixed with PI and the composite is aligned like PI itself. This structure is combined with the appropriate electrodes. There are also uniaxially aligned PL LCP, where rubbing substrate has been used[347].

(v) Luminescent guest molecules or polymers are also aligned, when their host matrix is mechanically aligned, which leads to polarized emission with suitable materials. In polarizing EET, luminescent guest molecules, or polymers, are located in an aligned host matrix containing sensitizers. Unpolarized light is absorbed by randomly distributed and randomly oriented sensitizer molecules resulting in excitation, which is passed on to the aligned guests and recombined, leading to polarized emission. If both guest and host belong to the LMW LCs, this structure can be sandwiched and switched by electric field between in-plane and out-of-plane alignments. For polymers, the PL EET system is developed containing a uniaxially aligned UHMW PE host, a substituted poly(*p*-phenylene-ethylene) (PPE) guest as a luminescent polymer, and selected sensitizers (coumarines)[337]. This concept combines low degree of polarization in the absorption and high degree of polarization in the emission[348]. Therefore, the composite material can utilize a larger part of the excitation light than the aligned molecules alone but still showing a high degree of polarization in emission. This leads to high PL efficiency.

(vi) The approach where π-conjugated polymer is incorporated into the aligned blend approach may be further developed by using block-*co*-polymers instead of a generic viscoelastic host. In one specific application synthetic modification of PPE is used for domain specific incorporation into polystyrene-b-polyisoprene-b-polystyrene (SIS) triblock copolymer with a cylindrical morphology. The orientation of the host via roll cast templates leads to an axial alignment of the guest PPE and polarized PL[349,350].

(vii) CP light can be produced using assembled molecules, such as PATs. CP light can in turn be transferred into linearly polarized light or, on the other hand, CP light can be used as such in LCDs containing chiroselective molecules or polymers. In these cases, conjugated polymers, especially PATs, are modified using chiral side groups[341].

## 4.2 Primary Photoexcitations in π-Conjugated Polymers

### 4.2.1 Excitons, Polaron Pairs, Excimers, and Aggregates

The π-conjugated polymers contain molecular segments, chromophores which emit photons after the decay of the excitation. In the terms of molecular orbital theory, photoexcitation involves an excited state generated in a fluorophore by a photon promoting an electron from the highest occupied molecular orbital (HOMO) or ground state to the lowest unoccupied molecular orbital (LUMO). Different types of decay pathways exists for the radiative relaxation process of this excitation, fluorescence or phosphorescence, and for the nonradiative transitions, internal conversion into phonons or intersystem crossing (ISC) (where the electronic state of the system is changed) or, on the other hand, by photochemical reactions.

Most fluorescence will result in radiation in the visible spectrum where the relaxation of excitation competes with nonradiative processes. The intensity of emission is much below than that used in excitation and the energy of the emitted photons lower than used in excitation. The loss of efficiency is described by a PLQY (Chapter 4.5) and the energy by the redshift (Stokes shift). The PL spectrum of organic molecules is broad due to the vibronic structures and general inhomogeneity. The smallest energy corresponds usually to $\pi \rightarrow \pi^*$ excitation. That is the case in PF2/6. By comparison, the molecules where it corresponds to the $n \rightarrow \pi^*$ transition are usually weakly fluorescent. This mostly refers to the heteroatoms and heterocyclic aromatic compounds. However, PPY shows fluorescence in the solid state, see refs. in Chapter 4.2.2.

The excitations in π-conjugated polymers[28,44] should be described via many-body physics[351] which is exceedingly difficult. A few guidelines of primary photoexcitations and their relations to the molecular and intermolecular or supramolecular structure are discussed. According to Conwell[352], the intramolecular excitons and intermolecular polaron pairs are the primary photoexcitations in π-conjugated polymers. How they may relate to the structure has to be considered.

The (singlet) excitons, bound electron-hole pairs with opposite spins, are created by initial photoexcitation of a π-conjugated moiety. The decay of the photoexciton occurs through radiative (PL) and nonradiative processes. In the structure the excitons in π-conjugated polymers are spatially spread over several monomers (6-7 for PPV[352]) and occupy a *single* chain.

In general, when a photon excites an electron into the conduction band, it leaves behind a hole in the valence band. In the single-body picture the energies of these two excitations could simply be added. Since the electron and hole are charged particles (and if we consider rather low temperature where no free charge carriers screen them) they may lower their energy by binding together by the Coulomb attraction. Such a

bound electron-hole pair is called exciton. The excitons are characterized by their radius. If the binding is considered weak and the electron and hole are at a large distance (much larger than the lattice spacing) from each other the exciton is called Mott-Wannier excition. If they instead are tightly bound and sit on the same site (on the scale of a few Ångströms), they form a Frenkel exciton. In general, Mott-Wannier excitons reflect semiconductive character while Frenkel exciton takes place in an insulator. In π-conjugated polymers the former have stronger interchain character but they are not referred to be of charge separated polaronic species (see below), whereas the latter is a purely intrachain excitation. Most of the excitons in PPY, for instance, are of the Frenkel type[105].

Excitons have two characteristic total spin states. The singlet excitons (S) has total spin S=0 (antisymmetric spin function), whereas the total spin of the triplet (T) (symmetric spin function) excitons is S=1. It is expected that the non-degenerate ground state of the π-conjugated molecules generally has S=0. There is, however, a discussion on the triplet ground state[353].

Since the radiative recombination of an exciton has to conserve spin, the singlet excitons decay through fluorescent emission but the triplet excitons do not result in fluorescence. Nonradiative singlet quenching occurs via singlet-singlet annihilation or singlet-triplet annihilation or singlets may become triplets via intersystem crossing (ISC). All these processes decrease the emission yield. Singlets may also disappear by creating another singlet in another, different molecule via process called energy transfer. The life time of a singlet is typically of the order of 300 ps. Longer half-life favors ISC.

Polaron pairs, unlike excitons, consist of an excited electron and hole separeated onto adjacent chains. The polaron pairs consist of a negative and a positive polaron (*cf.* Figure 3) bound by the Coulomb attraction and localized by the characteristic chain deformations. On the other hand the thermal energy tends to separate the pair to chains which are further apart. The polaron pair has an attraction greater than *kT*. Otherwise the polarons will separate. Polaron pairs are also called indirect excitons or charge transfer excitons, since, in principle, the pair could be located at the different conjugation segments rather than in different chains.

The excited dimers, called excimers, consist of a pair of identical molecules which repel each other in the ground state but become attractive, if one molecule is excited. The dimer does *not* have a stable ground state and the interaction occurs between a chain segment in its excited state and a chain segment with its ground state. These molecules must have a contact distance of the order of 4 Å, in order to induce an overlap but still maintain their molecular identity. This distance is so large that only the most loosely bound electrons take part in excimer formation. If the distance is increased the excimer disappears. In practice, the red emission seen in solid state disappears in dilute solution. Also no ground state absorption is associated with the red emission.

Exciplex, instead, consists of a pair of non-identical molecules with similar interaction character to excimers. Also in reality, an excimer is stable without an exact match and especially in the case of long conjugation lengths, where the properties depend a little on the lengths, the polaron pairs behave as excimers. The excimers arise from excitations fully located at one partner and excitation then resonate between partners realizing s.c. Förster energy transfer for symmetry reasons. It may also happen that the charge transfer state in the particular polymer has an energy near the excited state and resonates between the partners, too. Altogether, the attraction of the partners is due to the interaction between (i) the excitons on two partners, (ii) two charge transfer states, and (iii) the excited state on one partner and the charge transfer state on the other partner.

Physical aggregates differ from the excimers because of their *stable* associated ground state. So, the interchain interaction occurs between two chains in their ground states. The coupling between the chains is stronger than in excimers. The aggregate can consist of π-conjugated segments on only two polymer chains, a dimer, or spread over several chains. The different spectra in dilute solution, concentrated solution, and in solid state, indicate the formation of an aggregate.

The isolated chain exciton transition is seen in solution while the aggregate leads to the existence of additional absorption at lower energies and a lower frequency emission in thin films. The excimers and aggregates have a broad emission spectrum and the stable ground state may result in some phonon feature in the latter case. The excimers are lower energy configurations than single chain excited states. However, there may be also energy transfer from single chain excitons to the aggregates or eximers, which is related to the emission after excitation at energies which are much below those of single chain exciton absorption.

In PLEDs the excitation is made by subsequent injection of electrons and holes yielding EL[6,30]. The discussion on the exciton formation via charge recombination in EL is omitted. However, in the usual scenario the spin statistics implies a 1:3 probability to the formation of singlets and triplets in OLEDs, respectively. In PF (paper **V**) it is suggested that less than one triplet is formed for each singlet due to the higher cross section for singlet than triplet formation upon charge carrier recombination in EL[354].

### 4.2.2 Photoexcitations in PPY, PPY(CSA)$_x$, and PF2/6

The photoexcitations in PPY are known in detail[58,87,92,97,108]. PPY exhibits blue PL in solution and green in solid state films. The blue has a maximum at 2.9 eV and green a broad maximum at 2.3 eV and a shoulder at 2.6 eV. The excitation profiles are near the absorption spectra and the absorption peak position changes only slightly from 3.4 eV to 3.25 eV when going from the solution to the film. The Stokes shift is only of the order of 0.5 eV with respect to the excitation maximum in solution whilst the peak in solid state is much redshifted (0.9 eV).

The blue PL in solution is due to the fluorescence because of the decay of the first excited singlet state ($S_1$). The lifetime is about 10 ps. The green PL might originate either from the decay of the first exited triplet state ($T_1$), or that of the intermolecular photoexcitations, excimers or aggregates. The latter possiblities have proved incorrect based on the protonation photophysics of PPY[87]. The arguments are that the solution PL does not show coexistence of excimer and monomer PL at any concentration[58] and there are no big differences in the absorption band profiles between the solution and the solid-state. Also the intermolecular photoexcitations should result in lower quantum yield but the PLQY of PPY is higher in the solid-state than in solution[87] (Chapter 4.5).

The interpretation of green PL lies on both delayed fluorescence phosphorescence and of lifetimes 1.1 ns and 4.8 ns, respectively. The amplitudes and lifetime values of these components are highly dependent on the wavelength of PL so that the lifetimes of the components vary from 0.4 ns and 2.3 ns to 1.1 ns and 4.8 ns for delayed fluorescence and phosphorescence, respectively. The shorter lived component has a maximum at 2.6 eV matching with the spectral position of the solution fluorescence while the main PL maximum at 2.3 eV is related to the the longer lived component arising from the radiative decay of a first excited triplet. These components are very much overlapped but generally the delayed fluorescence increases with increasing excitation pulse energy while phosphorescence dominates at lower energies (<100μJ/pulse). Excimers are not present, except for curiosity at low temperature (20 K)[108].

Absorption spectra of PPY has a maximum at 3.2 eV and shoulders at 3.0 eV and 3.4 eV equally spaced in energy corresponding to the vibrations of C=C and CCN bonds[58]. After initial CSA complexation with $x$=0.25 or 0.5 the entire spectrum becomes redshifted by 0.1 eV. After further complexation the maximum blueshifts up to 3.4 eV and the shoulder features become less prominent. Finally, the absorption spectrum of PPY(CSA)$_{1.0}$ is featureless and corresponds to that observed for PPY solution. This situation is seen in the case of further complexation, too. However, when axially aligned films are considered (*Cf.* 4.3), the absorption maximum of the component parallel to the **c** axis is redshifted with the respect to the perpendicular component. This behaviour depends on the degree of alignment. Some smaller redshift is also observed in aligned PPY blend[105] and is suggested to be due to the larger delocalization length in the oriented chain related to a small number of delocalized excited states with high polarizability in chain direction, *i.e*. Mott-Wannier excitons generated by transferring one electron to a neighbouring chain[105]. These excitons are generated by light linearly polarized perpendicular to the chain. This result is based on the electroabsorption measurements of stretched PPY-PVA so the analogy may fail. Nevertheless, see an example of PPY(CSA)$_{0.5}$(HRES)$_{0.5}$ in paper **III** and PPY(CSA)$_{0.5}$(OG)$_{0.5}$ after partial cleavage in paper **IV**. This is concluded in[123] (see **Appendix**)

In PL, CSA complexation simply reveals some blueshift of the maximum at 2.3 eV. At higher complexation, $x$=0.75 or 1.0, a new blue feature appears at 2.7 eV approaching what is seen in solutions. The shoulder becomes more distinct for PPY(CSA)$_{1.0}$[87]. The further complexation with amphiphiles does not change the shape of the PL spectrum compared to the PPY(CSA)$_x$ which is described in papers **III** and **IV**. Unlike absorption, polarized PL does not result in shifts. Instead, PLQY is much reduced.

The photoexcitations of PF2/6[355,356] have been widely studied, too, especially with the energy transfer dopants like benzil[357] or porphyrines[156,358] and at low temperatures[157]. The schematic Jablonski diagram of PF2/6 describing the primary energy levels and optical transitions related to singlet, triplet and charged (polaron pair) excitations is presented in ref. 111. According to these authors, the absorption of a photon in PF2/6 results in the promotion of an electron in $\pi \rightarrow \pi^*$ transition. This is seen as a broad featureless absorption maximum at 3.3 eV. PF2/6 reveals blue PL spectrum with two peaks at ~ 2.9 eV, 2.8 eV and smaller maxima at ~2.6 eV, 2.4 eV, and 2.2 eV. The overlap between the absorption and emission spectra is small. The shapes are essentially not dependent on the polarization direction but they are somewhat redshifted upon annealing (paper **VI**). These peaks are interpreted as prompt fluorescence and the highest peak at 2.88 eV[357] corresponds to the decay of the first singlet to the ground state. The possible peak at 2.15 eV[357] is due to the phosphorescence arising from the decay of the lowest triplet exciton. PF2/6 does not show prominent polaron features in optical spectroscopy because of low energetic disorder and traps which could stabilize them. The low energetic disorder is related to the relatively high charge carrier mobility, generally observed in this class of polymers[10].

### 4.2.3 Photoexcitations vs. Morphology in π-Conjugated Polymers

The π-conjugated structure favours the fluorescence ultimately because the energy states allowing a suitable gap and because of the quasiparticle formation. Upon quasiparticle formation there is a change in the equilibrium configuration of the molecule and the quasiparticles move in a rapid fs to ps time scale to the lower energy segments of longer π-conjugation so that the PL spectrum is redshifted. The excitations tend to migrate so that their recombination occurs spatially in a lower energy site which is not the one they are created in. This occurs via energy transfer (EET or electron transfer) or by exciton hopping leading to the spatial relaxation. The intermolecular structure not only the local electronic structure effects on the PL process by preventing or facilitating their movement or by facilitating their movements to the quench sites where the nonradiative processes occurs. This can be optimized in a systematic though very laborious and time-consuming way by applying synthetic chemistry, structural studies, and quantum mechanical modelling combined[3]. In papers **III-IV**, some optimization was performed in a less elegant way by screening the best examples by trial and error. The drawback of the work is that the supramolecules of PPY never reproduce the PL of pure PPY. This is suggested to be due to sulfonic acid and is thus an inherent disadvantage of the current material compared to polyfluorenes, for instance.

The impact on PL is related to two issues, the increasing of conjugation length and the control of the electronic environment by substituents. They reflect some phenomenological tendencies which may hold also for charge transport in PLEDs.

The increase in the extent of π-conjugation increases the mobility of π-electrons and many times the fluorescence. The increase in planarity and rigidity indirectly enhances fluorescence because that is related to the conjugation length and so helps to increase the mobility of π-electrons. For instance, it is suggested[87] that the planarity of PPY is affected by CSA complexation so that PLQY is reduced but no significant difference in the ground and excited energy levels is seen. In the solid state pure PPY is essentially stacked[39] but upon CSA protonation the interchain interactions are reduced allowing the pyridine units to revert back to their more twisted state and thus lower energy configuration. This results in blue shift and decrease of PLQY as in solution. This is seen mostly for $x$=0.75 and 1.0 while $x$=0.25 and 0.5 show more green PL and almost as high PLQY as pure PPY. As described in paper **V**, $PPY(CSA)_{0.25}$ and $PPY(CSA)_{0.5}$ do not show significant twisting but equatorial stacking peak which disappears for further CSA protonation. The $x$=1.0 case is soft which may support this assumption but the complexes for which $x,y$~0-0.5 are relatively hard. So the softness and the stacking seem to be more related to the CSA than the amphiphiles. This proves the expectation[87] on the existence of the planar regions for $x$=0-0.5 and the solution like behavior and higher triplet formation for higher CSA complexation. The same is seen for the further amphiphile complexation so that the same spectral phenomena are seen depending on the CSA complexation independently on amphiphiles, albeit the PLQY is reduced much more (Chapter 4.5). Hence, the twisting argument is expected to hold in papers **III** and **IV**. This argument, however, is qualitative, because XRD probes a different length scale and do not measure the skeletal disorder.

All the constituents -covalently bonded or external additions- which enhance exciton mobility usually increase fluorescence. This, however, is a much more complicated issue than the increase of rigidity and the substituents may easily just act as fluorescence quenchers. Depending on the Förster transfer[359], the overlap of the absorption spectrum of the dopant end emission spectrum of the polymers, the energy trasfer dopants alter the emission by the radiative or nonradiative energy transfer by photon or phonon, respectively, from the quasiparticles of the polymer to the dopant and back before their recombination.

Added molecules may make the backbone more planar and thus increase the conjugation length and so the mobility of the excitons. This all depends on the ntature of defects, too. From that point of view, this case is also demonstrated in ref. 87 where $PPY(CSA)_x$ shows better PLQY compared to the other sulfonic acids or *m*-cresol for the mentioned torsion angle argument. Sometimes, a simultaneous introduction of electron donor and electron withdrawing substituents may enhance fluorescence. However, that is not true in the present supramolecules (Papers **III** and **IV**) where e-donating species, like hydroxyl groups, and e-withdrawing groups, like sulfonic or carbonyl group, are combined. Large bulky atoms, like bromine usually decrease the efficiency. The end bromines of PPY[35,91] (paper **V**) do not have a considerable effect. However, sometimes Ph-Br is finally added in order to prevent the end bromines in PPP which is somewhat analogically synthesized via coupling by starting from Br-Ph-Br [216]. Instead, large bulky side groups weaken intermolecular interactions and may also increase the intrinsic rigidity of the backbone.

Besides the morphology of the polymer and dopants the surrounding materials have an impact. For instance, charge carrier polymers are employed to enhance the EL by assisting an effective carrier injection compared to the metal interface, by confining the carriers within the EL layer and thus increasing the radiative recombination property, as well as by shifting the recombination zone out of the metal and thus preventing the quenching the excitons at the electrode interface.

## 4.3 Linearly Polarized Photoabsorption

The aligned rodlike polymers reveal anisotropic absorption processes, dichroism, and polarized PA[105] which have been utilized in papers **III-IV**, and **VI**. Besides PA the electro-absorption is widely used to study orientation of common π-conjugated polymers like poly[2-methoxy,5-(2'-ethyl-hexoxy)-p-phenylene-vinylene] (MEH-PPV)[360] and also aligned PPY[101]. In this work the studied materials were not expected to show CP light.

The transitions between electronic states, described as a superposition of one-electron transitions and a generalized definition of transition charge density. The electron transition moments can be employed to determine the symmetry of the molecules related to the molecular states and the macroscopic orientation of the specimen. The linearly polarized light, electric vector oscillating in one direction perpendicular to the propagation direction, was considered and for convenience, the polarization direction of the light is directed along a particular molecular axis. In the present papers the polarized photoabsorption has been employed to probe the axial alignment along the **z** direction which corresponds to the direction of shearing (papers **III-V**) or the rubbing direction of PI (paper **VI**). The natural choice of consideration was axis **c**. Since, the transmission geometry was used, the propagation direction of the light then equates to the normal direction of the sample, denoted as vector **x** in the mentioned papers.

The dichroism is seen as a different probability of absorption as a function of the relative orientation of the molecule and the electric field of the probe light, and is understood to arise from the aligned electron transition dipole moments $\bar{M}_f$ in molecules. The origin of the transition dipole moments is in the transient oscillations in the molecular charge density induced by the interaction with the electric field of the probe light. Experimentally, the absorption probability $W_f$ for the *f*:th transition is proportional to the square of the projection of $\bar{M}_f$ into the direction $\bar{e}$ of the electric field of the probe light, and now $\bar{e}$ lies along *y* or *x*.

$$W_{if} \sim (\bar{M}_i \cdot \bar{e}_i)^2 = |M_i|^2 \cos^2 \varphi , \tag{4.2.1}$$

where $\varphi$ is the angle between the transition dipole $\bar{M}_f$ and the unit vector $\bar{e}$ within the molecule-fixed coordinates *x*, *y* and *z*. The strength of the dipole moment is simply the length of the vector

$$D_f = |\bar{M}_f|^2 , \tag{4.2.2}$$

and its experimental manifestation (given the transitions are not forbidden) the dichroic ratio is defined as a quotient of the components of the probe light absorbed for a given energy and transition

$$d_f = \frac{E_z(\hat{\nu}_f)}{E_y(\hat{\nu}_f)} . \tag{4.2.3}$$

So the molecular transition can be characterized by its energy and its direction related to the transition moment and we can obtain both. In the simple structural framework, for the aligned rodlike polymers, besides the photon energy corresponding to the transition we consider the axis with the highest $d_f$. It is the **c** axis in the papers **III-IV**, and in paper **VI** which on the average is best aligned with *z*. Several other parameters are commonly used to describe originally the same phenomenon. A couple is used in paper **VI**.

## 4.4 Linearly Polarized Fluorescence/Photoluminescence

The detailed physical description of PL of aligned π-conjugated polymers, like MEH-PPV[361] is known. In the solid state, both the energy transfer and the reabsorption and (also light scattering and obviously the nonideality/misalignement of the polarizers) cause depolarization of the emission so the material must be highly aligned in order to achieve polarized PL. If the cooperative phenomena with the near environment are neglected, the spatial anisotropy in PL may be qualitatively described. Outside the dilute solution assumption this cannot be generally done.

The anisotropy of PL is defined as a ratio of the polarized component to the total PL. Like the anisotropic absorption properties of rigid molecules, the fluorescence polarization is understood regarding the rodlike moieties as oscillating dipoles having an oscillating dipole moment of the form

$$\mu = \mu_0 \cos \omega_L t , \tag{4.3.1}$$

where $\omega_L$ is the angular frequency of the emitted light and $t$ is the time. Correspondingly, the transition dipole moments for excitation and emission may be called the absorption and emission dipoles. The electric field of this dipole "radiated antenna" is from a distance proportional to $\sin\psi$ where $\psi$ is the angle away from the **z** axis, the molecular axis taken along the rodlike fluorophore which corresponds to the **c** axis in papers **III**-**IV**, and in paper **IV** and

$$A = A_0 \sin\psi . \tag{4.3.2}$$

The observed energy and intensity radiated are then proportional to the square of the electric field intensity (amplitude) $I \sim |A|^2$.

Given that the dipole is oriented along the **z** axis an equal intensity is observed along the **x** and **y** axes. When the fluorophores are excited by a photon and when they are aligned and sideways packed onto the surface, this flat solid state sample yields polarized photoluminescence. Usually both the absorption and the emission dipoles of π-conjugated polymers are parallel (*Cf.* papers **III**-**IV**, and **VI**) or nearly parallel[360,361] and the deviations are readily used to determine the molecular structure of more complicated molecules, such as branched π-conjugated polymers[362]. These dipoles are however not generally colinear and the electric dipole of a fluorophore does not need to be exactly oriented with the *z* axis in order to absorb light along this axis. Instead, the probability of absorption is proportional to $\cos^2\phi$ where $\phi$ is the angle between the absorption dipole and z axis, which is seen as a photoselection is seen, that is to say the polarized excitation which arises from the excited molecules symmetrically distributed around the *z* axis. The existence of that limits the degree of anisotropy that is independent of the energy of the emission.

The experimental effects arising from the spectrometer in the papers **III**-**IV**, and in paper **VI** are taken into account by correcting the spectra using G factor

$$G = I_{HV} / I_{HH} , \tag{4.3.3}$$

where $I_{HV}$ and $I_{HH}$ denote the intensities measured as a function of energy for the optically isotropic matter, for instance green-emitting Coumarin solution in papers **III** and **IV**, and blue-emitting solution in paper **VI**, placing that between crossed (horizontal-vertical) and parallel (horizontal-horizontal) polarizers with the respect to the experimental facility. In the current arrangements the monochromator before the first polarizer had vertical slit and the aligned polymers were assigned **c** axis vertically. The *G* factor is, unlike the intrinsic anisotropy, energy dependent.

## 4.5 Solid State Photoluminescence Quantum Yield

The high efficiency in the PL properties in π-conjugated polymers are one of the reasons to work with them and important in PLED applications. Basically, the radiative decay of singlet excitons - the process by which light emission occurs in π-conjugated polymers - should be detected[363]. High PL is needed for PLEDs and therefore photoluminescence quantum yield (PLQY) $\Phi_{PL}$ has been studied here. Also, PPY and PF2/6 are very efficient in this sense. PLQY is well-known for several hairyrods, such as PATs (1-10% in solid state) [223] or selected fluorene co-polymers[364] where, for instance, a large variation between solution, 45-60%, depending on the conditions, and solid state, 35%, have generally been observed.

There are several methods to determine the (absolute) solid state PLQY. Primary methods are introduced by Greenham[365,366], de Mello[367], and Pålsson and Monkman[368]. The latter which is a modification of that introduced by de Mello is applied in paper **III** and **IV** and it employs a spectrofluorimeter in combination with an integrating sphere. In this work, a PTFE coated integrating sphere was mounted on a fluorimeter so that the entry and output ports were in a perpendicular angle configuration (in the spectrometer plane) which meant that the design geometry of the fluorimeter was also used in the integrating sphere measurements. The sample material was coated onto a 10 mm diameter quartz substrate and mounted about 20 mm into the sphere from a holder in the entry port facing the excitation light beam. The measured spectra were background corrected by subtracting the spectrum obtained using a blank substrate and subsequently corrected for the wavelength sensitivity of the fluorimeter and the spectral response of the sphere. The spectral response of the sphere was determined using a calibrated tungsten lamp and the fluorimeter as the detector. The spectral correction factor of the fluorimeter was also obtained using the calibrated tungsten lamp. These two normalisation curves were then used to correct the recorded luminescence spectrum of the sample. This correction is applied to all subsequently measured emission spectra in the measurement of the sample PLQY. PLQY was calculated using equation[368]

$$\Phi_{PL} = \frac{E_i(\lambda) - (1-A)\cdot E_0(\lambda)}{L_e(\lambda)\cdot A}, \qquad (4.4.1)$$

where $E_i(\lambda)$ and $E_o(\lambda)$ are respectively, the integrated luminescence as a result of direct excitation of the film and secondary excitation. The latter emission is due to reflected excitation light from sphere walls hitting the sample, which in turn is not directly in the path of the excitation beam. $A$ is the film absorbance which is determined by

$$A = \frac{L_0(\lambda) - L_i(\lambda)}{L_0(\lambda)}. \qquad (4.4.2)$$

$A$ is found by measuring the integrated excitation profiles, i.e. the emission signal measured across the excitation wavelength (± 5 nm), for two situations: $L_i(\lambda)$ is the integrated excitation when the film is directly excited and $L_0(\lambda)$ is the integrated excitation when the excitation light first hits the sphere wall as previously explained. $L_e(\lambda)$ is the integrated excitation profile for an empty sphere.

The pure PPY and PPY(CSA)$_x$ where $x$~0.25-0.5 reveal high PLQY[58,85,87] (>20%) values in solid state, which are twice as high as those in solution. Instead, higher protonation $x$~0.75-1.0 results in the drop in PLQY mirroring the solution formation like the more blue solution like emission instead of solid-state type green (Chapter 4.2.3). In order to obtain high PLQY the pure PPY must be of high quality which cannot be easily achieved at all. In the early studies relatively low PLQY values of 5% were obtained[69,79]. In the papers **III** and **IV** PLQY of further complexes and that after the cleavage[123](**Appendix**) were studied. In general, PLQY of the complexes is always much lower than that of PPY or PPY(CSA) and therefore they have little to provide comparison to the polyfluorenes, for instance. The explanation may be that the amphiphiles provide efficient quenching sites. Instead, after cleavage the PLQY raises substantially but of course do not exceeds that of the pure components. In the papers **III** and **IV** it may be assumed that amphiphiles quench the exciton in singlet exciton quenching. The PL peak is only very slightly shifted by the further complexation (after CSA complexation).

The PLQY of PF2/6 is high in the solid state. Rothe *et al.*[356] observed values of 20 % for the same material as used in paper **VI** but there are also results of PLQY of 50-60% [111] for PF2/6. In the present study a value of 32% was observed[369].

# 5 Self-Organized Hairy-Rodlike Polypyridine, Polyaniline, and Polyfluorene

## 5.1 Self-Organized Supramolecular Hairy-Rodlike Polypyridine

### 5.1.1 Self-Organized, Aligned, and Cleaved Structures

The first section of this thesis concerns self-organized supramolecular hairy-rodlike polymers.The first primary outcome of this section is presented in Figure 23. This comprises (a) the formation supramolecules, (b) the self-organization of supramolecular hairy-rodlike polymers, their (c) overall alignment, and (d) the cleavage of the side groups as well as physical characterization thereof. The procedure has certain problems.

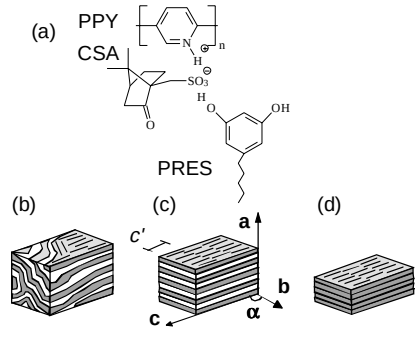


**Figure 23 (a)** Supramolecule of poly(2,5-pyridinediyl) (PPY), camphorsulfonic acid (CSA), and pentylresorcinol (PRES), and their suggested interactions. **(b)** Self-assembled local structure. White layers denote side chain regions. **(c)** Aligned structure. The structure is characterized by alternating polar and nonpolar layers, the stacking of main chain rings, and the length of the repetition unit of the rigid main chain along **a**, **b**, and **c** axes, in the normal, equatorial *out-of-plane*, almost in the equatorial, equatorial *in-plane*, and in the meridional direction, respectively, forming a monoclinic unit cell with lattice parameters *a*, *b*, and *c*, $\alpha \neq 90^{o}$. Additional order, *c'*, is present along **c** axis corresponding to the tentative length of PPY. **(d)** Solid films where the side chains have been cleaved. Adapted from paper **V**.

The first step, the formation of supramolecules has an obvious and serious difficulty. In order to prepare complexes, the molecules must be mixed and a common solvent has to be found. The problem is that unsubstituted rodlike polymers are almost fundamentally soluble only in strong acids. Acids, on the other hand, are chemically reactive towards most amphiphiles. Therefore, a great deal of chemical optimization was required to select common and inert solvent to this particular purpose. Still, although formic acid is employed throughout this thesis, it is not inert toward the used alkylresorcinols. When the evaporation is done in minutes, no serious damage is obtained, as revealed by FTIR spectroscopy. Selected alkylresorcinols are not stable themselves either. *E.g.* PRES should be stored under nitrogen. The feasiblity of the solvent options and their reactions in complex formation were studied elsewhere[121].

The second step, the self-organization has also obvious and even more fundamental difficulties and limitations. The core limitation is described in theoretical view on the self-organization of supramolecular hairy-rodlike polymers of Subbotin *et al.*[9] and in the theoretical discussion in paper **VII**: The supramolecular character results fundamentally in macrophase separation without a careful balance between interactions. This means that there are limited options to select the number of monomers in the coil, the ratio between the volumes of a coil monomer and the backbone section between two consecutive branching sites and thus only very few side groups are feasible.

The second step relies on the concepts known from block-*co*-polymers. On the other hand, the amphiphiles can be regarded as solvents and the concepts of lyotropic solutions can be visited. Since the accessible window of uniform solution in classic theory of rodlike polymers[137,177] is particularly narrow, it is also from this side plausible that only limited concentration range can be considered. Theoretically, it is possible to highlight the general tendencies to which direction the system is to be adjusted. However, in order to experimentally obtain the uniform self-organized phase, extensive experimental optimization procedures must be performed. Also, obtained structures may not necessarily be thermodynamically stable but only frozen-in and may tend to macrophase separate still. When the self-organized phase is obtained, a second optimization procedure in order to maximize the degree of local order is carried on.

This type work comprising self-assembly of $PPY(MSA)_{1.0}(OG)_y$ was presented earilier[298,370] but neiter further steps nor strict structural interpretation or optimization were discussed. The morphology of $PPY(MSA)_{1.0}(OG)_{2.0}$ was speculated but it was not shown to be lamellar until in paper **I**. Some previous conclusions[370] are also inaccurate or false interpreted in the light of this thesis. First of all, a WAXS peak at 1.8 $Å^{-1}$, which corresponds to the equatorial *020* reflection of P3HTs[1,2], was suggested to be due to the co-crystallinity of three compounds. Because the presented WAXS peak of $PPY(MSA)_{1.0}(OG)_{2.0}$ is in the

stacking direction of PPY, identically seen for example in $PPY(CSA)_{0.25}$ *without* any amphiphile, this cannot be the case. Secondly, PPY(MSA) is soluble in *m*-cresol and, unlike previously thought, three hydroxyl groups are not required for the structure formation but *e.g.* OP with one hydroxyl group can be employed. Moreover, the measured curve presented in the insert of Figure 6 does not correspond to sample as stated in the figure legend of ref. 370. The correct sample was $PPY(MSA)_{1.0}$, not $PPY(MSA)_{1.0}(OG)_{2.0}$.

## 5.1.2 Axial Alignment in Thin Films

The third step described in Figure 23, the thermotropic shear alignment, has an obvious problem. It requires necessarily bulky samples. All the published work with PPY has been carried out by shear oriented films, thickness of 10 μm or more. This is far too much to any (even speculative) thin film application. Shear alignment has clear problems regarded to the surface quality. Moreover, in our studies the shearing conditions were not always easy to reproduce, which means that the discussion on the degree of alignment is somewhat meaningless. Instead, the work with PF2/6 has been done employing the rubbed substrates and films thinner than 100 nm.

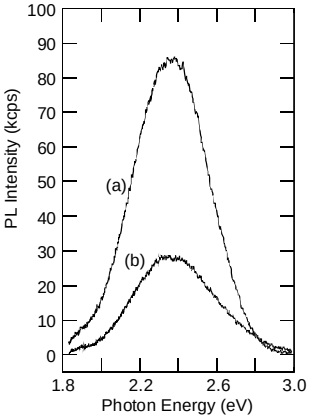


The fourth step, the cleavage of the side groups utilizes the macrophase separation in vacuum and high temperatures. The major problem of this step is that this can be properly done only in thin films (<100 nm) while thicker films allow only partial cleavage.

As described in the papers **II** and **V** (and also in **III** and **IV**) supramolecular hairy rods do self-organize in the thin films of 100 nm or less, too, and the natural question on the use of rubbed substrates arises. Therefore, alongside our PF2/6 studies PPY-based complexes were *also* aligned using PI substrates. This proved to work relatively well but we have not optimized this yet. An unpublished example is shown in Figure 24.

**Figure 24** Polarized PL spectra of *axially aligned* thin film (<60 nm) of $PPY(CSA)_{0.5}(OG)_{0.5}$. The excitation light (360 nm) was taken from the maximum of the excitation profile and was linearly polarized in the meridional **z** direction which is parallel to the crystallographic **c** axis along the polymer rod. **(a)** Polarizer after sample along the **c** axis. **(b)** Polarizer perpendicular to the **c** axis. The complex was aligned using rubbed PI and annealing at 120°C for 10 minutes.

## 5.1.3 Aligned Hierarchic Structures of Rodlike Polymers

The second primary outcome of the first section comprises the structural *hierarchy* in aligned supramolecular system of rodlike π-conjugated polymers. This is clear from the Figure 3 of paper **III**. The selection of the OP in it and its use as a discussed combination, the morphology of $PPY(CSA)_{0.5}(OP)_{1.0}$ (Figure 25), and systems alike are described in papers **III**-**V**, and in ref. 123. The further details are discussed here.

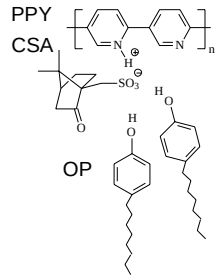


**Figure 25** Schematics of $PPY(CSA)_{0.5}(OP)_{1.0}$

The order where the rodlike backbones tend to form organizations where the chain ends are distributed in planes whose spacing corresponds to the end-to-end distance of the chains, has been observed for few PLC materials. These are lyotropic poly{5,7-dodecadiyne-1.12-diol-bis[((4-butoxy-carbonyl)-methyl)urethane]}[371] and smectic poly(α,L-glutamic acid) derivative owing to monodispersity in chain length[372]. However, this work presents such system for *supramolecular* PLC and also for π-conjugated polymer, which is unique. In purview of this work two classes of material selections revealing supramolecular hierarchy were formed, characterized, and interpreted. It is first noted that PPY is polydisperse ($M_w/M_n$= 1.2-1.6) [107].

The optical micrographs of $PPY(CSA)_{0.5}(OP)_{1.0}$ showed highly birefringent and essentially uniform fluid at 60°C, which suggests the formation of complex, see Figure 26. The other compositions were studied letting *x* vary from 0 to 1 and *y* from 0 to 3. This is done in paper **V** for the other materials. They all are macrophase separated. Also, the discussed composition exhibits irreversible macrophase separation upon further heating. However, because CSA is hygroscopic, a careful drying and thus heating at 60° overnight is required.

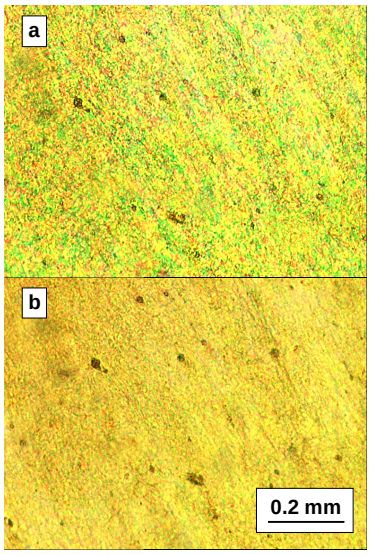


**Figure 26** The optical micrograph of fluid $PPY(CSA)_{0.5}(OP)_{1.0}$ at 60°C, *i.e.* above the melting point of OP ($T_m$=44-45°C). **(a)** Crossed polarizers employed. **(b)** The same area as above without the crossed polarizers.

The complex formation was supported by FTIR spectroscopy. While the FTIR spectra of the constituents of the complex are well-known, the spectrum of the complex is more complicated. Nevertheless, by making a comparison by the spectra of the constituents and the spectrum of the complex, first $PPY(CSA)_x$ and then $PPY(CSA)_x(OP)_y$, the arising or diminishing features and non-superposition due the complexation can be seen (Table I, page 64).

Now the mentioned two classes are observed. First, as described in paper **III** and **V**, relatively spotlike meridional reflections are seen in the samples of small side chain concentration, $x,y$~0.25. In fact they are also observed for $PPY(CSA)_{0.25}$, when no "proper" side chains are present. These features appears sometimes upon heating for the samples where $x,y$~0.5. These samples are rather brittle but it is still possible to induce orientation by using strong stress. All other peaks, *100*, *020*, and *004* (*Cf.* paper **III** and **V**) are also seen clearly indicating the layers, π-π stacking, and the short range order within the chains. Nevertheless, the normal reflections are considerably broadened and as a consequence the coherence length is decreased (paper **V**).

More importantly, as is described in papers **III-V**, streak meridional reflections definitely indicate nematic organization for PLC $PPY(CSA)_{0.5}(OP)_{1.0}$ complex. Since *all the other features*, normal order due to the alternating layers of polar and nonpolar parts of the complex, equatorial order because of the π-π-stacking, and the meridonal order related to the monomer units are *simultaneously* present, the hierarchy is evident. In this case the coherence length based on the reflection *100* is still very high, of order of 750 Å. As described in paper **V**, this is qualitatively the same as that of the other material combinations and among the best selections. As described in paper **V**, the period deduced from the meridional reflection *q'* (~70 Å) corresponds to the effective length of used PPY calculated from the SAXS curves of its solution and to the correlation length deduced from the meridional *004*.

**Figure 27** XRD patterns of hierarchic $PPY(CSA)_{0.5}(OP)_{1.0}$ fluid showing the first observation of hierarchic structure of hairy-rodlike π-conjugated polymer. The (meridional) reflection *q'* at ~ 0.09 $Å^{-1}$ corresponds to the period of 70 Å. In normal direction, the reflection *100* at 0.234 $Å^{-1}$ corresponds to the period of 25.8 Å. Pure OP has peak at 0.215 $Å^{-1}$ and $PPY(CSA)_{0.5}$ at 0.3458 $Å^{-1}$ so phase separated OP cannot be the cause. Amorphous halo, *q''*, is seen as a broad maximum and the equatorial reflection *020* and the meridional reflection, *004*, arise from the π-π stacks and monomer units, respectively. This all is presented in paper **IV** (Fig. 3), **V** (Fig. 2C), and **VI** (Fig. 4). The 2nd order peak, *200*, is typically tiny but *400*, too, is seen at paper **IV**.

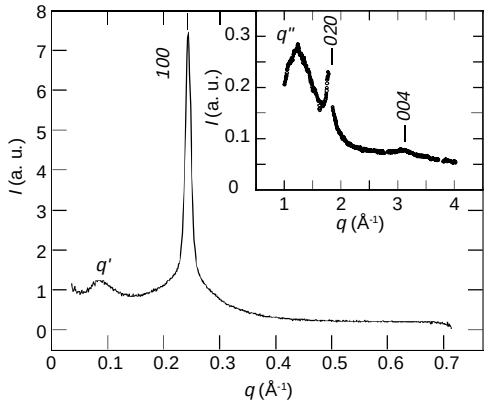


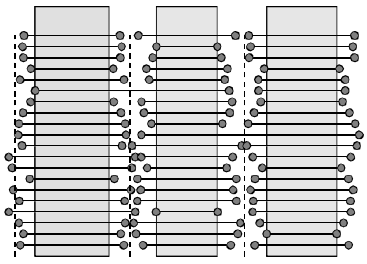

**Figure 28** Model of the head-to-head morphology of $PPY(CSA)_{0.5}(OP)_{1.0}$ related to peak *q'* of Figure 27. Bromines at the both ends of the rodlike chains induce relatively large scattering constrast. The LC character of the matter allows chains to achieve the most advantageous structure freely and the defects are concentrated on the bromine rich regions. The meridional "head-to-head" order is essentially one-dimensional and differs from that of $PPY(CSA)_{0.25}$ $PPY(CSA)_{0.25}(PRES)_{0.25}$ and $PPY(CSA)_{0.25}(HRES)_{0.25}$ where spots rather than streaks are seen at the low scattering angle. See papers **III-V**.

**Table 1** Selected characteristic FTIR peaks of $PPY(CSA)_{0.5}(OP)_{1.0}$ and its components having major distinctions from each other thus suggesting the formation of complexes. Differences between $PPY(CSA)_{0.5}$, OP, and $PPY(CSA)_{0.5}(OP)_{1.0}$ are seen in the fingerprint region. Br[91,373] of PPY and Br and I[35,373] of rrPPY are also observed in the X-ray fluorescence spectra. The FTIR result for PPY is equivalent with ref. 82. *For substitution at <1000 $cm^{-1}$ N of pyridine is treated as a substituent[374]. Despite the vacuum drying of CSA (60° overnight) (and all the components) tiny traces of water exist.

| rnd PPY | rr PPY | CSA | $PPY(CSA)_{0.5}$ | OP | $PPY(CSA)_{0.5}(OP)_{1.0}$ | Suggestive interpretation |
|---|---|---|---|---|---|---|
| | | | | | ~3400 $cm^{-1}$ (broad) | H-bonded hydroxyl |
| ~3050 $cm^{-1}$ (w) | ~3050 $cm^{-1}$ (w) | | | | | Ar in general |
| ~3015 $cm^{-1}$ (w) | ~3015 $cm^{-1}$ (w) | | | | | Ar in general |
| | | 2964 $cm^{-1}$ (s) | | 2965 $cm^{-1}$ (w) | | $-CH_3$ |
| | | | 2956 $cm^{-1}$ (m) | 2956 $cm^{-1}$ (w) | 2956 $cm^{-1}$ (w,) | $-CH_2-$ |
| | | 2892 $cm^{-1}$ (w) | 2892 $cm^{-1}$ (w) | | | -CH< |
| | | | 2887 $cm^{-1}$ (w) | | | |
| | | | | 1884 $cm^{-1}$ (w) | | |
| | | 1747 $cm^{-1}$ (s) | | | | >C=O |
| | | | 1740 $cm^{-1}$ (m) | | 1740 $cm^{-1}$ (m) | >C=O |
| | | | | 1678 $cm^{-1}$ (w) | | Ar in general |
| | | | 1614 $cm^{-1}$ (w) | | 1614 $cm^{-1}$ (w) | |
| | | | | 1597 $cm^{-1}$ (m) | | Ar in general |
| | | | 1590 $cm^{-1}$ (w) | | 1590 $cm^{-1}$ (w) | |
| 1586 $cm^{-1}$ (s) *Cf.*[82] | 1581 $cm^{-1}$ (s) | | | | | Ar in general |
| | | | 1540 $cm^{-1}$ (w) | | 1540 $cm^{-1}$ (w) | |
| | | | | 1516 $cm^{-1}$ (m) | 1516 $cm^{-1}$ (m) | Ar in general |
| 1458 $cm^{-1}$ (s) *Cf.*[82] | 1455 $cm^{-1}$ (s) | | | | | Conjugated ring |
| 1434 $cm^{-1}$ (w) | 1434 $cm^{-1}$ (w) | | | | | Conjugated ring |
| | ~1396 $cm^{-1}$ (w) | | | | | |
| | ~1351 $cm^{-1}$ (w) | | | | | |
| | ~1280 $cm^{-1}$ (w) | | | | | R-Br or R-I |
| | | | | 1260 $cm^{-1}$ (m) | | |
| | | | | 1251 $cm^{-1}$ (w) | | OH in general |
| | | | | | 1230 $cm^{-1}$ (m) | |
| ~1225 $cm^{-1}$ (w) | ~1220 $cm^{-1}$ (w) | | | | | R-Br or R-I |
| | | | | | 1203 $cm^{-1}$ (m) | |
| | | | | 1174 $cm^{-1}$ (w) | | |
| | | | | | 1170 $cm^{-1}$ (m) | $-SO_3-$ ? |
| 1074 $cm^{-1}$ (m) | 1074 $cm^{-1}$ (w) | | | | | Ar in general |
| | | 1045 $cm^{-1}$ (m) | | | | $-SO_3-$ |
| | | | 1038 $cm^{-1}$ (m) | | | $-SO_3-$ |
| 1010 $cm^{-1}$ (s) *Cf.*[82] | 1010 $cm^{-1}$ (s) | | | | | Ar in general |
| | | 970 $cm^{-1}$ (m) | | | | |
| | | 937 $cm^{-1}$ (w) | | | | |
| | | 915 $cm^{-1}$ (w) | | | | |
| | | 890 $cm^{-1}$ (m) | | | | |
| | | | | 862 $cm^{-1}$ (w) | | Isolated H |
| | | 853 $cm^{-1}$ (w) | | | | |
| | | | 835 $cm^{-1}$ (w) | | | |
| | | | | | 831 $cm^{-1}$ (m) | |
| 825 $cm^{-1}$ (s) *Cf.*[82] | | | | | | *p*-coupling |
| | | | | 821 $cm^{-1}$ (m) | | *p*-coupling |
| 822$cm^{-1}$ (s) | 820$cm^{-1}$ (s) | | | | | *p*-coupling |
| 795 $cm^{-1}$ (m) | | | | | | *m*-coupling* |
| | 785 $cm^{-1}$ (m) | | | | | *m*-coupling* |
| | | | | | 778 $cm^{-1}$ (w) | |
| | | | | | 750 $cm^{-1}$ (w) | |
| 741 $cm^{-1}$ (m) | ~ | | | | | *o*-coupling* |
| | | | | | 738 $cm^{-1}$ (w) | |
| | | | | 723 $cm^{-1}$ (m) | | $-CH_2-$ |
| | | | | | 710 $cm^{-1}$ (w) | |
| | | | | | 700 $cm^{-1}$ (w) | |
| | | | | | 691 $cm^{-1}$ (w) | |
| | | | | | 671 $cm^{-1}$ (w) | |
| | | | | | 646 $cm^{-1}$ (w) | |
| | | | | | 633 $cm^{-1}$ (w) | |
| | ~625 $cm^{-1}$ (w) | | | | | R-I |
| | | | | | 557 $cm^{-1}$ (w) | |
| | | | | 546 $cm^{-1}$ (w) | | |
| | | | | | 524 $cm^{-1}$ (w) | |
| | | | | 507 $cm^{-1}$ (w) | | |
| | | 490 $cm^{-1}$ (m) | | | | |

After all, the result is interpreted as a structure where the rodlike chains are organized in "head-to-head" manner due to the formation of π-π stacks which cannot be accommodated by bromine end groups. Then the polydispersity results in less densely filled and less densely ordered zones which may contain the residual dopants and amphiphiles (Figure 28). Note, in particular, that PPY is not tilted but both **c** axis and reflection *q'* (Figure 27) are seen in the same, meridional direction, along the **z** axis. It is plausible that the peaks arising from the order of the rodlike chains are related to this shearing direction. Note also that the simultaneous very good equatorial order is an evidence of strong inherent stacking tendency (paper **V**).

# 5.2 Hexagonal Cylidrical Phase of Polyaniline

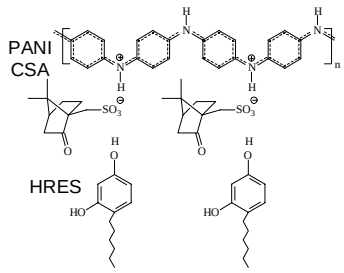


**Figure 29.** Chemical structure of $PANI(CSA)_{0.5}(HRES)_{1.0}$

PANI has been considered in paper **II**.

One of the important issues is that the procedure steps (a) and (b) in Figure 23 can be generalized. This is seen in the work of PANI where, however, a problem of solubility had to be overcome. Analogous to the previous work where formic acid was used as solvent for PPY[370], formic acid was tried to use for PANI, too. Surprisingly, complexation by CSA and hexyl resorcinol (HRES) (Figure 2, paper **II**) occurred also when PANI was not completely soluble. Nevertheless, it did it well when completely soluble Durham-PANI[127,128] was employed. In both cases the use of formic acid did make the proper complexation and thus well-defined morphology of PANI doped by CSA and HRES (Figure 29, paper **II**) possible. Nevertheless, this material is self-organized and plastiziced but no proper thermotropic PLC. So, the overall alignement, the step (c) is problematic. Also, as seen in paper **II**, it does not really show a decent order in thin spin coated films.

The polymeric structure of different forms of PANI[2,302,306,375-380], especially that of emeraldine base (EB) *i.e.* $[(-C_6H_4-NH-C_6H_4-NH-)_{1-x}][-C_6H_4-N=C_6H_4=N-)_x])_n$, where $x=0.5$[381,382] are well-known. The structure of CSA protonated PANI[383-385] and chiral CSA protonated PANI[386] as well as the single crystal structure of its oligomeric analogy[387] are widely discussed in literature. In particular, EB is a semicrystalline polymer of semiflexible chains. The deviations from the planarity of EB are $\pm 30^0$ for the subsequent rings with respect to the average line chain plane in the crystalline form of EB[388]; and $-15^o$, $+15^o$, $-25^o$, and $+5^o$ for three benzoidal and one quinoidal rings, respectively, with respect to the average chain plane for the amorphous form of EB[306].

Upon protonation by CSA PANI forms modest *lamellar* structure intercalated by the bulky acid[383]. Instead, a further complexation with HRES, leads to the well-ordered *hexagonal* mesomorphic structure. This was performed for the first time in summer 1999 and is presented in this thesis in Figure 30. This very discovery was the crucial base for a later study of the same cylindrical phase and several papers[389-391].

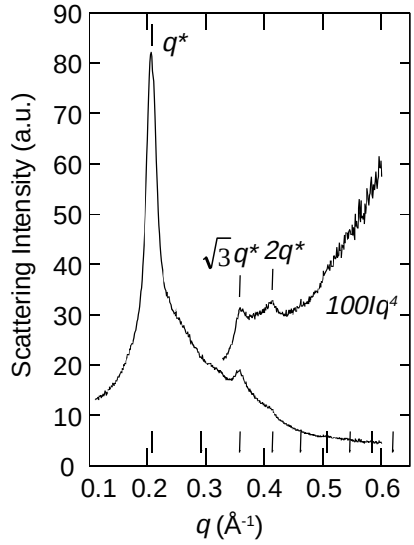


**Figure 30** The chronologically first XRD patterns of the hexagonal cylindrical morphology of the sample of $PANI(CSA)_{0.5}$ complexed by one mole of hexyl resorcinol made from the dilute formic acid solution. The primary peak of the same data has been presented elsewhere[298]. See, in particular, the clear, pronounced square root three reflection $\sqrt{3}\ q^*$ indicating cylindrical phase. Ticks seen at the bottom represents the positions of the square root of index times the position of main reflection where the index get the values from one to nine. Corresponding values are 0.2070 $Å^{-1}$, 0.2927 $Å^{-1}$, 0.3585 $Å^{-1}$, 0.4140 $Å^{-1}$, 0.4629 $Å^{-1}$, 0.5070 $Å^{-1}$, 0.5477 $Å^{-1}$, 0.5855 $Å^{-1}$, and 0.6210 $Å^{-1}$.

## 5.3 Self-Organized Polyelectrolyte

Poly(4-vinylpyridine) (P4VP) has been considered in paper **II**.

Unlike in the case of rodlike PPY, the corresponding complex formation for flexible P4VP is far easier and macrophase separation is always avoided. However, when P4VP is used instead of PPY in $P4VP(MSA)_{1.0}(OG)_{2.0}$ somewhat analogous phase behavior is seen. This comprises of a isotropic phase above 180 °C and a liquid birefringent phase below that. The material melts at 100 °C that is probably related to side chain crystallization. Both transitions are described using optical microscopy with crossed polarizers (Figure 31) and DSC in ref. 298. Furthermore, ODT is demonstrated in Figure 32 using SAXS. The birefringent phase is related to the lamellar self-organized structure of $P4VP(MSA)_{1.0}(OG)_{2.0}$. The lamellar structure is shown in the curve (a) in the insert of Figure 32. By contrast, as seen in the curve (b) in the insert of Figure 32, $P4VP(MSA)_{1.0}$ shows no well-defined structure. This is in agreement with the behaviour of PPY(MSA)[298,370].

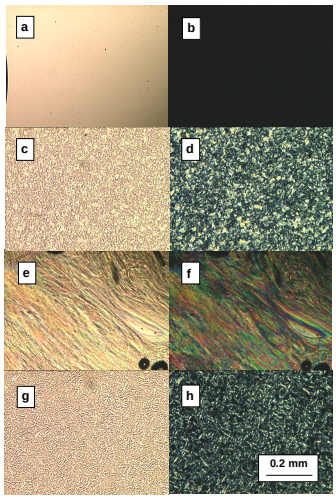


**Figure 31** Optical micrographs of $P4VP(MSA)_{1.0}(OG)_{2.0}$ as a function of temperature described without (on the left) and with crossed polarisers (on the right). Above ca 180 °C (here at 230 °C) this composition is an isotropic liquid (**(a)** and **(b)**), whereas below this temperature (here at 160 °C) (**(c)** and **(d)**) it becomes birefringent fluid. At room temperature the system crystallizes (**(g)** and **(h)**). The transition temperature is (again) approximately 100 °C. The effect of the slight shearing at this temperature is presented in **(e)** and **(f).** Adapted from ref. 298.

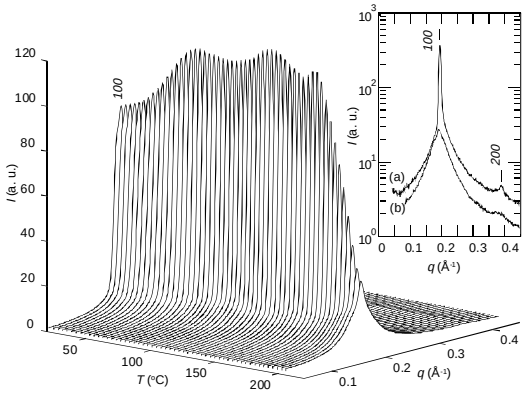


**Figure 32** The SAXS intensity patterns of $P4VP(MSA)_{1.0}(OG)_{2.0}$ indicate self-assembled structure with ODT at ca. 180°C. Insert: **(a)** $P4VP(MSA)_{1.0}(OG)_{2.0}$ shows the sharp first order peak at 0.195 $Å^{-1}$ and clear second order peak at 0.38 $Å^{-1}$ at 124 °C, indicating lamellar structure. Data lifted for clarity. **(b)** $P4VP(MSA)_{1.0}$ shows no sharp peaks at low scattering angle.

In the previous work[298,370] there is a discussion about the character of conductivity of the studied complexes. PPY cannot be made conductive by protonation, like PANI. Instead it has to be *n*-doped *e.g.* by Sodium. The Na-doping is widely described in the literature[69,74,106,392]. PPY itself is a true insulator. Instead, the present complexes show weak thermally induced conductivity which occurs *only* in the melt state. Otherwise they are insulators, too. Their conductivity obeys the exponential relation to the temperature and is definitely due to the ionic motion.

Figure 33 shows simple DC-conductivity characteristics of $P4VP(MSA)_{1.0}$ and self-organized $P4VP(MSA)_{1.0}(OG)_{2.0}$. DC-conductivity level of and its complexes with gallates is low and is of course ionic due to mobile protons and/or sulfonate species in the melt state. If the four probe configuration is applied and the voltage measured when the direct-current is supplied, their relation seems somewhat linear for $P4VP(MSA)_{1.0}(OG)_{2.0}$ but not at all linear for $P4VP(MSA)_{1.0}$. When the current is applied for longer time the linear-like dependence seems more permanent for the self-organized matter than disordered complex which do not show such behavior. However, there is no general relation between the self-organized structure of the studied complexes and this kind of conductivity characteristic. $PPY(MSA)_{1.0}$ do not show self-organized structure but $PPY(MSA)_{1.0}(OG)_{2.0}$ does. Both still exhibit the similar I-V curve as $P4VP(MSA)_{1.0}(OG)_{2.0}$. The smaller ions generally exhibit higher conducting tendency. Moderately large methane sulphonate anion combined with the head of OG might have some effect on the molecular association that could result in decreased ionic mobility. This might cause effect on the ionic motion.

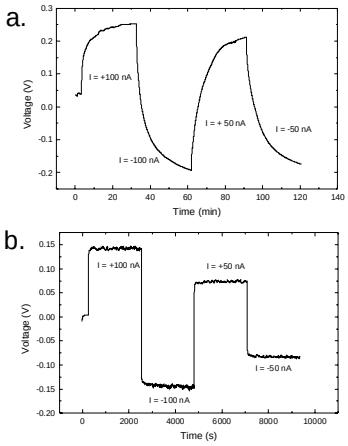


Though the detailed microscopic explanation remains completely open, the observation may prove to be interesting. This complex is white or transparent conductor instead of many times colorful conductive polymers. Transparency combined to the inexpensivity is usually required in bulky coating applications such as paper, other plastics etc.

**Figure 33** Voltage stability measurement of $P4VP(MSA)_{1.0}$ - complex suggesting ionic conductor character **(a)** and the same of the ionic conductor, $P4VP(MSA)_{1.0}(OG)_{2.0}$ **(b)** above crystallisation temperature (~ 100 °C). This curve is very similar to that of $PPY(MSA)_{1.0}$ or $PPY(MSA)_{1.0}(OG)_{2.0}$ Measurements were made using a four-probe method. Adapted from ref. 298.

# 5.4 Self-Organized Hairy-Rodlike Polyfluorene

## 5.4.1 Multiple Orientation

The second section of this thesis concerns self-organized hairy-rodlike polymers. Both their self-organized structure formation[8] and thermotropic alignment lie on the same principles as in their supramolecular counterparts. Therefore, the covalent hairy rods represent natural and necessary parallel line of research. Besides the similarities, the obvious difference and crucial benefit compared to supramolecules is that covalent materials do not macrophase separate. Also, as described in Chapter 5.1.2, one major problem in the supramolecular work in general is based on the shear alignment which is clearly not well suited for thin films used in opto-electronic research and applications of π-conjugated polymers. Therefore, thin film alignment and used rubbed PI substrates were employed.

When working aligned PF, however, another experimental problem is faced. Compared to the work with thick freestanding aligned films, the XRD characterization of the oriented thin films on PI substrate is nontrivial and GIXD set up is required. This experimental arrangement is schematically shown in Figure 34. The first problem is that PF and PI are rather similar materials. Both are rodlike polymers (Figures 6 and 10) and their densities and thus critical angles are near to each other. Secondly, PI shows reflections near those of PF2/6. Although the incident angle is kept below critical angle, the penetration depth of hard X-rays may still be large up to 100 Å. For instance, PI shows a *006* reflection also at 0.8 $Å^{-1}$ in GIXD data[393], near to *005* of PF2/6 (paper **V**) and a possible contribution from PI should be considered. However, as we were not able to resolve other *00l* reflections of PI which should appear for instance at 0.4 $Å^{-1}$, this contribution appears not to be significant here. A peak at 0.8 $Å^{-1}$ was also observed when PF2/6 was spun on glass. Thirdly, PI layer is characteristically not as flat as silicon or quartz which are conveniently used in this type studies and therefore there are stronger local variations in the angle of incidence.

**Figure 34** The schematics of the GIXD technique in the studies of aligned thin films. Refracted beam is omitted. The substrate in paper **VI** comprises ITO on the glass below PI (*Cf.* Figure 10).

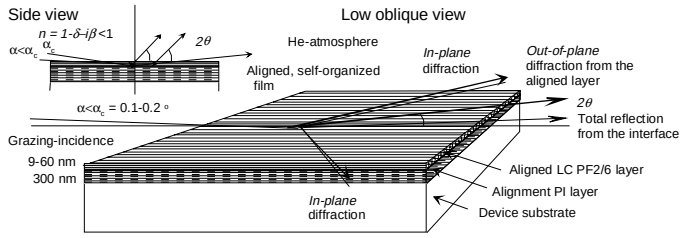

A structural study of PF in thin films is discussed in the pioneer work of Kawana *et al.*[149]. They prepared a PF layer on a PI alignment layer and performed GIXD scan with the incident angle near the critical angle and observed a halo centered at $q$=1.18 Å$^{-1}$ ($d$=5.3 Å). They pointed out that this halo was not observed for the LC phase sample without an alignment layer. Also, they reported that no distinct peak was observed in their scattering geometry for LC phase regardless of the existence of an alignment layer and the origin of this halo to be unclear.

PI is widely used as windows in X-ray studies and it causes a halo as described above. So we expected that PI may easily result in strong halo compared to the very weak signal of PF. Also, any indefinable scattered radiation which is ignored in the work with bulky organic or inorganic thin samples contamines the detected data. In paper **VI** these experimental problems were mostly solved by making first a measuring trip to learn how to use the facility itself. Then the conditions were further optimized by a combination of careful positioning as well as several lead masks, two successive beam stops, and a He-chamber. The decisive details presented in the measurement diary are shown in Figure 35. They allowed the results discussed thereafter. However, several things can be still improved. As Figure 35 shows, the positions of the beam stops cannot be controlled outside the hutch. This makes the rocking of the specimen unnecessarily time-consuming.

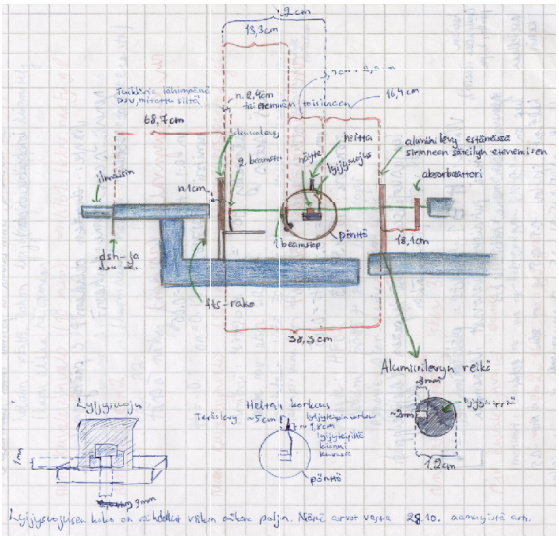


**Figure 35** First-hand information of the experimental arrangement. An authentic laboratory note of the GIXD set up used in paper VI. Finnish terms "lyijy", "alumiini", and "teräs" denote lead, aluminium, and steel, respectively. Both words "heltta" and "suojus" refer to a shield, whilst a term "pönttö" refers to a He-chamber constructed in our laboratory.

The orientation scheme of PF2/6 is the first primary outcome of the second section of this thesis. Two coexistent orientation phases have been described in paper **VI**. These types comprise 30° tilt respect to each other and the difference between them is illustrated in Figure 36. An example of the GIXD data indicating the multiple orientation of PF2/6 is shown in Figure 37.

Among π-conjugated high polymers any resembling phenomenon is to date reported only for PPV by Winokur[307] and for P3HT by Sirringhaus[7]. The crucial difference beetween the present work and these previous reports is that the present observations comprise the in-plane *and* unixially aligned true thin films on the rubbed substrate, while the previous work dealt with uniaxially aligned but clearly thicker films[307] or thin films but only in-plane aligned[7]. On the one hand, for instance the work of Sirringhaus has obvious major results in the mobility relation between the different orientation types, which does not require axial alignment. Still, as pointed out by Sirringhaus, the axial alignment by itself improves greatly the axial charge carrier mobility of PF[10]. In paper **VI**, the multiple orientation shows thickness dependence. In general, the thickness dependent properties of PF films are described to be important *e.g.* in ref. 394.

There are, as is well-known, two interchain structural organizations of PANI, amorphous and semi-crystalline, for instance, and their existence is also dependent on the processing conditions[395]. However, these forms do not represent proper self-organized structure and orientation of the hairy rods or "well-ordered" polymers discussed here. This is due to the fact that both the degree of crystallinity (<60%) and the coherence length of unsubstituted PANI (70 Å) remain modest. *Cf.* the study of self-organized hexagonal, hairy-rodlike PANI. We omit the discussion of the phenomena in generic polymers due to the scope of π-conjugated matter.

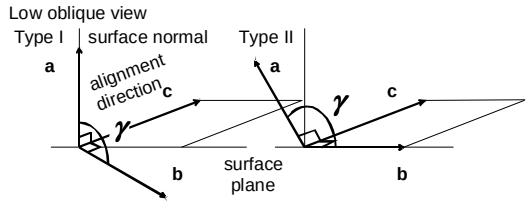


**Figure 36** The mutual orientation of the orientation type I and type II with the respect of the surface plane. *Cf.* paper **VI**

In the presented cases the degree of alignment is naturally interesting. In the current papers, this topic is not deeply investigated mainly because the alignment produced by shear varied much from sample to sample. Also, when the articles were made, the emphasis was on the qualitative demonstration of alignment and the use of alignment as a tool when obtaining more XRD information compared to the unaligned samples. Further, because the present specimens in our studies show very high dichroic ratio nearly 20, the further consideration has been postponed to more samples.

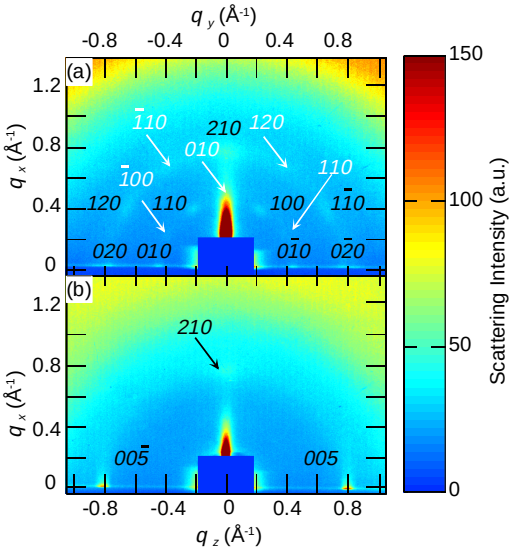


**Figure 37** The GIXD patterns of Case III of paper **VI**, where annealing at 175°C for 3.5 hours were used. This is discussed but not shown in paper **VI**. **(a)** (*xy*0) plane. **(b)** (*x*0*z*) plane. The black dashed lines show primary reflection planes of orientation type I, and white those of type II. The reflection *210* which belong to the type I, (marked with the black indices) is not in the same plane as the reflections *-110* and*120* which belong to the type II (marked with the white indices). The proportion between the intensities of the types is roughly 2.5. The thickness of the film is around 9 nm. Adapted from ref. 369.

However, we may use some simple estimates for orientation with respect to **z** axis. Taking the averaged integrated intensity of a given reflection ideally appearing along one plane only and comparing that to the trace seen on the other plane, we get a ratio given by

$$\tilde{f} = \frac{\langle I_{y-z} \rangle}{\langle I_{x-z} \rangle}, \qquad (5.2.1)$$

where the subindices refer to the planes which here are suited to the consideration in paper **VI**. This simple consideration obviously requires similar measuring conditions for both planes and careful background subtraction and holds practically for distinct Bragg reflections only. As an example the degree of axial orientation for the orientation type I in PF2/6 can be determined according to Equation (5.2.1). If a *120* reflection is taken, clearly seen on the (*xy*0) plane, of the orientation type I from the data of 60 nm thick film (paper **VI)** and calculate the integrated intensity of that reflection on the (*xy*0) plane as an average along the **y** and **z** axes and the integrated intensity of the trace of this reflection on the (*x*0*z*) plane as an average along the **x** and **z** axes, this ratio is about twenty. Clearly, this ratio means higher axial orientation than can ever be expected based on the photoabsorption data (*cf.* paper **VI** and Chapter 4.3). One reason is that conceptually every PF2/6 polymer in the matter contributes in photoabsorption, whether it is amorphous or crystalline or LC, while XRD reflections are in the first instance due to the aligned crystalline part only.

## 5.4.2 Aligned Structure of PF2/6 in Thin Films

In the paper **VI** PF2/6 was found to form two types of orientation from which type I mostly dominant. This urged us to discuss the stucture of this type in somewhat more detail. The purpose was to investigate the structural behaviour of type I in order to clarify whether the structure differs from that observed in aligned fibres[154]. No large variation was originally expected. This, however, is the second primary outcome of the second section of this thesis.

The observed relative structure factors, $|F_{hkl}|^2$, are listed in paper **VI** for the hexagonal ($l$=0) reflections. They were corrected for pixel size, $1/\sin 2\theta$, and Lorentz factor (*Cf.* Chapter 3.2.1), which accounts for differences in the efficiency of scattering resulting from variations in experimental conditions. Atomic structure factor was omitted as a unity approximation, because PF2/6 is a carbohydrate. The measurements were not in absolute units but relative scattering factors were used throughout. For type I they are 30±1, 100, 30±1, 32±4, 2±2, 37±8, and 31±11, for $n=h^2+k^2+hk$=1, 3, 4, 7, 9, 12, and 13, and for type II 1.5±0.1 and 6.7±0.5 for $n$=1 and 3, respectively. The first case is shown in Figure 38.

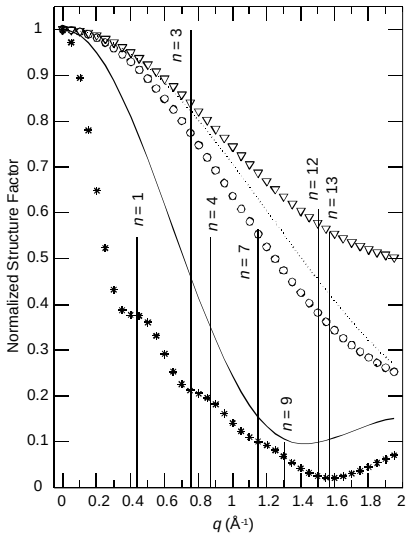


**Figure 38** Normalized structure factor of the different ideal PF2/6 chains of ten monomer period as a function of the magnitude of the scattering vector. 10/1 (stars), 10/2 (solid line), 10/3 (circles), 10/4 (dotted line), and 10/5 helices (triangles) calculated using Equation 5.2.4. The vertical lines represent the normalized measured structure factors of aligned PF2/6 in thin film for the orientation type I, when $n = h^2+hk+k^2$ = 1, 3, 4, 7, 9, 12, and 13, respectively. The minimum at $n$ = 9 for 5/1 helix is in agreement with the measured value.

The strongest reflection at $n$ = 3, not at $n$ = 1[270], suggests the packing of the three helices in a unit cell. It is pointed out that the choice of $Z$ = 3 has also done based on the combined density and fibre diffraction experiments for hexagonal-like structure elsewhere[154]. As pointed out by Lieser *et al.*[154], this selection is *not* compatible with 6-fold symmetry and the unit cell may be selected to be trigonal instead of hexagonal. In paper **VI**, it is called hexagonal-like. As comprehensively described in paper **VI** for type I, this packing is rotated 30° from what is conventionally expected for the orientation of the hexagons onto the surface. The lattice vector **a** is parallel to the surface normal (see discussion in Chapter 5.4.1) and so one of the unit cell edges is normal to the surface.

The rather large reflections $n$=1 etc. indicate a slight deviation from the ideal (8 Å) hexagonal arrangement. A single helix chain does not posses the three-fold symmetry either. In order to illustrate this the (electron)density map perpendicular to the helical axis was constructed for the orientation type I by calculating the complex structure amplitude using the close packing positions ($x$,$y$) and drawing maps using the experimental amplitudes but keeping the phases from the calculated amplitudes.

The comparison with observed structure factors, loosely speaking a variant of the direct method (Chapter 3.1.2) was applied. There were no practical possibilities to heavy atom incorporations, the most structural information originated from the intermolecular, not atomic packing, and there were reasonable initial understanding of the structure of PF2/6 preferentially consisting of hexagonal-like packing of 5/$q$ helices (*i.e.* $q$ turns in 5 units) and the ideal chains of bond-angle 22.86°[154] between neighbouring monomer bonds. Therefore, somewhat different approach was used. In the simple idea, the structure of PF2/6 consists of rigid monomer backbones and flexible side groups and depends on the bond angle $\theta$ between the neighbouring monomers and the dihedral angle $\phi$ describing the rotation of each unit. The monomers form periodic polymers of ten units interval. First, the different types of ideal helical PF2/6 structures were formed and compared keeping the mentioned bond angle constant and letting the- dihedral angle $\phi$ between the bonds vary. For comparison, the values of the helices having all the observed periodicity 8.18 Å (*Cf.* paper **VI**) are tabulated. This is presented in Table 2

**Table 2** The different ideal PF2/6 helices when the constant monomer-monomer bond angle $\theta$ (observed in ref. 154) is employed. Primed parameters refer to the case when the constant meridional lattice parameter $c$ (observed in paper VI) is used. $\phi$ is the dihedral angle, $L_1$ the repeat unit, and $\delta\rho$ the calculated density fluctuation after optimization of the helix positions ($x$, $y$) which minimizes $\delta\rho$. The optimized position is in fractionalized coordinates.

| Helix | $\theta$ | $\phi$ | $L_1$ | $\delta\rho$ | $x$ | $y$ | $\theta'$ | $\phi'$ | $L_1'$ | $\delta\rho'$ | $x'$ | $y'$ |
|---|---|---|---|---|---|---|---|---|---|---|---|---|
| 10/1 | 22.86 | 27.9980 | 6.60 | 0.0566 | 0.3587 | 0.0159 | 11.9998 | 34.0038 | 8.18 | 0.1549 | 0.3555 | 0.0145 |
| 5/1 | 22.86 | 68.7442 | 8.10 | 0.1518 | 0.3532 | 0.0126 | 23.4350 | 68.5798 | 8.18 | 0.1500 | 0.3532 | 0.0126 |
| 10/3 | 22.86 | 106.3062 | 8.35 | 0.1785 | 0.3532 | 0.0148 | 33.3676 | 104.2970 | 8.18 | 0.1676 | 0.3532 | 0.0152 |
| 5/2 | 22.86 | 143.2458 | 8.42 | 0.1899 | 0.3548 | 0.0105 | 40.4870 | 141.5399 | 8.18 | 0.1782 | 0.3543 | 0.0102 |
| 2/1 | 22.86 | 180.0000 | 8.44 | 0.2360 | 0.5096 | 0.0104 | 38.5160 | 180.0000 | 8.18 | 0.2395 | 0.5096 | 0.0104 |

Then, the helices were placed in the unit cell so that the projected density along the helical axis was the flattest (showed least fluctuation, cf. Table I). As pointed out in paper **VI** three helices per unit cell with a three-fold symmetry was assumed. This is a crucial thing yielding the general positions to the three helices on the (*ab*0) plane: (*x*,*y*), (-*x*,*x*-*y*), and (*y*-*x*,-*x*). This, together with the measured periodicity $L_1$ =8.18 Å was used as a base when constructing the density map. This period is the closest match for 5/1 helix[154] and the bond angle may originally chosen to meet this requirement. The chains were packed by simply minimizing the (electron) density fluctuation $\delta\rho$,

$$\delta\rho = \left\langle \rho - \bar{\rho} \right\rangle . \tag{5.2.2}$$

As presented in Table 2 this was first done by letting the periodicity vary and finally it was set to be the same as experimentally observed. In the latter case the results are close to the each others, because the radius of the helix is directly related to the periodicity. The ringlike 10/1 helix and planar 2/1 configuration are self evidently wrong choices. Among the rest, 5/1 helix tend to fill the unit cell most efficiently. Also, the weak $n$=9 reflection is compatible with the chain diameter of the 5/1 helix because of the minimum in the structure factor for a single 5/1 helix is located at the position for $n$=9. This is shown in Figure 38, where the structure factors of the distinct model chains are calculated as Bessel functions using formulas

$$F^2(\bar{q}) = \sum_{ij} \exp(i\bar{q} \cdot \bar{r}_{ij}) \text{, and} \tag{5.2.3}$$

$$\sqrt{\left\langle F^2(\bar{q}) \right\rangle} = \sqrt{\sum_{ij} \frac{1}{2\pi} \int_0^{2\pi} \exp(iqr_{ij}\cos\varphi) d\varphi} \sim \sqrt{\sum_{ij} J_0(qr_{ij})} , \tag{5.2.4}$$

where $J_0$ denotes zeroth order Bessel function (the effect of short range order) and where $r_{ij}$ is the component of interatomic vector normal to chain axis.

In paper **VI** the electron density map for the Case I was calculated using the observed diffraction intensities to derive the magnitudes of the structure factors. A density projection on *ab*-plane using Fourier synthesis[396] was formed for the experimental amplitudes $\left|F_{hk0}\right|$. 10/1, 10/3, 5/2, and 5/1 helices were tried with ideal lateral close packing and with the phases obtained from these different models. It was deduced that the 5/2 helix fitted best the unit cell close packing motif. In paper **VI** the structure of PF2/6 chain was also calculated using molecular mechanics. The calculated structure is less dense than based on XRD, though the discussed cases - aligned fibre, thin aligned film, and calculation *in vacuo*- represent a slightly different environment and somewhat different results are expected. The computational result, however, was completely consistent with 5/2 helicity suggested by the fibre diffraction[154] and therefore PF2/6 is assumed to favor the 5/2 helix. Since 5/1 helicity may not be completely excluded, Figure 39 shows the corresponding map when a 5/1 helix is employed.

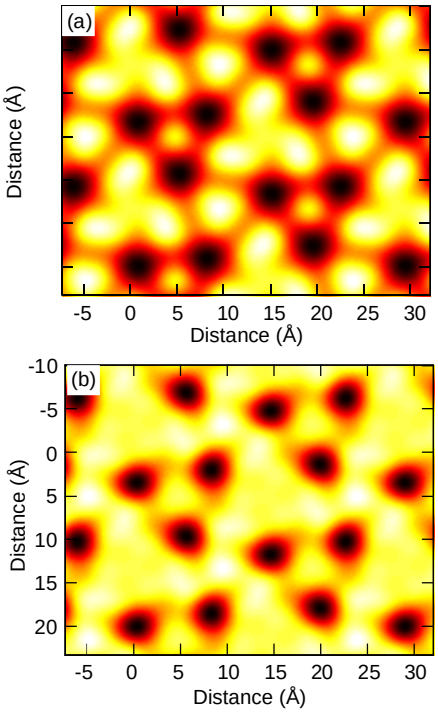


**Figure 39** Density maps of 5/1 helix of the PF2/6 in real space on (*ab*0) plane. **(a)** Model based on the monomer size presented in ref. 154. **(b)** Calculated map where the phase has been taken from the model **(a)** and where the relative structure factors amplitudes of were taken from the measurement. The initial angle of the placement of PF2/6 with respect to the surface plan was taken at one degree intervals from zero to 360° and the presented map is an average of the calculated results. The actual form of the image depends on the values used for the original (*x*,*y*) and the rotation of the helix. No significance should be put on the fine details of the picture. The helices are arranged in layers which are again tilted with respect to the originals layers. As seen on the paper **VI** and this Figure, the crystallization of the helical structures relies on the formation of "triplets" of the helices which together possess the three-fold symmetry which itself is not clearly compatible with 5-fold symmetry.

In both case, the observed lateral packing has unusual features for helices which lack of suitable symmetry of a lattice (which are 5/*q* helices[154]). Commonly, either triclinic unit cell with *Z*=1 or unit cell with equal number of left and right handed helices is found[396]. However, in PF2/6, the suggested number of helices is three in a hexagonal or a closely hexagonal unit cell. It is stressed that the map is not unique but depends on the choice of phase angles. Also the trigonal symmetry has been maintained. Nevertheless, it is concluded that the arrangement as suggested by the map is far from the "usual" packing where each chain would be surrounded by six neighbors. Instead, a more distinct motif of the three helices is indicated by the reflection intensities $|F_{hk0}|^2$. The map agrees more with the 5/2 helix, which has a smaller cross section diameter compared to 5/1[154]. Still, both the map presented in paper **VI** and that presented in Figure 39 produce qualitatively similar result where the initial triplet of helices is slightly rotated.

The crystallization of the helical structures seems to rely on the formation of triplets of the helices making the three-fold symmetry possible. Also, in this respect, there seems to be no difference between type I and II apart from the fact that the type II has more direct indication of the helicity (*Cf.* paper **VI**). The nature of the orientation type may in turn be related to these differences discussed in Chapter 5.4 so that the more convenient form of orientation, type II, is suggested to be a consequence of the helicity, whereas the slightly less ordered phase realizes itself as a type I. Thus the crystallinity seems to affect the orientation.

The 5/2 helix approximate 5 sided structure which does not allow for long range order but there is a tendency to pack on a triangular lattice. Some packed 2D arrays of metal pentagons show a triangular lattice repeat despite the lack of obvious angular order[397,398]. On this basis one might say PF2/6 to represent a frozen LC rotator phase: Orientationally-disordered crystals consist of molecules that lie on a crystalline lattice, but which retain orientational degrees of freedom. At high temperatures the molecules rotate freely when their state is called the rotator phase. (For instance, in the nematic phase the molecules can rotate about one axis, but are mobile in three directions, while in the smectic phase the molecules can again only rotate around one axis, but are only mobile in two directions.) The consideration is obviously not limited to the PLCs and besides rodlike materials[399] solid-rotator transitions have been widely studied in the case of proper liquids, like 1,17-heptadecanediol[400]. Also paper **VII** may be understood to present such transition even if as a function of composition.

In conclusion, the frustration of packing locally may be a cause for the rather large coherence lengths (*cf.* Table I in paper **VI**) and the suggested three chain unit cell is an anomaly. This is studied in detail later by the powder diffraction and advanced modelling combined[401].

# 6 Conclusion

This thesis is concerned with the supramolecular and covalent hairy-rodlike π-conjugated polymers. The interdisciplinary view and methods comprising physics, chemistry, and materials science have been consolidated and employed. The following results and outcomes of the work are summarized as concluding remarks.

First of all, this thesis is aimed at developing of the well-ordered supramolecular LCPs. In particular, locally highly ordered, supramolecular hairy-rodlike π-conjugated polymer materials family has indeed been developed and characterized. A complex structural hierarchy - the head-to-head organization, self-organized layers, and rodlike polymers within the layers - unique in π-conjugated polymers, has been found. Several new phases have been discovered and the phase behavior has been studied in parallel with the theoretical predictions. Alongside the structural work the materials selection and composition have been rather succesfully optimized with respect to photoluminescence. The achieved liquid crystalline phase has been used for overall alignment of all the levels of hierarchy. The orientation of *all* the levels has made the detailed structural characterization possible and the axial alignment has resulted in polarized photoluminescence. The axially aligned bare rigid chains have been achieved by cleaving the supramolecular side groups, and simultaneously the diminished photoluminescence quantum yield has lifted up to the high level of pure polymer.

Altogether, the general concepts originating from the tradition of supramolecular science and the physics of block-*co*-polymers and π-conjugated materials have been integrated in a way hitherto not known. There are enormous amount of different supramolecules but specifically a *π-conjugated* unsubstituted polymer was considered here. This may have implications for processing routes and controlled nanoscale structures of rigid rodlike polymers, in particular electroactive polymers.

Secondly, the structural nature of hairy-rodlike polyfluorene in axially thin films has been clarified in detail when important rubbed polyimide substrate and thermotropic alignment have been applied. In order to overcome the background of the alignment substrate, a careful experimental work has been performed. Multiple orientation, scarce among π-conjugated polymers, and first in polyfluorenes and in axially aligned thin films has been identifed. These findings may be considered in the design of polarized LEDs.

The previously found 5/2 helix (ref. 154) was observed. A strong tendency to pack on a triangular lattice is an anomaly which should not allow long range order which, however, was found. The polyfluorene may be understood as the representative of a frozen liquid crystal rotator phase and the frustration of packing locally may be cause for the rather large coherence lengths.

In addition, an unambigous experiment and observation of hexagonal self-organized supramolecular phase of polyaniline has been performed. Self-organized white polyelectrolyte has been discussed.

For future reasons, a large documented database comprising scattering and chemical information and practical aspects of the studied materials and methods and other tools and documents was created and partially discussed in the papers and this book.

# 7 References


[1] E. J. Samuelsen and J. Mårdalen, The Structure of Polythiophenes, in *Handbook of Organic Conductive Molecules and Polymers*; (Eds: H. S. Nalwa) Wiley, New York, **1997**, pp. 87.

[2] M. J. Winokur, Structural Studies of Conducting Polymers, in *Handbook of Conducting Polymers*; (Eds: T. A. Skotheim, R. L. Elsenbaumer, and J. R. Reynolds) Marcel Dekker, New York, **1998**, pp. 707.

[3] L. R. Dalton, *J. Phys.: Condens. Matter*, **2003**, *15*, R897.

[4] M. J. Winokur and W. Chunwachirasiri, *J. Polym. Sci. B: Polym. Phys.*, **2003**, *41*, 2630.

[5] A. Kraft, A. C. Grimsdale, and A. B. Holmes, *Angew. Chem. Int. Ed.*, **1998**, *37*, 402.

[6] R. H. Friend, R. W. Gymer, A. B. Holmes, J. H. Burroughes, R. N. Marks, C. Taliani, D. D. C. Bradley, D. A. Dos Santos, J. L. Brédas, M. Lögdlund, and W. R. Salaneck, *Nature*, **1999**, *397*, 121.

[7] H. Sirringhaus, P. J. Brown, R. H. Friend, M. M. Nielsen, K. Bechgaard, B. M. W. Langeveld-Voss, A. J. H. Spiering, R. A. J. Janssen, E. W. Meijer, P. Herwig, and D. M. de Leeuw, *Nature*, **1999**, *401*, 685.

[8] R. Stepanyan, A. Subbotin, M. Knaapila, O. Ikkala, and G. ten Brinke, *Macromolecules*, **2003**, *36*, 3758.

[9] A. Subbotin, R. Stepanyan, M. Knaapila, O. Ikkala, and G. ten Brinke, *Eur. Phys. J. E.*, **2003**, *12*, 333.

[10] H. Sirringhaus, R. J. Wilson, R. H. Friend, M. Inbasekaran, W. Wu, E. P. Woo, M. Grell, and D. D. C. Bradley, *Appl. Phys. Lett.*, **2000**, *77*, 406.

[11] H. Sirringhaus, P. J. Brown, R. H. Friend, M. M. Nielsen, K. Bechgaard, B. M. W. Langeveld-Voss, A. J. H. Spiering, R. A. J. Janssen, and E. W. Meijer, *Synth. Met.*, **2000**, *111-112*, 129.

[12] A. P. H. J. Schenning, C. Elissen-Román, J.-W. Weener, M. W. P. L. Baars, S. J. van der Gaast, and E. W. Meijer, *J. Am. Chem. Soc.*, **1998**, *120*, 8199.

[13] A. El-Ghayoury, E. Peeters, A. P. H. J. Schenning, and E. W. Meijer, *Chem. Comm.*, **2000**, *19*, 1969.

[14] A. El-Ghayoury, A. P. H. J. Schenning, P. A. Van Hal, J. K. J. Van Duren, R. A. J. Janssen, and E. W. Meijer, *Angev. Chem. Int. Ed.*, **2001**, *40*, 3660.

[15] A. El-Ghayoury, A. P. H. J. Schenning, P. A. van Hal, C. H. Weidl, L. J. Joost, R. A. J. Janssen, U. S. Schubert, and E. W. Meijer, *Thin Solid Films*, **2002**, *403-404*, 97.

[16] A. P. H. J. Schenning, P. Jonkheijm, J. Hofkens, S. De Feyter, T. Asavei, M. Cotlet, F. C. De Schryver, and E. W. Meijer, *Chem. Comm.*, **2002**, *12*, 1264.

[17] M. C. T. Fyfe and J. F. Stoddart, *Acc. Chem. Res.*, **1997**, *30*, 393.

[18] P. G. de Gennes and J. Prost, *The Physics of Liquid Crystals*, 2 ed. (Oxford University Press, Oxford, **1998**).

[19] R. J. Andres, T. Bein, M. Dorogi, S. Feng, J. I. Henderson, C. P. Kubiak, W. Mahoney, R. G. Osifchin, and R. Reifenberger, *Science*, **1996**, *272*, 1323.

[20] L. Y. Gorelik, A. Isacsson, M. V. Voinova, B. Kasemo, R. I. Shekhter, and M. Jonson, *Phys. Rev. Lett.*, **1998**, *80*, 4526.

[21] M. Park, C. Harrison, P. M. Chaikin, R. A. Register, and D. H. Adamson, *Science*, **1997**, *276*, 1401.

[22] A. Aoki, M. Nakaya, and T. Miyashita, *Macromolecules*, **1998**, *31*, 7321.

[23] C. J. Drury, C. M. J. Mutsaers, C. M. Hart, M. Matters, and D. M. de Leeuw, *Appl. Phys. Lett.*, **1998**, *73*, 108.

[24] H. Sirringhaus, N. Tessler, and R. H. Friend, *Science*, **1998**, *280*, 1741.

[25] E. R. Holland, D. Bloor, A. P. Monkman, A. Brown, D. De Leeuw, M. M. Bouman, and E. W. Meijer, *J. Appl. Phys.*, **1994**, *75*, 7954.

[26] C. M. J. Mutsaers, D. M. De Leeuw, and C. J. Drury, *Methods of manufacturing field-effect transistor substantially consisting of organic materials, PCT Int. Appl. WO9910939*, **1999**. 17 pp.

[27] G. Frey, K. J. Reynolds, H. Sirringhaus, and R. H. Friend, *Organic field effect transistor and fabrication thereof, PCT Int. Appl. WO0341184*, **2003**. 22 pp.

[28] D. Baeriswyl, D. K. Campbell, and S. Mazumdar, An Overview of the Theory of pi-Conjugated Polymers, in *Conjugated Conducting Polymers*; (Eds: H. Kiess) Springer-Verlag, Berlin, **1992**, pp. 7.

[29] W. Rehwald and H. G. Kiess, Charge Transport in Polymers, in *Conjugated Conducting Polymers*; (Eds: H. Kiess) Springer-Verlag, Berlin, **1992**, pp. 135.

[30] R. H. Friend and N. C. Greenham, Electroluminescence in Conjugated Polymers, in *Handbook of Conducting Polymers*; (Eds: T. A. Skotheim, R. B. Elsenbaumer, and J. R. Reynolds) Marcel Dekker Inc, New York, **1998**.

[31] E. Smela, O. Inganäs, and I. Lundström, *Science*, **1995**, *268*, 1735.

[32] G. Decher, *Science*, **1997**, *277*, 1232.

[33] E. Braun, Y. Eichen, U. Sivan, and B.-Y. Gdalyahy, *Nature*, **1998**, *391*, 775.

[34] C. P. Collier, E. W. Wong, M. Belohradský, F. M. Raymo, J. F. Stoddart, P. J. Kuekes, R. S. Williams, and J. R. Heath, *Science*, **1999**, *285*, 391.

[35] L. E. Horsburgh, A. P. Monkman, C. Wang, and M. R. Bryce, *Mater. Res. Soc. Symp. Proc.*, **2002**, *665*, 169.

[36] A. D. Schlueter and Z. Bo, Synthesis of conjugated polymers for materials science, in *Handbook of Organopalladium Chemistry for Organic Synthesis*; (Eds: E.-I. Negishi) John Wiley & Sons Inc., Hoboken, **2002**, pp. 825.

[37] S. S. Zhu, P. J. Carroll, and T. M. Swager, *J. Am. Chem. Soc.*, **1996**, *118*, 8713.

[38] D. A. P. Delnoye, R. P. Sijbesma, J. A. J. M. Vekemans, and E. W. Meijer, *J. Am. Chem. Soc.*, **1996**, *118*, 8717.

[39] E. J. Samuelsen, A. P. Monkman, L. A. A. Pettersson, L. E. Horsburgh, K. E. Aasmundtveit, and S. Ferrer, *Synth. Met.*, **2001**, *124*, 393.

[40] A. J. Heeger, *Angew. Chem., Int. Ed.*, **2001**, *40*, 2591.

[41] J. L. Brédas, K. Cornil, F. Meyers, and D. Beljonne, Electronic Structure and optical Response of Highly Conducting and Semiconducting Conjugated Polymers and Oligomers, in *Hanbook of Conducting Polymers*; (Eds: T. A. Skotheim, R. L. Elsenbaumer, and J. R. Reynolds) Marcel Dekker Inc, New York, **1998**.

[42] A. J. Heeger, S. Kivelson, J. R. Schrieffer, and W.-P. Su, *Rev. Mod. Phys.*, **1988**, *60*, 781.

[43] W. R. Salaneck, S. Stafström, and J.-L. Bredas, *Conjugated polymer surfaces and interfaces* (Cambridge University Press, Cambridge, **1996**).

[44] H. G. Kiess and G. Harbege, Optical Properties of Conducting Polymers, in *Conjugated Conducting Polymers*; (Eds: H. Kiess) Springer-Verlag, Berlin, **1992**, pp. 175.

[45] A. O. Patil, A. J. Heeger, and F. Wudl, *Chem. Rev.*, **1988**, *88*, 183.

[46] G. Wegner and W. Schermann, *Colloid Polym Sci*, **1974**, *252*, 655.

[47] M. Wintger, A. Grupp, M. Mehring, and H. Sixl, *Chem. Phys. Lett.*, **1987**, *133*, 482.

[48] K. E. Huggins, S. Son, and S. I. Stupp, *Macromolecules*, **1997**, *30*, 5305.

[49] L. S. Li and S. I. Stupp, *Macromolecules*, **1997**, *30*, 5313.

[50] D. Fichou and C. Ziegler, Structure and properties of oligothiphenes in the solid state: single crystals and thin films, in *Handbook of Oligo- and Polythiophenes*; (Eds: D. Fichou) Wiley-VCH GmbH, Weinham, **1999**, pp. 183.

[51] E. M. Conwell, *Proceedings of the International School of Physics "Enrico Fermi", 149th(Organic Nanostructures: Science and Applications)*, **2002**, 67.

[52] G. Boiteux-Steffan, T. Pascal, C. Naccache, and J. F. Dutel, *Ann de Physique (Paris)*, **1986**, *11*, 83.

[53] P. A. Heiney, J. E. Fischer, D. Djurado, J. Ma, D. Chen, M. J. Winokur, N. Coustel, P. Bernier, and F. E. Karasz, *Phys. Rev. B*, **1991**, *44*, 2507.

[54] M. J. Winokur, P. Wamsley, J. Moulton, P. Smith, and A. J. Heeger, *Macromolecules*, **1991**, *24*, 3812.

[55] T. J. Prosa, M. J. Winokur, J. Moulton, P. Smith, and A. J. Heeger, *Phys. Rev. B*, **1995**, *51*, 159.

[56] K. Tashiro, M. Kobayashi, T. Kawai, and K. Yoshino, *Polymer*, **1997**, *38*, 2867.

[57] L. Pauling, *The Nature of the Chemical Bond and the Structure of Molecules and Crystals*, 3 ed. (Cornell University Press, Ithaca, New York, **1973**).

[58] A. P. Monkman, M. Halim, S. Dailey, I. D. W. Samuel, M. Sluch, and L. E. Horsburgh, *Proc. SPIE-Int. Soc. Opt. Eng.*, **1997**, *3145*, 208.

[59] N. F. Mott, *Phil. Mag.*, **1968**, 835.

[60] N. F. Mott, *Metal-Insulator Transitions*, 2nd ed. (Taylor & Francis Ltd., London, **1990**).

[61] F. M. Gray, *Solid Polymer Electrolytes* (VCH, New York, **1991**).

[62] J. Koryta, J. Dvorak, and L. Kavan, *Principles of Electrochemistry*, 2 ed. (John Wiley & Sons, Chichester, **1993**).

[63] T. Yamamoto, T. Ito, and K. Kubota, *Chem. Lett.*, **1988**, 153.

[64] T. Yamamoto, T. Ito, K. Sanechika, and M. Hishinuma, *Synth. Met.*, **1988**, *25*, 103.

[65] T. Yamamoto, *Japanese Journal of Applied Physics, Part 2: Letters*, **1989**, *28*, L875.

[66] T. Yamamoto, Z.-H. Zhou, T. Kanbara, and T. Maruyama, *Chem. Lett.*, **1990**, *2*, 223.

[67] T. Yamamoto, T. Maruyama, Z.-H. Zhou, T. Ito, and T. Kanbara, *Synth. Met.*, **1991**, *42*, 1587.

[68] T. Yamamoto, T. Maruyama, Z. Zhou, T. Ito, T. Fukuda, Y. Yoneda, F. Begum, T. Ikeda, S. Sasaki, H. Takezoe, A. Fukuda, and K. Kubota, *J. Am. Chem. Soc. (Supplementary materials)*, **1994**, *116*, 4832.

[69] T. Yamamoto, T. Maruyama, Z.-H. Zhou, T. Ito, T. Fukuda, Y. Yoneda, F. Begum, T. Ikeda, S. Sasaki, H. Takezoe, A. Fukuda, and K. Kubota, *J. Am. Chem. Soc.*, **1994**, *116*, 4832.

[70] J. W. Blatchford, S. W. Jessen, L.-B. Lin, J.-J. Lih, D. D. Gebler, Y. Wang, T. L. Gustafson, A. J. Epstein, H.-L. Wang, T. M. Swager, A. G. MacDiarmid, T. Yuzawa, T. Tahara, S. Yamaguchi, and H.-O. Hamaguchi, in *Photoexcitations in Electroluminescent Conducting Polymers: Time Resolved Absorption, Luminescence, and Infrared Spectroscopy of Pyridine Based Polymers*, Los Alamos Natl. Lab. LA (U. S.), 1995 (CAS), p. 77.

[71] T. Yamamoto, Y. Yoneda, and K. Kizu, *Macromol. Rapid Commun.*, **1995**, *16*, 549.

[72] D. D. Gebler, Y. Z. Wang, J. W. Blatchford, S. W. Jessen, L.-B. Lin, T. L. Gustafson, H. L. Wang, T. M. Swager, A. G. MacDiarmid, and A. J. Epstein, *J. Appl. Phys.*, **1995**, *78*, 4264.

[73] T. Miyamae, D. Yoshimura, H. Ishii, Y. Ouchi, K. Seki, T. Miyazaki, T. Koike, and T. Yamamoto, *J. Chem. Phys.*, **1995**, *103*, 2738.

[74] J. W. Blatchford, T. L. Gustafson, and A. J. Epstain, *J. Chem. Phys.*, **1996**, *105*, 9214.

[75] J. W. Blatchford, S. W. Jessen, L.-B. Lin, T. L. Gustafson, D.-K. Fu, H.-L. Wang, T. M. Swager, A. G. MacDiarmid, and A. J. Epstein, *Phys. Rev. B*, **1996**, *54*, 9180.

[76] M. C. M. v. d. Sanden, C. Y. Yang, P. Smith, and A. J. Heeger, *Synth. Met.*, **1996**, *78*, 47.

[77] M. J. Percino and V. M. Chapela, Poly(2,6-Pyridinedivinylene), in *Polymeric Materials Encyclopedia*; (Eds: J. C. Salamone) CRC Press, Boca Raton, **1996**, pp. 6662.

[78] Y. Z. Wang, D. D. Gebler, L. B. Lin, J. W. Blatchford, S. W. Jessen, H. L. Wang, and A. J. Epstein, *Appl. Phys. Lett.*, **1996**, *68*, 894.

[79] J. W. Blatchford, S. W. Jessen, L. B. Lin, J. J. Lih, T. L. Gustafson, A. J. Epstein, D. K. Fu, M. J. Marsella, T. M. Swager, A. G. MacDiarmid, S. Yamaguchi, and H. Hamaguchi, *Phys. Rev. Lett.*, **1996**, *76*, 1513.

[80] J. W. Blatchford, T. L. Gustafson, and A. J. Epstein, *J. Chem. Phys.*, **1996**, *105*, 9214.

[81] J. W. Blatchford, S. W. Jessen, L. B. Lin, T. L. Gustafson, A. J. Epstein, D. K. Fu, H. L. Wang, T. M. Swager, and A. G. MacDiarmid, *Mat. Res. Soc. Symp. Proc.*, **1996**, *413*, 671.

[82] H. Yun, T. K. Kwei, and Y. Okamoto, *Macromolecules*, **1997**, *30*, 4633.

[83] H. Nishihara, Organometallic Conductive Polymers, in *Handbook of Organic Conductive Molecules and Polymers*; (Eds: H. S. Nalva) John Wiley & Sons, Chichester, **1997**, pp. 799.

[84] Y. Z. Wang, D. D. Gebler, D. K. Fu, T. M. Swager, A. G. MacDiarmid, and A. J. E. A. J., *Synth. Met.*, **1997**, *85*, 1179.

[85] M. Halim, I. D. W. Samuel, E. Rebourt, and A. P. Monkman, *Synth. Met.*, **1997**, *84*, 951.

[86] T. Miyamae, D. Yoshimura, H. Ishii, Y. Ouchi, T. Miyazaki, T. Koike, T. Yamamoto, Y. Muramatsu, H. Etori, T. Maruyama, and K. Seki, *Synth. Met.*, **1997**, *84*, 939.

[87] A. P. Monkman, M. Halim, I. D. W. Samuel, and L. E. Horsburgh, *J. Chem. Phys.*, **1998**, *109*, 10372.

[88] Y. Yao, J. J. S. Lamba, and J. M. Tour, *J. Am. Chem. Soc.*, **1998**, *120*, 2805.

[89] Y.-H. Liau and N. F. Scherer, *Proc. SPIE-Int. Soc. Opt. Eng.*, **1998**, *3279*, 203.

[90] M. Magnuson, L. Yang, J.-H. Guo, C. Såthe, A. Agui, J. Nordgren, Y. Luo, H. Ågren, N. Johansson, W. R. Salaneck, L. E. Horsburg, and A. P. Monkman, *Chem. Phys.*, **1998**, *237*, 295.

[91] L. E. Horsburgh, A. P. Monkman, and I. D. W. Samuel, *Synth. Met.*, **1999**, *101*, 113.

[92] A. P. Monkman, M. Halim, S. Dailey, I. D. W. Samuel, and L. E. Horsburgh, *Synth. Met.*, **1999**, *101*, 208.

[93] A. P. Monkman, S. Dailey, M. Halim, and L. E. Horsburgh, *Synth. Met.*, **1999**, *101*, 252.

[94] M. Magnuson, L. Yang, J.-H. Guo, C. Såthe, A. Agui, J. Nordgren, Y. Luo, H. Ågren, N. Johansson, W. R. Salaneck, L. E. Horsburgh, and A. P. Monkman, *J. Electron Spectrosc. Relat. Phenom.*, **1999**, *101-103*, 573.

[95] M. Jonforsen, S. Grigalevicius, M. R. Andersson, and T. Hjertberg, *Synth. Met.*, **1999**, *102*, 1200.

[96] M.-Y. Hwang, M.-Y. Hua, and S.-A. Chen, *Polymer*, **1999**, *40*, 3233.

[97] A. P. Monkman, M. Halim, S. Dailey, I. D. W. Samuel, and L. Horsburgh, *Synth. Met.*, **1999**, *101*, 253.

[98] L. J. Harwell, M. E. Vaschetto, L. E. Horsburgh, and A. P. Monkman, *Synth. Met.*, **1999**, *101*, 807.

[99] M. Halim, I. D. W. Samuel, J. N. G. Pillow, A. P. Monkman, and P. L. Burn, *Synth. Met.*, **1999**, *102*, 1571.

[100] Y. Z. Wang and A. J. Epstein, *Acc. Chem. Res.*, **1999**, *32*, 217.

[101] F. Feller and A. P. Monkman, *Phys. Rev. B*, **1999**, *60*, 8111.

[102] C. T. Wong and W. K. Chan, *Adv. Mater.*, **1999**, *11*, 455.

[103] F. Meghdadi, G. Leising, Y. Z. Wang, D. D. Gebler, T. M. Swager, and A. J. Epstein, *Synth. Met.*, **1999**, *102*, 1085.

[104] C. Wang, M. Kilitziraki, J. A. H. MacBride, M. R. Bryce, L. E. Horsburgh, A. K. Sheridan, A. P. Monkman, and I. D. W. Samuel, *Adv. Mater.*, **2000**, *12*, 217.

[105] F. Feller and A. P. Monkman, *Phys. Rev. B*, **2000**, *61*, 13560.

[106] G. Greczynski, N. Johansson, M. Lögdlund, L. A. A. Pettersson, W. R. Salaneck, L. E. Horsburgh, A. P. Monkman, D. A. dos Santos, and J. L. Brédas, *J. Chem. Phys.*, **2001**, *114*, 4243.

[107] M. Tammer, L. E. Horsburgh, H. Burrows, W. Brown, and A. P. Monkman, *Adv. Funct. Mat.*, **2002**, *12*, 447.

[108] S. Sinha, C. Rothe, A. Beeby, L. E. Horsburgh, and A. P. Monkman, *J. Chem. Phys.*, **2002**, *117*, 2332.

[109] F. Feller, D. Geschke, and A. P. Monkman, *J. Phys.: Condens Matter*, **2003**, *14*, 8455.

[110] T. Maruyama and T. Yamamoto, *J. Phys . Chem. B*, **1997**, *101*, 3806.

[111] U. Scherf and E. J. W. List, *Adv. Mater.*, **2002**, *14*, 477.

[112] S. Dailey, A. P. Monkman, and I. D. W. Samuel, *Synth. Met.*, **1999**, *102*, 945.

[113] B.-K. Choi and T. Yamamoto, *Electrochem. Comm.*, **2003**, *5*, 566.

[114] Y. Eichen, G. Nakhmanovich, V. Gorelik, O. Epstein, J. M. Poplawski, and E. Ehrenfreund, *SPIE*, **1997**, *3148*, 345.

[115] Y. Eichen, G. Nakmanovich, V. Gorelik, O. Epshtein, J. M. Poplawski, and E. Ehrenfreund, *J. Am. Chem. Soc.*, **1998**, *120*, 10463.

[116] P. Baxter, J.-M. Lehn, A. DeCian, and J. Fischer, *Angew. Chem. Int. Ed. Engl.*, **1993**, *32*, 69.

[117] P. N. W. Baxter, J.-M. Lehn, J. Fischer, and M.-T. Youinou, *Angew. Chem. Int. Ed. Engl.*, **1994**, *33*, 2284.

[118] D. Gust, *Nature*, **1994**, *372*, 133.

[119] P. Ceroni, F. Paolucci, C. Paradisi, A. Juris, S. Roffia, S. Serroni, S. Campagna, and A. J. Bard, *J. Am. Chem. Soc.*, **1998**, *120*, 5480.

[120] B. M. Ginzburg, N. V. Mikhailova, V. I. Nikitina, A. S. Sidorovich, S. Tupchiyev, and S. Y. Frenkel, *Polym. Sci. USSR*, **1967**, *9*, 2694.

[121] M. Knaapila, *Special Assignment: Feasibility of Methanesulfonic Acid Solvent of Construct Supramolecular Structures of Octyl Gallate and Poly(p-pyridine)* (Helsinki University of Technology; Materials Physics Laboratory, **1999**).

[122] G. Mao, M. J. Winokur, and F. E. Karasz, *Phys. Rev. B*, **1998**, *58*, 4089.

[123] M. Knaapila, L. E. Horsburgh, A. P. Monkman, and O. Ikkala, *A Method of Aligning Polymer Chains, PCT Int. Appl. FI0300245*, **2003**. 46 pp.

[124] M. Knaapila, L. E. Horsburgh, A. P. Monkman, and O. Ikkala, *Menetelmä polymeeriketjujen suuntaamiseksi, Finnish Patent Application 20020615*, **2002**. 46 pp.

[125] A. G. MacDiarmid, *Rev. Mod. Phys.*, **2001**, *73*, 701.

[126] Y. S. Negi and P. v. Adhyapak, *J. Macromol. Sci; Polym. Rev.*, **2002**, *C42*, 35.

[127] P. N. Adams, P. J. Laughlin, A. P. Monkman, and A. M. Kenwright, *Polymer*, **1996**, *37*, 3411.

[128] P. N. Adams, P. Devasagayam, S. J. Pomfret, L. Abell, and A. P. Monkman, *J. Phys.: Condens. Matter*, **1998**, *10*, 8293.

[129] J. Eiffler, H. P. Schneider, P. N. Adams, D. Bloor, and A. P. Monkman, *Crosslinked conjugated polymers for films and fibers of high strength and conductivity, Eur. Pat. Appl. EP577406*, **1994**. 14 pp.

[130] S. J. Pomfret, P. N. Adams, N. P. Comfort, and A. P. Monkman, *Adv. Mater.*, **1998**, *10*, 1351.

[131] P. N. Adams, A. P. Monkman, and S. J. Pomfret, *Fluid polymer mixtures for preparation of conductive polymer compositions from sulfonic acid-doped polyanilines, PCT Int. Appl. WO9924991*, **1999**. 18 pp.

[132] S. J. Pomfret, P. N. Adams, N. P. Comfort, and A. P. Monkman, *Polymer*, **1999**, *41*, 2265.

[133] J. Zhou, G. Tzamalis, N. A. Zaidi, N. P. Comfort, and A. P. Monkman, *J. Appl. Polym. Sci.*, **2001**, *79*, 2503.

[134] C. Ober and G. Wegner, *Adv. Mat.*, **1997**, *9*, 17.

[135] R. S. Kohlman, A. Zibold, D. B. Tanner, G. G. Ihas, T. Ishiguro, Y. G. Min, A. G. MacDiarmid, and A. J. Epstein, *Phys. Rev. Lett.*, **1997**, *78*, 3915.

[136] J. Yang, S. M. Burkinshaw, J. Zhou, A. P. Monkman, and P. J. Brown, *Adv. Mater.*, **2003**, *15*, 1081.

[137] A. Y. Grosberg and A. R. Khokhlov, *Statistical Physics of Macromolecules* (American Institute of Physics, **1994**).

[138] Y. Cao, P. Smith, and A. J. Heeger, *Synth. Met.*, **1992**, *48*, 91.

[139] Y. Cao and P. Smith, *Polymer*, **1993**, *34*, 3139.

[140] T. Vikki, L.-O. Pietilä, H. Österholm, L. Ahjopalo, A. Takala, A. Toivo, K. Levon, P. Passiniemi, and O. Ikkala, *Macromolecules*, **1996**, *29*, 2945.

[141] A. G. MacDiarmid and A. J. Epstein, *Synth. Met.*, **1994**, *65*, 103.

[142] M. Reghu, C. O. Yoon, C. Y. Yang, D. Moses, P. Smith, A. J. Heeger, and Y. Cao, *Phys. Rev. B*, **1994**, *50*, 13931.

[143] C. Y. Yang, Y. Cao, P. Smith, and A. J. Heeger, *Synth. Met.*, **1993**, *53*, 293.

[144] H. Cheun, B. Tanto, W. Chunwaschirasiri, B. Larson, and M. J. Winokur, *Appl. Phys. Lett.*, **2004**, *84*, 22.

[145] M. Grell, D. D. C. Bradley, G. Ungar, J. Hill, and K. S. Whitehead, *Macromolecules*, **1999**, *32*, 5810.

[146] M. Grell, W. Knoll, D. Lupo, A. Meisel, T. Miteva, D. Neher, H.-G. Nothofer, U. Scherf, and A. Yasuda, *Adv. Mater.*, **1999**, *11*, 671.

[147] M. Grell, D. D. C. Bradley, M. Inbasekaran, G. Ungar, K. S. Whitehead, and E. P. Woo, *Synth. Met.*, **2000**, *111-112*, 579.

[148] K. S. Whitehead, M. Grell, D. D. C. Bradley, M. Jandke, and P. Strohriegl, *Appl. Phys. Lett.*, **2000**, *76*, 2946.

[149] S. Kawana, M. Durrell, J. Lu, J. E. MacDonald, M. Grell, D. D. C. Bradley, P. C. Jukes, R. A. L. Jones, and S. L. Bennett, *Polymer*, **2002**, *43*, 1907.

[150] J. M. Lupton, M. R. Craig, and E. W. Meijer, *Appl. Phys. Lett.*, **2002**, *80*, 4489.

[151] M. J. Winokur, J. Slinker, and D. L. Huber, *Phys. Rev. B*, **2003**, *67*, 184106/1.

[152] G. Fytas, H. G. Nothofer, U. Scherf, D. Vlassopoulos, and G. Meier, *Macromolecules*, **2002**, *35*, 481.

[153] M. J. Banach, R. H. Friend, and H. Sirringhaus, *Macromolecules*, **2003**, *36*, 2838.

[154] G. Lieser, M. Oda, T. Miteva, A. Meisel, H.-G. Nothofer, U. Scherf, and D. Neher, *Macromolecules*, **2000**, *33*, 4490.
[155] M. Tammer, R. W. T. Higgins, and A. P. Monkman, *J. Appl. Phys.*, **2002**, *91*, 4010.
[156] B. P. Lyons, K. S. Wong, and A. P. Monkman, *J. Chem. Phys.*, **2003**, *118*, 4707.
[157] S. Sinha, C. Rothe, R. Güntner, U. Scherf, and A. P. Monkman, *Phys. Rev. Lett.*, **2003**, *90*, 127402(1).
[158] L. Kinder, J. Kanicki, J. Swensen, and P. Petroff, *Proc. SPIE Int. Soc. Opt. Eng.*, **2003**, *5217*, 35.
[159] Y. Geng, A. Trajkovska, D. Katsis, J. J. Ou, S. W. Culligan, and S. H. Chen, *J. Am. Chem. Soc.*, **2002**, *124*, 8337.
[160] J.-M. Lehn, *Supramolecular Chemistry* (VCH, Weinham, **1995**).
[161] U. Müller, *Inorganic Structural Chemistry*, 2 ed. (John Wiley & Sons, Chichester, **1993**).
[162] M. Muthukumar, C. K. Ober, and E. L. Thomas, *Science*, **1997**, *277*, 1225.
[163] F. S. Bates and G. H. Fredrickson, *Annu. Rev. Phys. Chem.*, **1990**.
[164] I. W. Hamley, *The Physics of Block Copolymers* (Oxford University Press, Oxford, **1998**).
[165] J. Ruokolainen, M. Saariaho, O. Ikkala, G. ten Brinke, E. L. Thomas, M. Torkkeli, and R. Serimaa, *Macromolecules*, **1999**, *32*, 1152.
[166] F. S. Bates, *Macromolecules*, **1984**, *17*, 2607.
[167] S. I. Stupp and P. V. Braun, *Science*, **1997**, *277*, 1242.
[168] S. I. Stupp, M. Keser, and G. N. Tew, *Polymer*, **1998**, *39*, 4505.
[169] S. A. Jenekhe and X. L. Chen, *Science*, **1998**, *279*, 1903.
[170] E. R. Zubarev, M. U. Pralle, L. Li, and S. I. Stupp, *Science*, **1999**, *283*, 523.
[171] J. F. Rosedale, F. S. Bates, K. Almdal, K. Mortensen, and G. D. Wignall, *Macromolecules*, **1995**, *28*, 1429.
[172] F. Vögtle, *Supramolecular Chemistry* (John Wiley & Sons, Chichester, **1991**).
[173] S. Menzer, A. J. P. White, D. J. Williams, M. Belohradský, C. Hamers, F. M. Raymo, A. N. Shipway, and J. F. Stoddart, *Macromolecules*, **1998**, *31*, 295.
[174] P. Kohli, K. K. Taylor, J. J. Harris, and G. J. Blanchard, *J. Am. Chem. Soc.*, **1998**, *120*, 11962.
[175] L. Brunsveld, B. J. B. Folmer, E. W. Meijer, and R. P. Sijbesma, *Chem. Rev.*, **2001**, *101*, 4071.
[176] V. V. Tsukruk, *Progress in Polym Sci*, **1997**, *22*, 247.
[177] P. J. Flory, *Adv. Polym. Sci.*, **1984**, *59*, 1.
[178] M. A. Osipov, Molecular Theory of Cholestic Polymers, in *Liquid Crystalline and Mesomorphic Polymers*; (Eds: V. P. Shiparew and L. Lam) Springer Verlag, New York, **1994**.
[179] V. P. Shipaev, Y. S. Freidzon, and S. G. Kostromin, Molecular Architecture and Structure of Thermotropic Liquid Crystal Polymers with Mesogenic Side Groups, in *Liquid Crystalline and Mesomorphic Polymers*; (Eds: V. P. Shiparew and L. Lam) Springer Verlag, New York, **1994**.
[180] A. H. Windle, Structure of Thermotropic Main-Chain Polymers, in *Liquid Crystalline and Mesomorphic Polymers*; (Eds: V. P. Shiparew and L. Lam) Springer Verlag, New York, **1994**.
[181] L. Lam, Bowlings, in *Liquid Crystalline and Mesomorphic Polymers*; (Eds: V. P. Shiparew and L. Lam) Springer Verlag, New York, **1994**.
[182] G. ten Brinke, J. Ruokolainen, and O. Ikkala, *Europhys. Lett.*, **1996**, *35*, 91.
[183] V. V. Tsukruk and J. H. Wendorff, *Trends in Polym. Sci.*, **1995**, *3*, 82.
[184] P. J. Flory, *Principles of Polymer Chemistry* (Cornel University Press, Ithaca, New York, **1953**).
[185] P.-G. de Gennes, *Scaling Concepts in Polymer Physics* (Cornell University Press, Ithaca, **1979**).
[186] T. Tsuda, Ladder Polymers (Cycloaddition Copolymerization of Cyclic Diynes), in *Polymeric Materials Encyclopedia*; (Eds: S. J. C.) CRC Press, Boca Raton, **1996**.
[187] J. Grüner, P. J. Hamer, R. H. Friend, H.-J. Huber, U. Scherf, and A. B. Holmes, *Adv. Mater.*, **1994**, *6*, 748.
[188] N. Grassie and I. C. McNeill, *J. Chem. Soc.*, **1956**, 3929.
[189] N. Grassie and I. C. McNeill, *J. Polym. Sci.*, **1958**, *27*, 207.
[190] L. K. H. van Beek, *J. App. Polym. Sci.*, **1965**, *9*, 553.
[191] H. Teoh, D. MacInnes, and P. D. Metz, *J. Phys. (Paris)*, **1983**, *44*, 687.
[192] T.-C. Chung, Y. Schlesinger, S. Etemad, A. G. MacDiarmid, and A. J. Heeger, *Journal of Polymer Science*, **1984**, *22*, 1239.
[193] G. Mengoli, C. Pagura, R. Salmaso, R. Tomat, and S. Zecchin, *Synth. Met.*, **1986**, *16*, 173.
[194] J. L. Bredas and W. R. Salaneck, *J. Chem. Phys.*, **1986**, *85*, 2219.
[195] C. L. Renschler and L. V. Salgado, *Polym. Mater. Sci. Eng.*, **1988**, *59*, 1058.
[196] L. H. Peebles, P. Peyser, A. W. Snow, and W. C. Peters, *Carbon*, **1990**, *28*, 707.
[197] L. H. Peebles, A. W. Snow, and W. C. Peters, *J. Poly. Sci: Part A: Polymer Chemistry*, **1995**, *33*, 2069.
[198] L. L. Bircumschaw, F. M. Tayler, and D. H. Whiffen, *J. Am. Chem. Soc.*, **1954**, *931*, 931.
[199] E. Polushkin, G. O. R. Alberda van Ekenstein, M. Knaapila, J. Ruokolainen, M. Torkkeli, R. Serimaa, W. Bras, I. Dolbnya, O. Ikkala, and G. ten Brinke, *Macromolecules*, **2001**, *34*, 4917.
[200] H. Menzel, Hairy Rod-Like Polymers, in *Polymer Materials Encyclopedia*; (Eds: J. C. Salamone) CRC Press, Boca Raton, **1996**, pp. 2916.
[201] M. Ballauf, *Makromol. Chem., Rapid Commun.*, **1986**, *7*, 407.
[202] R. Duran, M. Ballauf, M. Wenzel, and G. Wegner, *Macromolecules*, **1988**, *21*, 2897.
[203] M. Ballauf and G. F. Schmidt, *Makromol. Chem., Rapid Commun.*, **1987**, *8*, 93.
[204] M. Ballauf, *Angew. Chem. Int. Ed. Engl.*, **1989**, *28*, 253.
[205] M. Ballauff, *J. Polym. Sci., Part B, Polym.*, **1987**, *25*, 739.
[206] J. J. Ge, A. Zhang, K. W. McCreight, R.-M. Ho, S.-Y. Wang, X. Jin, F. W. Harris, and S. Z. D. Cheng, *Macromolecules*, **1997**, *30*, 6498.
[207] F. Helmer-Metzmann, M. Ballauff, R. C. Schulz, and G. Wegner, *Makromol. Chem.*, **1989**, *190*, 985.
[208] M. Wenzel, M. Ballauff, and G. Wegner, *Makromol. Chem.*, **1987**, *188*, 2865.
[209] G. Wegner, *Macrom. Chem. Phys.*, **2003**, *204*, 347.
[210] T. Bjornholm, T. Hassenkam, and N. Reitzel, *J. Mater. Chem.*, **1999**, *9*, 1975.
[211] M. Itoh and M. Itaru, *J. Polym. Sci.: Part A: Polymer Chemistry*, **1994**, *32*, 1581.
[212] G. Petekidis, D. Vlassopoulos, G. Fytas, N. Kountourakis, and S. Kumar, *Macromolecules*, **1997**, *30*, 919.
[213] G. Petekidis, D. Vlassopoulos, G. Fytas, R. Rülkens, and G. Wegner, *Macromolecules*, **1998**, *31*, 6128.

[214] G. Petekidis, D. Vlassopoulos, G. Fytas, R. Rülkens, G. Wegner, and G. Fleischer, *Macromolecules*, **1998**, *31*, 6139.
[215] T. Liu, R. Rulkens, G. Wegner, and B. Chu, *Macromolecules*, **1998**, *31*, 6119.
[216] S. Vanhee, R. Rulkens, U. Lehmann, C. Rosenauer, M. Schulze, W. Köhler, and G. Wegner, *Macromolecules*, **1996**, *29*, 5136.
[217] W. Zheng, K. Levon, T. Taka, J. Laakso, and J.-E. Österholm, *J. Polym. Sci.: Part B: Polymer Physics*, **1995**, *33*, 1289.
[218] S.-A. Chen and J.-M. Ni, *Macromolecules*, **1992**, *25*, 6081.
[219] K. Levon, E. Chu, K.-S. Ho, T. K. Kwei, J. Mao, W.-Y. Zheng, and J. Laakso, *J. Polym. Sci. :Part B: Polymer Physics*, **1995**, *33*, 537.
[220] P. M. Cotts, T. M. Swager, and Q. Zhou, *Macromolecules*, **1996**, *29*, 7323.
[221] E. Mena-Osteritz, A. Meyer, B. M. W. Langeveld-Voss, R. A. J. Janssen, E. W. Meijer, and P. Bäuerle, *Adv. Mater.*, **2000**, *39*, 2680.
[222] J. Roncali, *Chem. Rev.*, **1992**, *92*, 711.
[223] M. Theander, O. Inganäs, W. Mammo, T. Olinga, M. Svensson, and M. R. Andersson, *J. Phys. Chem. B*, **1999**, *103*, 7771.
[224] P. Dyreklev, M. Berggren, O. Inganäs, M. R. Andersson, O. Wennerström, and T. Hjertberg, *Adv. Mater.*, **1995**, *7*, 43.
[225] M. Grell and D. D. C. Bradley, *Adv. Mater.*, **1999**, *11*, 895.
[226] B. M. W. Langeveld-Voss, R. A. J. Janssen, M. P. T. Christiaans, S. C. J. Meskers, H. P. J. M. Dekkers, and E. W. Meijer, *J. Am. Chem. Soc.*, **1996**, *118*, 4908.
[227] B. M. W. Langeveld-Voss, R. A. J. Janssen, and E. W. Meijer, *J. Mol. Struct.*, **2000**, *521*, 285.
[228] P. J. Brown, D. S. Thomas, A. Kohler, J. S. Wilson, J.-S. Kim, C. M. Ramsdale, H. Sirringhaus, and R. H. Friend, *Phys. Rev. B.*, **2003**, *67*, 064203/1.
[229] M. J. Winokur, D. Spiegel, Y. Kim, S. Hotta, and A. J. Heeger, *Synth. Met.*, **1989**, *28*, C419.
[230] K. Tashiro, K. Ono, Y. Minagawa, M. Kobayashi, T. Kawai, and K. Yoshino, *J. Polym. Sci. B: Polym. Phys.*, **1991**, *29*, 1223.
[231] K. Tashiro, K. Ono, Y. Minagawa, K. Kobayashi, T. Kawai, and K. Yoshino, *Synth. Met.*, **1991**, *41*, 571.
[232] T. J. Prosa, M. J. Winokur, J. Moulton, P. Smith, and A. J. Heeger, *Macromolecules*, **1992**, *25*, 4364.
[233] K. C. Park and K. Levon, *Macromolecules*, **1997**, *30*, 3175.
[234] T. J. Prosa, J. Moulton, A. J. Heeger, and M. J. Winokur, *Macromolecules*, **1999**, *32*, 4000.
[235] K. E. Aasmundtveit, E. J. Samuelsen, M. Guldstein, C. Steinsland, O. Flornes, C. Fagermo, T. M. Seeberg, L. A. A. Pettersson, O. Inganäs, R. Feidenhans'l, and S. Ferrer, *Macromolecules*, **2000**, *33*, 3120.
[236] K. E. Aasmundtveit, E. J. Samuelsen, W. Mammo, M. Svensson, M. R. Andersson, L. A. A. Pettersson, and O. Inganäs, *Macromolecules*, **2000**, *33*, 5481.
[237] D. W. Breiby, E. J. Samuelsen, L. Groenendaal, and B. Struth, *J. Polym. Sci. B: Polym. Phys.*, **2003**, *41*, 945.
[238] L. Groenendaal, F. Jonas, D. Freitag, H. Pielartzik, and J. R. Reynolds, *Adv. Mater.*, **2000**, *12*, 481.
[239] J. J. Apperloo, R. A. J. Janssen, P. R. L. Malenfant, L. Groenendaal, and J. M. J. Fréchet, *J. Am. Chem. Soc.*, **2000**, *122*, 7042.
[240] K. Kishikawa, M. C. Harris, and T. M. Swager, *Chem. Mater.*, **1999**, *11*, 867.
[241] E. Lankinen, G. Sundholm, P. Talonen, H. Granö, and F. Sundholm, *J. Electroanal. Chem.*, **1999**, *460*, 176.
[242] V. Balzani, M. Gómez-López, and J. F. Stoddart, *Acc. Chem. Res.*, **1998**, *31*, 405.
[243] F. M. Raymo and J. F. Stoddart, *Chem. Rev.*, **1999**, *99*, 1643.
[244] J. F. Stoddart, *Acc. Chem. Res.*, **2001**, *34*, 410.
[245] Y. Wei, W. W. Focke, G. E. Wnek, A. Ray, and A. MacDiarmid, *J. Phys. Chem.*, **1989**, *93*, 495.
[246] A. J. Berresheim, M. Müller, and K. Müllen, *Chem. Rev.*, **1999**, *99*, 1747.
[247] L. Schidt-Mende, A. Fechtenkötter, K. Müllen, E. Moons, R. H. Friend, and J. D. MacKenzie, *Science*, **2001**, *293*, 1119.
[248] A. Van de Craats, N. Stutzmann, R. H. Friend, and H. Sirringhaus, *Aligned discotic liquid crystals for devices, PCT Int. Appl. WO 2003023506*, **2003**. 41 pp.
[249] A. M. van de Craats, N. Stutzmann, O. Bunk, M. M. Nielsen, M. Watson, K. Müllen, H. D. Chanzy, H. Sirringhaus, and R. H. Friend, *Adv. Mater.*, **2003**, *15*, 495.
[250] J. M. Robertson, *J. Chem. Soc.*, **1935**, 615.
[251] J. M. Robertson, *J. Chem. Soc.*, **1936**, 1195.
[252] J. M. Robertson and I. Woodward, *J. Chem. Soc.*, **1937**, 219.
[253] R. P. Linstead, *Ber. Deutsch. Chem. Ges.*, **1939**, *A72*, 93.
[254] R. P. Linstead, *J. Chem. Soc.*, **1953**, 2873.
[255] C. F. van Nostrum and R. J. M. Nolte, *Macromol. Symp.*, **1994**, *77*, 267.
[256] M. Hanack and M. Lang, *Adv. Mat.*, **1994**, *6*, 819.
[257] W. Knoll, L. Angermaier, G. Batz, T. Fritz, S. Fujisawa, T. Furuno, H.-J. Guder, M. Hara, M. Liley, K. Niki, and J. Spinke, *Synth. Met.*, **1993**, *61*, 5.
[258] J. M. Fox, T. J. Katz, S. Van Elshocht, T. Verbienst, M. Kauranen, A. Persoons, T. Thongpanchang, T. Krauss, and L. Brus, *J. Am. Chem. Soc.*, **1999**, *121*, 3453.
[259] C. F. van Nostrum, S. J. Picken, A.-J. Schouten, and R. J. M. Nolte, *J. Am. Chem. Soc.*, **1995**, *117*, 9957.
[260] T. Verbiest, S. van Elshocht, M. Kauranen, L. Hellemans, J. Snauwaert, C. Nuckolls, T. J. Katz, and A. Persoons, *Science*, **1998**, *282*, 913.
[261] M. Sommerauer, C. Rager, and M. Hanack, *J. Am. Chem Soc.*, **1996**, *118*, 10085.
[262] D. M. Knawby and T. M. Swager, *Chem. Mater.*, **1997**, *9*, 535.
[263] F. Fernández-Lázaro, T. Torres, B. Hauschel, and M. Hanack, *Chem. Rev.*, **1998**, *98*, 563.
[264] *Neutron and Synchrotron Radiation for Condensed Matter Studies; Theory, Instruments, and Methods*; HERCULES - Higher European Research Course for Users of Large Experimental Systems*Vol. I*, edited by J. Baruchel, J.-L. Hodeau, M. S. Lehmann, J.-R. Regnard, and C. Schlenker (Springer-Verlag, Berlin, 1993).
[265] *Neutron and Synchrotron Radiation for Condensed Matter Studies; Application to Solid State Physics and Chemistry*; HERCULES - Higher European Research Course for Users of Large Experimental Systems*Vol. II*, edited by J. Baruchel, J.-L. Hodeau, M. S. Lehmann, J.-R. Regnard, and C. Schlenker (Springer-Verlag, Berlin, 1993).
[266] D. Attwood, *Soft X-Rays and Extreme Ultraviolet Radiation: Principles and Applications* (Cambridge University Press, Cambridge, **2000**).
[267] H. Winick, *X-Ray Data Booklet* (Lawrence Berkeley National Laboratory, University of California, Berkeley, **2001**).

[268] B. E. Warren, *X-Ray Diffraction* (Addison Wesley, Reading Massachusetts, **1969**).
[269] K. Fontell, X-ray Diffraction by Liquid Crystals-Amphiphilic Systems, in *Liquid Crystals and Plastic Crystals*; (Eds: G. W. Cray and P. A. Windor) Chichester, **1974**, pp. 81.
[270] H. P. Klug and L. E. Alexander, *X-Ray Diffraction Procedures for Polycrystalline and Amorphous Materials* (John Wiley & Sons, New York, **1974**).
[271] G. Porod, General Theory, in *Small Angle X-ray Scattering*; (Eds: O. Glatter and O. Kratky) Academic Press, London, **1982**.
[272] L. A. Feigin and D. I. Svergun, *Structure Analysis by Small-Angle X-Ray and Neutron Scattering* (Plenum Press, New York, **1987**).
[273] F. J. Baltá-Calleja and C. G. Vonk, *X-ray Scattering of Synthetic Polymers* (Elsevier Publishers, Amsterdam, **1989**).
[274] D. D. L. Chung, P. W. Datinvan, and M. Arnold, *X-ray Diffraction at Elevated Temperatures* (VCH, New-York, **1993**).
[275] A. Guinier, *X-Ray Diffraction in Crystals, Imperfect Crystals, and Amorphous Bodies* (Dover Publications, New York, **1994**).
[276] M. J. Winokur, Studies of Local Structure in Polymers using X-Ray Scattering, in *Local Structure from Diffraction*; (Eds: S. J. L. Billinge and M. F. Thorpe) Plenum Press, New York, **1998**.
[277] R.-J. Roe, *Methods of X-Ray and Neutron Scattering in Polymer Science* (Oxford University Press, Oxford, **2000**).
[278] R. F. Kruh, Radial-Distribution Analysis, in *Handbook of X-rays*; (Eds: E. F. Kaelbe) New York, **1976**, pp. 22.
[279] W. Parrish, Powder and Related Techniques: X-ray Techniques, in *International Tables for Crystallography*; (Eds: A. J. C. Wilson) Kluwer Academic Publication, Dordrecht, **1993**, pp. 42.
[280] P. Suortti and L. D. Jennings, *Acta Crystallogr. Sect. A*, **1977**, *A33*, 1012.
[281] H. D. Bartunik, in *Handbook on Synchrotron Radiation*; (Eds: S. E. Bashi, M. Koch, and E. Rubenstein) Elsevier Science Publishers, Amsterdam, **1990**, pp. 147.
[282] J. R. Halliwell, *Macromolecular Crystallography with Synchtrotron Radiation* (Cambridge university press, Cambridge, **1992**).
[283] R. Kahn, P. Carpentier, C. Berthet-Colominas, M. Capitan, M.-L. Chesne, E. Fanchon, S. Lequien, D. Thiaudière, J. Vicat, P. Zielinski, and H. Stuhrmann, *J. Synchrotron Rad.*, **2000**, *7*, 131.
[284] L. Kissel, B. Zhou, S. C. Roy, S. K. Sen Gubta, and R. H. Pratt, *Acta Cryst.*, **1995**, *A51*, 271.
[285] J. E. Epperson and P. Thiyagarajan, *J. Appl. Cryst.*, **1988**, *21*, 652.
[286] D. Harker and J. S. Kasper, *Acta Crystallogr.*, **1948**, *1*, 70.
[287] J. Karle and H. Hauptman, *Acta Crystallogr.*, **1950**, *3*, 181.
[288] C. Giacovazzo, Direct Methods, in *International Tables for Crystallography*; (Eds: U. Shmuli) Kluwer Academic Publication, Dordrecht, **1993**, pp. 201.
[289] J. C. Dunitz, *X-ray analysis and the structure of organic molecules* (Cornell University Press, Ithaca, **1979**).
[290] D. W. Breiby and E. J. Samuelsen, *J. Polym. Sci. Part B: Polym. Phys.*, **2003**, *41*, 2375.
[291] U. Vainio, Master's Thesis, University of Helsinki, **2003**.
[292] N. Armstrong and W. Kalceff, *J. Appl. Cryst.*, **1998**, *31*, 453.
[293] N. Armstrong and W. Kalceff, *J. Appl. Cryst.*, **1999**, *32*, 600.
[294] T. Ida and H. Toraya, *J. Appl. Cryst.*, **2002**, *35*, 58.
[295] L. Alexander, *J. Appl. Phys.*, **1954**, *25*, 155.
[296] T. Ida and K. Kimura, *J. Appl. Cryst.*, **1999**, *32*, 634.
[297] T. Ida and K. Kimura, *J. Appl. Cryst.*, **1999**, *32*, 982.
[298] M. Knaapila, Master's Thesis, Helsinki University of Technology, **1999**.
[299] K. Jokela, R. Serimaa, M. Torkkeli, F. Sundholm, T. Kallio, and G. Sundholm, *J. Polym. Sci. B: Polym. Phys.*, **2001**, *40*, 1539.
[300] K. Jokela, A. Väänänen, M. Torkkeli, P. Starck, R. Serimaa, B. Löfgren, and J. Seppälä, *J. Polym. Sci. B: Polym. Phys.*, **2001**, *39*, 1860.
[301] R. J. Hunter, *Introduction to Modern Colloid Science* (Oxford University Press, Oxford, **1993**).
[302] M. J. Winokur and B. R. Mattes, *Phys. Rev. B*, **1996**, *54*, 12637.
[303] K. S. Vahvaselkä, R. Serimaa, and M. Torkkeli, *J. Appl. Cryst*, **1995**, *28*, 189.
[304] F. S. Bates, *Macromolecules*, **1985**, *18*, 525.
[305] J. Huh, O. Ikkala, and G. ten Brinke, *Macromolecules*, **1997**, *30*, 1828.
[306] J. Maron, M. J. Winokur, and B. R. Mattes, *Macromolecules*, **1995**, *28*, 4475.
[307] D. Chen, M. J. Winokur, M. A. Masse, and F. E. Karasz, *Polymer*, **1992**, *33*, 3116.
[308] A. Naudon, T. Slimani, and P. Goudeau, *J. Appl. Cryst.*, **1991**, *24*, 501.
[309] A. Naudon and D. Thiaudiere, *J. Appl. Cryst.*, **1997**, *30*, 822.
[310] T. Slimani, P. Goudeau, A. Naudon, G. Farges, and J. L. Derep, *J. Appl. Cryst.*, **1991**, *24*, 638.
[311] A. Njeh, T. Wieder, and H. Fuess, *Powder Diffraction*, **2000**, *15*, 211.
[312] T. P. A. Hase, E. M. Ho, J.-J. Freijo, S. M. Thompson, A. K. Petford-Long, and B. K. Tanner, *J. Phys. D: Appl. Phys.*, **2003**, *36*, A231.
[313] H. Dosch, Critical Phenomena at Surfaces and Interfaces, in *Springer Tracts in Modern Physics*; (Eds: G. Hoehler) Springer Verlag, Berlin, **1992**.
[314] J. Clarke, I. Pape, P. Normile, and B. K. Tanner, *J. Phys. D: Appl. Phys.*, **2003**, *36*, A209.
[315] J. Saenger, W. Gronski, H. Leist, and U. Wiesner, *Macromolecules*, **1997**, *30*, 7621.
[316] R. von Hosemann and W. Wilke, *Macromol. Chem.*, **1968**, *118*, 239.
[317] S. Sakurai, S. Okamoto, T. Kawamura, and T. Hashimoto, *J. Appl. Cryst.*, **1991**, *24*, 679.
[318] B. E. Warren and B. L. Averbach, *J. Appl. Phys.*, **1952**, *23*, 497.
[319] B. Tomberli, C. J. Benmore, P. A. Egelstaff, J. Neuefeind, and V. Honkimäki, *Journal of Physics B: Condens. Mater.*, **2000**, *12*, 2597.
[320] Y. D. Lee, P. J. Phillips, and J. S. Lin, *J. Polym. Sci. B: Polym. Phys.*, **1991**, *29*, 1235.
[321] M. Borsboom, W. Bras, I. Cerjak, D. Detollenaere, D. Glastra van Loon, P. Goedtkindt, M. Konijnenburg, P. Lassing, Y. K. Levine, B. Munneke, M. Overluizen, R. van Tol, and E. Vlieg, *J. Synchrotron Rad.*, **1998**, *5*, 518.
[322] W. Bras, *J. Macromol. Sci. Phys*, **1998**, *B37*, 557.
[323] W. Bras and A. J. Ryan, *Adv. Colloid Interface Sci.*, **1998**, *75*, 1.

[324] E. Homan, M. Konijnenburg, C. Ferrero, R. E. Ghosh, I. P. Dolbnya, and W. Bras, *J. Appl. Cryst.*, **2001**, *34*, 519.

[325] P. Debye, *Ann. Physik (Berlin)*, **1915**, *46*, 809.

[326] L. S. Ornstein and F. Zernike, *Proc. Acad. Sci. (Amsterdam)*, **1914**, *17*, 793.

[327] M. Plischke and B. Bergersen, *Equilibrium Statistical Physics*, 2 ed. (World Scientific, Singapore, **1994**).

[328] P. Debye and A. M. Bueche, *J. Appl. Phys.*, **1949**, *20*, 518.

[329] G. R. Strobl, *The Physics of Polymers*, 2nd ed. (Springer-Verlag, Berlin, **1997**).

[330] L. Rayleigh, *Proc. Roy. Soc. London*, **1911**, *A-84*, 25.

[331] R. G. Kirste and C. Oberthür, Synthetic Polymers in Solution, in *Small Angle X-ray Scattering*; (Eds: O. Glatter and O. Kratky) Academic Press, London, **1982**, pp. 387.

[332] O. Kratky and G. Porod, *J. Colloid Interface Sci.*, **1949**, *4*, 35.

[333] G. D. Wignall, in *Physical Properties of Polymers Handbook*; (Eds: J. E. Mark) American Institute of Physics, New York, **1996**.

[334] J. H. Burroughes, D. D. C. Bradley, A. R. Brown, R. N. Marks, K. Mackay, R. H. Friend, P. L. Burns, and A. B. Holmes, *Nature*, **1990**, *347*, 539.

[335] T. Yamamoto, *Polarizing polymer film, Patent, Jpn. Kokkai Tokkyo Koho JP03089202*, **1991**. 6 pp.

[336] N. A. J. M. van Aerle, M. Barmentlo, and R. W. J. Hollering, *J. Appl. Phys.*, **1993**, *77*, 3111.

[337] A. Montali, C. Bastiaansen, P. Smith, and C. Weder, *Nature*, **1998**, *392*, 261.

[338] D. Steiger, M. Ehrenstein, C. Weder, and P. Smith, *Macromolecules*, **1998**, *31*, 1254.

[339] C. Weder, C. Sarwa, C. Bastiaansen, and P. Smith, *Adv. Mater.*, **1997**, *9*, 1035.

[340] C. Weder, C. Sarwa, A. Montali, C. Bastiaansen, and P. Smith, *Science*, **1998**, *279*, 835.

[341] E. Peeters, M. P. T. Christiaans, R. A. J. Janssen, H. F. M. Schoo, H. P. J. M. Dekkers, and E. W. Meijer, *J. Am. Chem. Soc.*, **1997**, *119*, 9909.

[342] A. J. Heeger and D. Braun, *Visible Light Emitting Diodes Fabricated from Soluble Semiconducting Polymers, US Patent US5408109*, **1995**. 34 pp.

[343] Z. Bao and X. L. Chen, *Process for fabricating polarized organic phonics devices, PCT Int. Appl. EP1081774*, **2001**. 15 pp.

[344] J. Hegenbarth and D. R. Carpenter, *Oriented Crystalline Materials, US Patent US5772755*, **1998**. 5 pp.

[345] W. Caseri, T. Sauer, and G. Wegner, *Macromol. Chem., Rap. Commun.*, **1988**, *9*, 651.

[346] D. Lupo, A. Yasuda, M. Grell, D. Neher, and T. Miteva, *Polyimide layer comprising functional material, device employing the polyimide layer, manufacturing the device, Eur. Pat. Appl. EP1011154*, **2000**. 29 pp.

[347] G. Lüssem, R. Festag, A. Greiner, C. Schmidt, C. Unterlechner, W. Heitz, J. H. Wendorff, M. Hopmeier, and J. Feldmann, *Adv. Mater.*, **1995**, *7*, 923.

[348] C. Weder, C. Bastiaansen, A. Montali, and P. Smith, *Efficient photoluminescent polarizers, process for forming, and application in display devices, WO9939222*, **1999**. 76 pp.

[349] T. Deng, A. Craig, T. Breiner, T. M. Swager, and E. L. Thomas, *Abstracts, 31st Northeast Regional Meeting of the American Chemical Society, Saratoga Springs, NY, United States, June 15-18 (2003)*, **2003**.

[350] C. A. Breen, T. Deng, T. Breiner, E. L. Thomas, and T. M. Swager, *J. Am. Chem. Soc.*, **2003**, *125*, 9942.

[351] A. L. Fetter and J. D. Walecka, *Quantum Theory of Many-Particle Physics* (McGraw-Hill, New York, **1971**).

[352] E. Conwell, Intramolecular Excitons and Intermolecular Polaron Pairs as Primary Photoexcitations in Conjugated Polymers, in *Primary Photoexcitations in Conjugated Polymers*; (Eds: N. S. Sariciftci) World Scientific, Singapore, **1997**, pp. 99.

[353] A. P. Monkman, H. D. Burrows, L. J. Hartwell, L. E. Horsburgh, I. Hamblett, and S. Navaratnam, *Phys. Rev. Lett.*, **2001**, *86*, 1358.

[354] M. Wohlgenannt, K. Tandon, S. Mazumdar, S. Ramasesha, and Z. V. Vardeny, *Nature*, **2001**, *409*, 494.

[355] C. Rothe, R. Guentner, U. Scherf, and A. P. Monkman, *J. Chem. Phys.*, **2001**, *115*, 9557.

[356] C. Rothe, S. I. Hintschich, L.-O. Pålsson, A. P. Monkman, and U. Scherf, *Chem. Phys. Lett.*, **2002**, *360*, 111.

[357] C. Rothe, L.-O. Pålsson, and A. P. Monkman, *Chem. Phys.*, **2002**, *285*, 95.

[358] R. W. T. Higgins, A. P. Monkman, H.-G. Nothofer, and U. Scherf, *J. Appl. Phys.*, **2002**, *91*, 99.

[359] T. H. Förster, *Z. Naturforsch. Teil A*, **1949**, *4*, 55.

[360] T. W. Hagler, K. Pakbaz, and A. J. Heeger, *Phys. Rev. B*, **1994**, *49*, 10968.

[361] T. W. Hagler, K. Pakbaz, K. F. Voss, and A. J. Heeger, *Phys. Rev. B.*, **1991**, *44*, 8652.

[362] J. Yang, Q. He, H. Lin, J. Fan, and F. Bai, *Macrom. Rapid Comm.*, **2001**, *22*, 1152.

[363] S. R. Forrest, D. D. C. Bradley, and M. E. Thompson, *Adv. Mater.*, **2003**, *15*, 1043.

[364] L.-O. Pålsson, C. Wang, D. R. Russel, A. P. Monkman, M. R. Bryce, G. Rumbles, and I. D. W. Samuel, *Chem. Phys.*, **2002**, *279*, 229.

[365] N. C. Greenham, I. D. W. Samuel, G. R. Hayes, R. T. Phillips, Y. A. R. R. Kessener, S. C. Moratti, A. B. Holmes, and R. H. Friend, *Chem. Phys. Lett.*, **1995**, *241*, 89.

[366] N. C. Greenham, S. E. Burns, I. D. W. Samuel, R. H. Friend, S. C. Moratti, and A. B. Holmes, *Molecular Crystals and Liquid Crystals Science and Technology, Section A: Molecular Crystals and Liquid Crystals*, **1996**, *283*, 51.

[367] J. C. de Mello, H. F. Wittmann, and R. H. Friend, *Adv. Mater.*, **1997**, *9*, 230.

[368] L.-O. Pålsson and A. P. Monkman, *Adv. Mater.*, **2002**, *14*, 757.

[369] M. Knaapila, K. Kisko, P. B. Lyons, R. Stepanyan, J. P. Foreman, O. H. Seeck, U. Vainio, L.-O. Pålsson, R. Serimaa, M. Torkkeli, and A. P. Monkman, *J. Phys. Chem. B*, **2004**, accepted.

[370] O. Ikkala, M. Knaapila, J. Ruokolainen, M. Torkkeli, R. Serimaa, K. Jokela, L. Horsburgh, A. Monkman, and G. ten Brinke, *Adv. Mater.*, **1999**, *11*, 1206.

[371] W. Wang, G. Lieser, and G. Wegner, *Macromolecules*, **1994**, *27*, 1027.

[372] S. M. Yu, V. P. Conticello, G. Zhang, C. Kayser, M. J. Fournier, T. L. Mason, and D. A. Tirrell, *Nature*, **1997**, *389*, 167.

[373] L. E. Horsburgh, (Personal Communication, **2002**).

[374] R. M. Silverstein, G. C. Bassler, and T. C. Morrill, *Spectometric Identification of Organic Compounds*, 5 ed. (John Wiley & Sons, New York, **1991**).

[375] M. J. Winokur and B. R. Mattes, *Synth. Met.*, **1997**, *84*, 725.

[376] M. J. Winokur and B. R. Mattes, *55th Annual Technical Conference - Society of Plastics Engineers*, **1997**, *2*, 1325.

[377] M. J. Winokur and B. R. Mattes, *Macromolecules*, **1998**, *31*, 8183.

[378] P. Rannou, A. Gawlicka, D. Berner, A. Pron, M. Nechtschein, and D. Djurado, *Macromolecules*, **1998**, *31*, 3007.

[379] M. J. Winokur and B. R. Mattes, *Journal Reinforced Plastics and Composites*, **1999**, *18*, 875.
[380] H.-L. Wang, R. J. Romero, B. R. Mattes, Y. Zhu, and M. J. Winokur, *J. Polym. Sci.:Part B Polymer Physics*, **2000**, *38*, 194.
[381] J. Ma, J. E. Fischer, E. M. Scherr, A. G. MacDiarmid, M. E. Jozefowicz, A. J. Epstein, C. Mathis, B. Francois, N. Coustel, and P. Bernier, *Phys. Rev. B*, **1991**, *44*, 11609.
[382] J. E. Fischer, Q. Zhu, X. Tang, E. M. Scherr, A. G. MacDiarmid, and V. B. Cajipe, *Macromolecules*, **1994**, *27*, 5094.
[383] W. Luzny, E. J. Samuelsen, D. Djurado, and Y. F. Nicolau, *Synth. Met.*, **1997**, *90*, 19.
[384] E. Banka and W. Luzny, *Synth. Met.*, **1999**, *101*, 715.
[385] W. Lutzny and E. Banka, *Macromolecules*, **2000**, *33*, 425.
[386] M. J. Winokur, *Synth. Met.*, **2001**, *119*, 403.
[387] L. W. Shacklette, J. F. Wolf, S. Gould, and R. H. Baugham, *J. Chem. Phys.*, **1988**, *88*, 3955.
[388] M. E. Jozefowicz, R. Laversanne, H. H. S. Javadi, A. J. Epstein, J. P. Pouget, X. Tang, and A. G. MacDiarmid, *Phys. Rev. B*, **1989**, *39*, 12958.
[389] H. Kosonen, J. Ruokolainen, M. Knaapila, M. Torkkeli, K. Jokela, R. Serimaa, G. ten Brinke, W. Bras, A. P. Monkman, and O. Ikkala, *Macromolecules*, **2000**, *33*, 8671.
[390] H. Kosonen, J. Ruokolainen, M. Knaapila, M. Torkkeli, R. Serimaa, W. Bras, A. P. Monkman, G. ten Brinke, and O. Ikkala, *Synth. Met.*, **2001**, *121*, 1277.
[391] H. Kosonen, S. Valkama, J. Ruokolainen, M. Knaapila, M. Torkkeli, R. Serimaa, A. P. Monkman, G. ten Brinke, and O. Ikkala, *Synth. Met.*, **2003**, *137*, 881.
[392] T. Yamamoto, *J. Polym. Sci.:Part A, Polymer Chemistry*, **1996**, *34*, 997.
[393] B. J. Factor, T. P. Russell, and M. F. Toney, *Phys. Rev. Lett.*, **1991**, *66*, 1181.
[394] M. R. Craig, P. Jonkheijm, S. C. J. Meskers, A. P. H. J. Schenning, and E. W. Meijer, *Adv. Mater.*, **2003**, *15*, 1435.
[395] J. P. Pouget, M. E. Jozefowicz, A. J. Epstein, X. Tang, and A. G. MacDiarmid, *Macromolecules*, **1991**, *24*, 779.
[396] H. Tadokoro, *Structure of Crystalline Polymers* (John Wiley & Sons, New York, **1979**).
[397] P. F. Rodesiler, E. A. H. Griffith, N. G. Charles, and E. L. Amma, *Acta Cryst. C*, **1985**, *C41*, 673.
[398] W. J. Evans, J. L. Shreeve, J. W. Ziller, and R. J. Doedens, *Inorg. Chem.*, **1995**, *34*, 576.
[399] P. Bolhuis and D. Frenkel, *J. Chem. Phys.*, **1997**, *106*, 666.
[400] N. Nakamura, K. Uno, and Y. Ogawa, *Acta Cryst. C*, **2001**, *C57*, 585.
[401] B. Tanto, S. Guha, C. M. Martin, U. Scherf, and M. J. Winokur, *Macromolecules*, **2004**, *submitted*.

# Appendix

## A Method of Aligning Polymer Chains

A detailed description of the materials work of papers **III**, and **IV**, and partially of paper **V** can be found in this reference. A summary is presented here.

**(12) INTERNATIONAL APPLICATION PUBLISHED UNDER THE PATENT COOPERATION TREATY (PCT)**

**(19) World Intellectual Property Organization**
International Bureau

**(43) International Publication Date**
**9 October 2003 (09.10.2003)**

**PCT**

**(10) International Publication Number**
**WO 03/082948 A1**

**(51) International Patent Classification[7]:** **C08G 61/12**, C09K 11/06, 19/38

**(21) International Application Number:** PCT/FI03/00245

**(22) International Filing Date:** 28 March 2003 (28.03.2003)

**(25) Filing Language:** English

**(26) Publication Language:** English

**(30) Priority Data:**
20020615 28 March 2002 (28.03.2002) FI

**(71) Applicant** *(for all designated States except US)*: **TEKNILLINEN KORKEAKOULU** [FI/FI]; P.O. Box 1000, FIN-02015 Tkk (FI).

**(72) Inventors; and**
**(75) Inventors/Applicants** *(for US only)*: **KNAAPILA, Matti** [FI/FI]; Helsingin Yliopisto, Fysikaalisten tieteiden laitos, Gustaf Hällströmin katu 2, FIN-00560 Helsinki (FI). **HORSBURGH, Lockhart, E.** [GB/GB]; Department of Physics, University of Durham, South Road, Durham DH1 3LE (GB). **MONKMAN, Andrew, P.** [GB/GB]; Department of Physics, University of Durham, South Road, Durham DH1 3LE (GB). **IKKALA, Olli** [FI/FI]; Teknillisen fysiikan ja matematiikan osasto, P.O. Box 2200, FIN-02015 Tkk (FI).

**(74) Agent: SEPPO LAINE OY**; Itämerenkatu 3 B, FIN-00180 Helsinki (FI).

**(81) Designated States** *(national)*: AE, AG, AL, AM, AT (utility model), AT, AU, AZ, BA, BB, BG, BR, BY, BZ, CA, CH, CN, CO, CR, CU, CZ (utility model), CZ, DE (utility model), DE, DK (utility model), DK, DM, DZ, EC, EE (utility model), EE, ES, FI (utility model), FI, GB, GD, GE, GH, GM, HR, HU, ID, IL, IN, IS, JP, KE, KG, KP, KR, KZ, LC, LK, LR, LS, LT, LU, LV, MA, MD, MG, MK, MN, MW, MX, MZ, NI, NO, NZ, OM, PH, PL, PT, RO, RU, SC, SD, SE, SG, SK (utility model), SK, SL, TJ, TM, TN, TR, TT, TZ, UA, UG, US, UZ, VC, VN, YU, ZA, ZM, ZW.

**(84) Designated States** *(regional)*: ARIPO patent (GH, GM, KE, LS, MW, MZ, SD, SL, SZ, TZ, UG, ZM, ZW), Eurasian patent (AM, AZ, BY, KG, KZ, MD, RU, TJ, TM), European patent (AT, BE, BG, CH, CY, CZ, DE, DK, EE, ES, FI, FR, GB, GR, HU, IE, IT, LU, MC, NL, PT, RO, SE, SI, SK, TR), OAPI patent (BF, BJ, CF, CG, CI, CM, GA, GN, GQ, GW, ML, MR, NE, SN, TD, TG).

**Published:**
— *with international search report*

*For two-letter codes and other abbreviations, refer to the "Guidance Notes on Codes and Abbreviations" appearing at the beginning of each regular issue of the PCT Gazette.*

WO 03/082948 A1

**(54) Title:** A METHOD OF ALIGNING POLYMER CHAINS

**(57) Abstract:** A hierarchical self-assembly in comb-shaped supramolecules of conjugated rod-like polymers and a novel concept to obtain the aligned solid state via cleaving side groups from the supramolecules are described. The supramolecules may consist of poly(2,5-pyridinediyl), acid dopants, and hydrogen bonded side chains. Films thereof are fluids even without an additional solvent and show thermotropic liquid crystallinity. They reveal exceptional degree of self-assembled order and the fluid state allows facile overall alignment yielding anisotropic opto-electronic properties, such as high dichroism and polarized emission. After alignment, cleavage of the side chains results in stable solid films with high optical anisotropy and enhanced photonic efficiency, such as improved photoluminescence quantum yield.

# Summary of the Papers I-VII

**I** Polypyridines which are stable and good charge transport materials having high photoluminescence quantum yield have been studied. It is found that poly(2,5-pyridinediyl) forms supramolecules that form lamellar self-organized structures due to bonding between pyridine and sulphonic acid unit and polar nonpolar effects combined. The examples of the lamellar nanoscale structure are demonstrated using synchrotron radiation and small-angle X-ray scattering method.

**II** Rodlike poly(2,5-pyridinediyl), wormlike polyaniline, and flexible poly(4-vinylpyridine) are nitrogen-containing polymers that in bulk phase with selected amphiphilic oligomers form self-organized comb-shaped supramolecules due to protonation, hydrogen bonding and polar-nonpolar effects combined. By contrast, the formation of luminescent or conductive self-organized structures is studied here in thin spin-coated films. The structures have been characterized using glancing-angle and grazing-incidence X-ray diffraction. The uniformity has been studied and the possibility for macrophase separation excluded using atomic force microscopy and scanning near-field optical microscopy. The self-organization in the films of good macroscopic quality has been demonstrated.

**III** A hierarchical self-organization in hairy-rodlike supramolecules of a conjugated polymer is reported. The supramolecules consist of poly(2,5-pyridinediyl), acid dopants, and hydrogen bonded alkyl side chains. A thermotropic smectic state with exceptionally large coherence length is formed without additional solvent. This allows facile overall alignment resulting in rather high dichroism and polarized photoluminescence. Solid (not liquid crystalline) films of aligned polymers are formed by cleaving side groups from the supramolecules which retain the optical anisotropy together with the high photoluminescence quantum yield of pristine polymer.

**IV** A directed self-organization in supramolecules containing rodlike polymers is reported. The hairy-rodlike supramolecules consist of poly(2,5-pyridinediyl), camphorsulfonic acid, and hydrogen bonded amphiphilic side chains. Locally they form highly ordered lamellar structures in which the polymers are stacked. The liquid crystalline state allows facile overall alignment yielding absorption dichroism and polarized photoluminescence. After alignment, cleavage of the amphiphiles results in pristine films which retain this optical anisotropy with the high photoluminescence quantum yield.

**V** Detailed small/wide-angle X-ray scattering and grazing-incidence X-ray diffraction investigations of hairy-rodlike supramolecules of poly(2,5-pyridinediyl), acid dopant and hydrogen bonded amphiphilic side chains are reported. In solution, the polymers are dissolved rodlike particles, whilst the complexation causes the formation of loose aggregates. When the side-chains are introduced, polymers self-assemble into hierarchic liquid crystals in the solid state. The fractions of the constituents varied over the whole regime of microphase separation and the bulk material was studied as a function of temperature. Depending on the composition, glassy, smectic, and disordered phases and corresponding order-order and order-disorder transitions were found. Thermotropic or plasticized material have been aligned both in-plane and uniaxially. Diffraction patterns of aligned liquid crystalline complexes show axial *h00*, *020*, *040*, and *004* reflections, and additional small-angle reflections along the (meridional) polymer axis. In particular, the small-angle reflections show both nematic and smectic type organization and additionally the two dimensional patterns reveal hierarchic organization - liquid crystallinity within the liquid crystallinity. The data - including accurate lattice parameters and the coherence lengths in three directions - and interpretation of the structrural behavior over a wide range of concentration and temperarure are presented. After alignment the self-organized part of the material reveals essentially only aligned component in diffraction patterns. The behavior of the aligned and nonaligned amorphous component in scattering patterns is discussed and taken into account when considering the correlation functions of the scattering intensities in all three directions. In a particular result, a triangular correlation function and a very large correlation length is seen along the smectic axis. The interpretation of the features of the correlation function is given. The self-organization was also studied in thin films and all the major characteristics seen in thick films were found. Moreover, an aligned solid (not liquid crystalline) structure can be formed by cleaving the side chains from the aligned liquid crystals. Based on the grazing-incidence X-ray diffraction patterns, in thin films this pristine material is suggested to be almost pure polymer.

**VI** The detailed structural investigation of hairy-rodlike poly(9,9-bis(2-ethylhexyl)-fluorene-2,7-diyl) in aligned thin films is presented here. Formation of a thickness dependent triaxial texturing has been identified in thermotropically aligned films. X-ray reflectivity measurements reveal good macroscopic quality and polarized photoluminescence and dichroic ratios in absorption indicate clear axial alignment. Grazing-incidence X-ray diffraction shows axially aligned mesomorphic structure with a distinct arrangement of helices. Large correlation lengths indicate a high local lateral order. Both the experiments and the computational results produced using molecular mechanics methods suggest 5/2-helicity. Further options have been discussed, too. The polymer chains are parallel to the substrate in the **c** direction. The hexagonal-like cells are flattened in the direction of the surface normal and, in particular, reveal two kinds of coexistent crystallites, a multiple orientation where the greater proportion of the crystallites have a crystal axis **a** perpendicular to the substrate surface, whereas a smaller proportion is aligned with the crystal axis **a** parallel to surface. In thinner films the former class of orientation is usually dominant, whilst the proportion of the parallel orientation type increases with prolonged annealing.

**VII** The structure formation and phase behavior of supramolecular hairy-rod polymers consisting of rodlike polymer chains with physically bonded side chains was investigated in the melt state using small-angle X-ray scattering. The supramolecules consisted of poly(2,5-pyridinediyl), complexed by methanesulfonic acid to form poly(2,5-pyridinium methane sulfonates), to which octyl gallates were hydrogen bonded. These hairy-rodlike supramolecules have been found to self-organize in rodlike assemblies in a square or oblique lattice or to form lamellar structures. Moreover, nematic (solid) and macrophase separated structures have been observed. These results have been collected in a phase diagram in the high polymer fraction limit and they are in a clear qualitative resemblance with recent theoretical modeling. The differences and similarities between the experiments and theory are discussed. The study shows that the recent theoretical model is able to explain many peculiarities observed in the experiment, highlights the most important mechanisms responsible for the observed phenomena, and gives the trends in which direction the experimental system has to be adjusted to get desired effects.